

1 2 9 0



UNIVERSIDADE DE
COIMBRA

Andrew Murray

WHITE SANDS OF RIO MAIOR
GEOLOGICAL HISTORY, PALAEOENVIRONMENT, AND
ECONOMIC POTENTIAL

Dissertação no âmbito do Mestrado em Engenharia Geológica e de Minas orientada pela Professora Doutora Lídia Maria Gil Catarino e pelo Professor Doutor Fernando Antunes Gaspar Pita e apresentada ao Departamento de Ciências da Terra da Faculdade de Ciências e Tecnologia da Universidade de Coimbra.

Setembro de 2019



UNIVERSIDADE D
COIMBRA

Andrew Murray

WHITE SANDS OF RIO MAIOR:
GEOLOGICAL HISTORY, PALAEOENVIRONMENT, AND ECONOMIC
POTENTIAL

Dissertação de Mestrado em Engenharia Geológica e de Minas

Orientadores:

Prof. Lídia Maria Gil Catarino

Prof. Fernando Antunes Gaspar Pita

Coimbra, Setembro de 2019

Thanks:

I give my thanks to all who have helped in the completion of this dissertation. For their understanding and support I thank my family. For the opportunity to work at Sifucel I thank Gonçalo Pinheiro, and for their help in producing this dissertation I would like to thank André Filipe and Raquel Dias. I would also like to thank all of the Sifucel employees who have welcomed me and helped me make a contribution. Finally, I thank my professors for their help and guidance in this work.

Abstract

This work focuses on the mining work of the Sifucel - Sílicas, S.A. company, and the Parapedra Group which owns it. The aim is to propose the merits of expanding mining rights northwards from the current Via-Vai quarry, where approximately 21.38 million tonnes of sand could be available from areas currently owned by Sifucel. Expanding ownership rights, however, to a 47 hectare area placed between the local restricting features, could yield 99.772 million tonnes of sand. This could extend the life of sand mining in this area by Sifucel by 332.6 years (based on current production). This is based on a virtual model created from available data. The various issues relating to mining expansion and the information it is based on are discussed.

The extraction, refinement, and quality control methods are described. Particular focus is placed on the sorting methods to ensure a high quality of the product. This includes froth flotation, by which the purest siliceous sand is produced. Methods to maintain quality are outlined and the granulometric, chemical, and mineralogical compositions of the various Sifucel sand products are examined.

In order to better understand the Rio Maior sand deposit and identify patterns in the sand composition, the geological history is examined. During the Piacenzian, the Rio Maior basin was infilled with sand which, due to its aeolian transport, had a high silica content. This sand and the above diatomite and lignite complex are of particular geological interest as being the most complete Piacenzian deposits in Portugal. This understanding is combined with information obtained from previous studies and first hand analysis to achieve characteristic patterns in sand composition.

Keywords

Rio Maior sands; sedimentary basin; palaeoenvironment; lithostratigraphy; sand characterisation

Resumo

Este trabalho centra-se no trabalho de mineração da empresa Sifucel-Sílicas, S.A., e no grupo Parapedra, que é seu proprietário. O objetivo é propor argumentos para a expansão dos direitos minerários para o norte a partir da atual pedreira de Via-Vai, onde aproximadamente 21,38 milhões de toneladas de areia poderiam estar disponíveis nas áreas atualmente propriedade da Sifucel. Expansão dos direitos de propriedade, no entanto, para uma área de 47 hectares colocada entre as características locais de restrição, poderia render 99.772 milhões de toneladas de areia. Isso poderia prolongar a vida útil da mineração de areia nesta área pela Sifucel em 332,6 anos (com base na produção atual). Isso é baseado em um modelo virtual criado a partir de dados disponíveis. São discutidos os vários aspetos relacionados.

Os métodos de extração, refinamento e controlo de qualidade são descritos nesta dissertação. Um foco particular é colocado nos métodos de triagem para garantir uma alta qualidade do produto. Isso inclui flutuação, pela qual a mais pura areia siliciosa é produzida. Os métodos para manter a qualidade são descritos e as composições granulométricas, químicas e mineralógicas dos vários produtos de areia Sifucel são examinadas.

Para melhor compreender o depósito de areia de Rio Maior e identificar padrões na composição da areia, é examinada a história geológica. Durante o período Placenciano, a bacia do Rio Maior foi preenchida com areia que, devido ao seu transporte eólico, apresentava um elevado teor de sílica. Esta areia e o complexo de diatomite e lignite acima referido são de interesse geológico particular, sendo os depósitos do Placenciano mais completos em Portugal. Essa compreensão é combinada com informações obtidas de estudos anteriores e análise de primeira mão para atingir padrões característicos na composição da areia.

Palavras-chave

Areias de Rio Maior; bacias sedimentares; paleoambiente; litostratigrafia; caracterização de areias

Contents

1. Introduction	1
1.1. Background	1
1.2. Objectives	1
1.3. Organisation of work	2
2. Sifucel and the silica market	3
2.1 Sifucel - Sílicas, S.A.	3
2.2. Market and uses	4
2.2.1. Uses of silica	4
3. Extraction methods and refinement of the Rio Maior sand	6
3.1. Extraction and processing of sand	6
3.1.1. Extraction	7
3.1.2. Hopper	7
3.1.3. Trommel	8
3.1.4. Hydrocyclone	8
3.1.5. Vibrating screen	9
3.1.6. Gravity separation	10
3.1.7. Froth flotation	10
3.1.8. Stock	11
3.2. Quality control	14
3.2.1. Internal control	14
4. Composition of Sifucel sands	18
4.1. Granulometric analysis	18
4.2. Chemical composition	18
4.2.1. Non-flotation sand designations	19
4.2.2. Chemical composition of rejected sand	21
4.2.3. Chemical analysis of flotation sand	23
4.3. Mineralogical analysis	24
5. Geology and palaeoenvironment of the Rio Maior basin	26
5.1. Description of the Rio Maior basin	26
5.2. Previous studies	28
5.3. Geological history of the basin	29
5.3.1. Mesozoic	29
5.3.2. Paleogene and Miocene	30

5.3.3. Pliocene	31
5.4. Utility	33
6. Analysis of white sand and interpretation	35
6.1. Sand analysis	35
6.1.1. Granulometry	35
6.1.2. Chemistry	37
6.1.2.1. Silicon dioxide	37
6.1.2.2. Aluminium oxide	38
6.1.2.3. Potassium, sodium, and calcium oxides	39
6.1.2.4. Titanium dioxide	41
6.1.2.5. Iron oxide	41
6.1.2.6. Magnesium oxide	42
6.1.2.7. Other contaminants	43
6.1.2.8. Mineralogical indications	45
6.1.3. Structures	46
6.2. Interpretations	50
7. Areas of further exploitation	54
7.1. Need for further excavation	54
7.2. Virtual modelling	54
7.3. Area determination	55
7.3.1. Owned area	55
7.3.2. Factors for expansion	58
7.3.3. Proposed excavation location	61
7.4 Legal requirements	65
8. Conclusion and recommendations	67
8.1. Further excavation of sand	67
8.2. Further geological exploration	67
Bibliography	69

Index of Figures

Figure 2.1. Location of Sifucel, Rio Maior and arrangement of buildings on the site. Maps constructed using Google Earth and Apple Maps.	3
Figure 2.2. Average silica sand historical price volatility (98 US\$/tonne, from Kelly <i>et al.</i> , 2014 and modified by European Commission, 2014).	4
Figure 2.3. European silica consumption by market (industry estimate, modified from IMA-Europe, 2013).	5
Figure 3.1. Flowchart showing the processes used to produce sand (the sand classifications can be found in Table 4.1)	6
Figure 3.2. Dedger working inside the Via-Vai quarry (Grupo Parapedra, 2013).	7
Figure 3.3. Dedger working inside the Via-Vai quarry and pipeline transporting sand for processing.	7
Figure 3.4. Hopper feeding conveyor belt. Reservoir in the background.	8
Figure 3.5. Inside trommel.	8
Figure 3.6. Design of a hydrocyclone (Michaud, 2015).	9
Figure 3.7. Clarifier.	9
Figure 3.8. Kaolin filter press.	9
Figure 3.9. Vibrating screen used in washing.	10
Figure 3.10. Set of four sorting spirals.	10
Figure 3.11. Inside of spirals showing separation outlets.	10
Figure 3.12. Diagram of froth flotation, modified from Michaud (2013).	11
Figure 3.13. Rejected material concentrated in heavy minerals.	11
Figure 3.14. Grain fineness calculation from Brown (1936).	12
Figure 3.15. Storage silos.	13
Figure 3.16. Underneath storage silos with outlets labelled with the product.	13
Figure 3.17. Inside the drying and packing centre.	13
Figure 3.18. Revolving dryer.	13
Figure 3.19. Sifucel 'big bags'.	13
Figure 3.20. Sifucel packages.	13
Figure 3.21. Sieves used for dry granulometric analysis.	15
Figure 3.22. Preparation area for chemical analysis discs.	15
Figure 3.23. Malvern Panalytical Zetium machine.	15
Figure 3.24. Mastersizer 3000 machine.	17
Figure 3.25. Colorimeter.	17
Figure 3.26. Moisture scale.	17

Figure 4.1. S90/100 sand. Scale is 5 mm.	19
Figure 4.2. S90/100 sand. Scale is 1 mm.	19
Figure 4.3. S40 sand. Scale is 5 mm.	20
Figure 4.4. S40 sand. Scale is 1 mm.	20
Figure 4.5. S30/40 sand. Scale is 5 mm.	20
Figure 4.6. S30/40 sand. Scale is 1 mm.	20
Figure 4.7. S40/45 sand. Scale is 5 mm.	20
Figure 4.8. S40/45 sand. Scale is 1 mm.	20
Figure 4.9. S40/45 CF sand. Scale is 5 mm.	21
Figure 4.10. S40/45 CF sand. Scale is 1 mm.	21
Figure 4.11. Linha 1 rejected sand. Scale is 5 mm.	21
Figure 4.12. Linha 1 rejected sand. Scale is 1 mm.	21
Figure 4.13. Linha 2 rejected sand. Scale is 5 mm.	21
Figure 4.14. Linha 2 rejected sand. Scale is 1 mm.	21
Figure 4.15. S40/45 FL Linha 1 sand. Scale is 5 mm.	23
Figure 4.16. S40/45 FL Linha 1 sand. Scale is 1 mm.	23
Figure 4.17. S40/45 FL Linha 2 sand. Scale is 5 mm.	23
Figure 4.18. S40/45 FL Linha 2 sand. Scale is 1 mm.	23
Figure 5.1. Geological map of the area of interest showing the location of relevant boreholes (modified from Zbyszewski & Almeida, 1960 and Carvalho & Pereira, 1973).	27
Figure 5.2. Diagram showing the position of the Caldas da Rainha and Fonte da Bica diapirs (modified from Zbyszewski, 1959).	30
Figure 5.3. Mean variation of temperature and humidity in the Miocene of the Lower Tejo basin (modified from Pais, 2010, using data from Antunes & Pais, 1984, Antunes <i>et al.</i> , 2000).	31
Figure 5.4. Mean variation of temperature and humidity in the Pliocene of the Rio Maior basin (modified from Pais, 2010, using data from Diniz, 1984, 2003).	33
Figure 5.5. Map of the area showing the extent of the sand in the Rio Maior basin (modified from Carvalho & Pereira, 1973), the lignite basin (modified from Flores, 1996), and the location of the Via-Vai quarry.	34
Figure 6.1. Cumulative frequency curves showing average, maximum, and minimum percentages for each grade measured. A: Sieve matrix from >2 to <0.02 mm. B: Sieve matrix from >5.66 to <0.02 mm.	35
Figure 6.2. Average A.F.A. Fineness Number across basin. Map modified from Carvalho and Pereira (1973) data using RockWorks.	36
Figure 6.3. Cumulative frequency curve of SiO ₂ (data from Carvalho & Pereira, 1973).	38
Figure 6.4. Concentrations in <44 µm fraction (data from Carvalho & Pereira, 1973).	38

Figure 6.5. Cumulative frequency curve of Al ₂ O ₃ (data from Carvalho & Pereira, 1973).	39
Figure 6.6. Concentrations in <44 µm fraction (data from Carvalho & Pereira, 1973).	39
Figure 6.7. Cumulative frequency curve of K ₂ O (data from Carvalho & Pereira, 1973).	40
Figure 6.8. Concentrations in <44 µm fraction (data from Carvalho & Pereira, 1973).	40
Figure 6.9. Cumulative frequency curve of Na ₂ O (data from Carvalho & Pereira, 1973).	40
Figure 6.10. Concentrations in <44 µm fraction (data from Carvalho & Pereira, 1973).	40
Figure 6.11. Cumulative frequency curve of CaO (data from Carvalho & Pereira, 1973).	40
Figure 6.12. Concentrations in <44 µm fraction (data from Carvalho & Pereira, 1973).	40
Figure 6.13. Cumulative frequency curve of TiO ₂ (data from Carvalho & Pereira, 1973).	41
Figure 6.14. Concentrations in <44 µm fraction (data from Carvalho & Pereira, 1973).	41
Figure 6.15. Cumulative frequency curve of Fe ₂ O ₃ (data from Carvalho & Pereira, 1973).	42
Figure 6.16. Concentrations in <44 µm fraction (data from Carvalho & Pereira, 1973).	42
Figure 6.17. Cumulative frequency curve of MgO (data from Carvalho & Pereira, 1973).	43
Figure 6.18. Distribution of SiO ₂ throughout basin. Made using RockWorks.	43
Figure 6.19. Distribution of Al ₂ O ₃ throughout basin. Made using RockWorks.	43
Figure 6.20. Distribution of K ₂ O throughout basin. Made using RockWorks.	44
Figure 6.21. Distribution of Na ₂ O throughout basin. Made using RockWorks.	44
Figure 6.22. Distribution of TiO ₂ throughout basin. Made using RockWorks.	44
Figure 6.23. Distribution of Fe ₂ O ₃ throughout basin. Made using RockWorks.	44
Figure 6.24. Distribution of MgO throughout basin. Made using RockWorks.	45
Figure 6.25. Distribution of other contaminants throughout basin. Made using RockWorks.	45
Figure 5.26. Variation of chemical composition of sand samples according to depth in borehole AF 28 (data from Carvalho & Perreira, 1973).	45
Figure 6.27. Via-Vai quarry showing sample points. Created using GoogleEarth.	46
Figure 6.28. South west side of the Via-Vai quarry with bedding planes highlighted. Whole view is 350m.	47
Figure 6.29. Red and white sand lenses located in point α. Scale is 50cm.	47
Figure 6.30. Sample point δ1. Sloping delta beds are highlighted in blue, near-horizontal beds are highlighted in green. Scale is 10m.	49
Figure 6.31. Signs of black plant material in red sand located in point β. Scale is 5cm.	49
Figure 6.32. <i>Planorbarius</i> sp. Scale is 5cm.	49
Figure 6.33. Unidentified bivalve or brachiopod. Scale is 5cm.	49
Figure 6.34. Fragment of purple siltstone. Scale is 10cm.	50

Figure 6.35. Reconstruction of the Rio Maior basin during sand deposition. Map based on current sand deposits and elevations based on the upper horizon of the deposit. The source of the sand is the beach dunes, and three interpreted inputs are marked.	52
Figure 7.1. RockWorks stratigraphic model of the Rio Maior basin. Above model shows all stratigraphic units. Below model shows only white sand stratigraphic unit.	56
Figure 7.2. Map showing areas, and related approximate coordinates, owned by Sifucel. Map was created using GoogleEarth and AppleMaps.	56
Figure 7.3. RockWorks stratigraphic model of the Areas 1 and 2. Above model shows all stratigraphic units. Below model shows only surface deposits and white sand stratigraphic units.	57
Figure 7.4. Thickness of sand deposit in the Areas 1 and 2. Made using RockWorks.	57
Figure 7.5. Depth of the sand upper horizon in the Areas 1 and 2. Made using RockWorks.	57
Figure 7.6. Thickness of sand deposit in the Rio Maior basin. Made using RockWorks.	59
Figure 7.7. Depth of the sand upper horizon in the Rio Maior basin. Made using RockWorks.	59
Figure 7.8. Map showing areas, and related approximate coordinates, of proposed excavation location. Rua Central Eléctrica picked out. Map was created using GoogleEarth and AppleMaps.	60
Figure 7.9. Thickness of sand deposit in the proposed excavation location. Made using RockWorks.	61
Figure 7.10. RockWorks stratigraphic model of the proposed excavation location. Above model shows all stratigraphic units. Below model shows only the white sand stratigraphic unit.	62
Figure 7.11. Depth of the sand upper horizon in the Rio Maior basin. Made using RockWorks.	63
Figure 7.12. Distribution of Al ₂ O ₃ throughout proposed excavation location. Made using RockWorks.	63
Figure 7.13. Distribution of Fe ₂ O ₃ throughout proposed excavation location. Made using RockWorks.	63
Figure 7.14. RockWorks stratigraphic sections of the proposed excavation location. Above map was created using GoogleEarth and Applemaps, and shows section lines.	64

Index of Tables

Table 3.1. Types of sands produced and sold by Sifucel.	12
Table 4.1. Granulometric compositions of S40/45 sand types 1 and 2 and flotation sand (FL). Type 1 feeds line 1 and type 2 feeds line 2. The samples were collected at 16:00 on 27/02/2019.	18
Table 4.2. Granulometric compositions of S30/40 sand. The sample was collected at 16:00 on 27/02/2019.	18
Table 4.3. Granulometric compositions of S55/60 sand. The sample was collected at 16:00 on 27/02/2019.	18
Table 4.4. Chemical compositions of various sands produced by Sifucel. All samples were measured using the AREIRA calibration. SiO ₂ values are estimated. The construction sand was measured at 14:00 on 01/11/2018, while the other samples were collected at 16:00 on 27/02/2019.	19
Table 4.5. Typical chemical composition of sand for clear glass (Moura & Velho, 2012).	20
Table 4.6. Chemical compositions of construction sand, material rejected by hydraulic separation (S40/45 CF), and material rejected by flotation (Linha 1 & Linha 2 rejected). SiO ₂ values are estimated. The construction sand was measured at 14:00 on 01/11/2018, while the other samples were collected at 16:00 on 27/02/2019.	22
Table 4.7. Chemical compositions of sand entering flotation (Entrada) and leaving flotation (S40/45 FL). SiO ₂ values are estimated. The samples were collected at 16:00 on 27/02/2019.	24
Table 4.8. Approximate values for the percentage of heavy minerals in various granulometric fractions (Carvalho & Pereira, 1973).	24
Table 4.9. Identification of minerals from different granulometric sizes of samples of S 40 designation (Serpa, 2018).	25
Table 6.1. Chemical compositions of samples from the Via-Vai quarry. All samples were measured using the OMNIAN calibration conforming to Sifucel analysis procedures. SiO ₂ values are estimated. The samples were collected between 27/02/2019 and 16/05/2019.	48

1. Introduction

1.1. Background

This dissertation is part of the curriculum of the course Mestrado em Engenharia Geológica e de Minas, provided by the University of Coimbra.

The curricular internship was carried out at Sifucel - Sílicas, S.A. between 11th February 2019 to 3rd June 2019. It was supervised by Professors Lídia Gil Catarino and Fernando Gaspar Pita. André Filipe was the Sifucel supervisor who provided workplace instruction and oversaw the work.

The area around the city of Rio Maior has long been used to extract white, silica-rich sand, being the country's main producer (Moura & Velho, 2012). The main market for sand is construction, however, the purity of the Rio Maior sands make it suitable for various types of glass, metal casting, and ceramics (IMA-Europe, 2013). Although the sand has a high purity, clay and other contaminating minerals (iron oxides, micas, feldspars) have to be removed. The benefit of a high grade source is reduced treatment, more product, and less waste. The size of the deposit also suggests future work extracting the untapped areas of the deposit.

Sifucel - Sílicas, S.A. was founded in 1965, setting up its headquarters in Rio Maior. It was acquired by the Parapedra Group in 1995. Sifucel controls five excavation operations: Rio Maior, Alcácer do Sal, Mosteiros, Caldas da Rainha, and Nazaré/Pataias. The Rio Maior site focuses on the production of silica sand, the byproduct kaolin, and refined silica powder.

The high purity of the sand produced by Sifucel allow it to sell material for construction, various and specialised glass, ceramics, metallurgical industries, insulation, sport, and various other uses. While transporting around Portugal, Sifucel also export to Spain, France, Italy, North Africa, Asia, and South America.

1.2. Objectives

The purpose of this work is to examine possible areas of further sand excavation and exploitation, considering the factors which decide feasibility and profitability. Various other information will be analysed to better determine this objective.

This dissertation will collect and summarise previous work on the geological events that produced the Rio Maior sedimentary basin. Conclusions of the changing palaeoenvironment will also be presented. An analysis of the sand within the basin will be made using previous studies and an interpretation of the environmental conditions which produced the deposit proposed.

There will also be a description of the processes used in the Rio Maior site of Sifucel to extract and refine the sand from the Via-Vai quarry. This will discuss all aspects from extraction to packing and briefly mention the markets which this production supports.

1. Introduction

The areas currently owned, but not exploited by Sifucel will be analysed and a wider area of extraction proposed. The contents and features, both physical and chemical, will be explored through geological modelling. The work will estimate the content of sand and propose future work regarding the Rio Maior basin, both industrial and geological.

1.3. Organisation of work

This dissertation is divided into eight chapters.

This first chapter, Introduction, provides information on the framework of the internship and the Sifucel company, the objectives of the dissertation, and how it is organised.

The second chapter, Sifucel and the silica market, examines Sifucel - Sílicas, S.A. and discusses the market of siliceous sand, its uses and quality required by various industries.

The third chapter, Extraction methods and refinement of the Rio Maior basin, examines the processes of extraction, refinement, and quality control of Sifucel. The whole process and its constituent sections are described.

The fourth chapter, Composition of Sifucel sands, examines the granulometric, chemical, and mineralogical characteristics of the sands. These include sand produced by Sifucel at various stages of the refinement process.

The fifth chapter, Geology and Palaeoenvironment of the Rio Maior basin, summarises the previous work carried out relating to the geology of the Rio Maior area. The tectonic events which created the basin and the deposition of sand, diatomite and lignite in the basin are described. Included are the conclusions of studies stratigraphically above and below the sand deposit to identify the age and palaeoenvironment of the surrounding lithologies.

The sixth chapter, Analysis of white sand and interpretation, uses the results of previous studies and analysis carried out for this work. The physical and chemical characteristics are analysed using computer modelling to find patterns across the basin. After the results of these analyses are presented, they are interpreted to propose a reconstruction of the features which produced the sand deposit.

The seventh chapter, Areas of further exploitation, discusses the need for further exploitation of the Rio Maior basin and the factors that limit this expansion. The areas owned but not yet exploited by Sifucel are examined and a new area of excavation proposed.

The eighth chapter, Conclusion and recommendations, suggests the way in which the current Sifucel extraction process can be expanded. Also discussed are the issues, both geological and commercial, for further exploration of the Rio Maior basin.

2. Sifucel and the silica market

2.1. Sifucel - Sílicas, S.A.

Parapedra - Sociedade Transformadora de Pedras, is a group that was founded in Rio Maior in 1979 and began to grow rapidly in the 1990s. The Parapedra Group deal in rocks and sands, producing around 18 000 tons of product per day. The group includes the companies: Parapedra, Interbritas, Tecnicálcio, Calcitrans, and Sifucel.

Sifucel was founded in 1965 as a company which specialised in the treatment of sand for commercial use, selling product to other companies in Portugal and abroad. It was acquired by the Parapedra Group in 1995 and, in 1997, began exploring the sand deposits of the Rio Maior basin in the search for commercially exploitable material.

The company opened the Via-Vai Quarry Project to extract the white sand. The quarry itself covers 20.5 ha, with an additional 2.5 ha providing an exclusion zone. The refinement works are located to the south of the quarry as part of the Rio Maior Industrial Park and occupy about 5 ha (Figure 2.1).

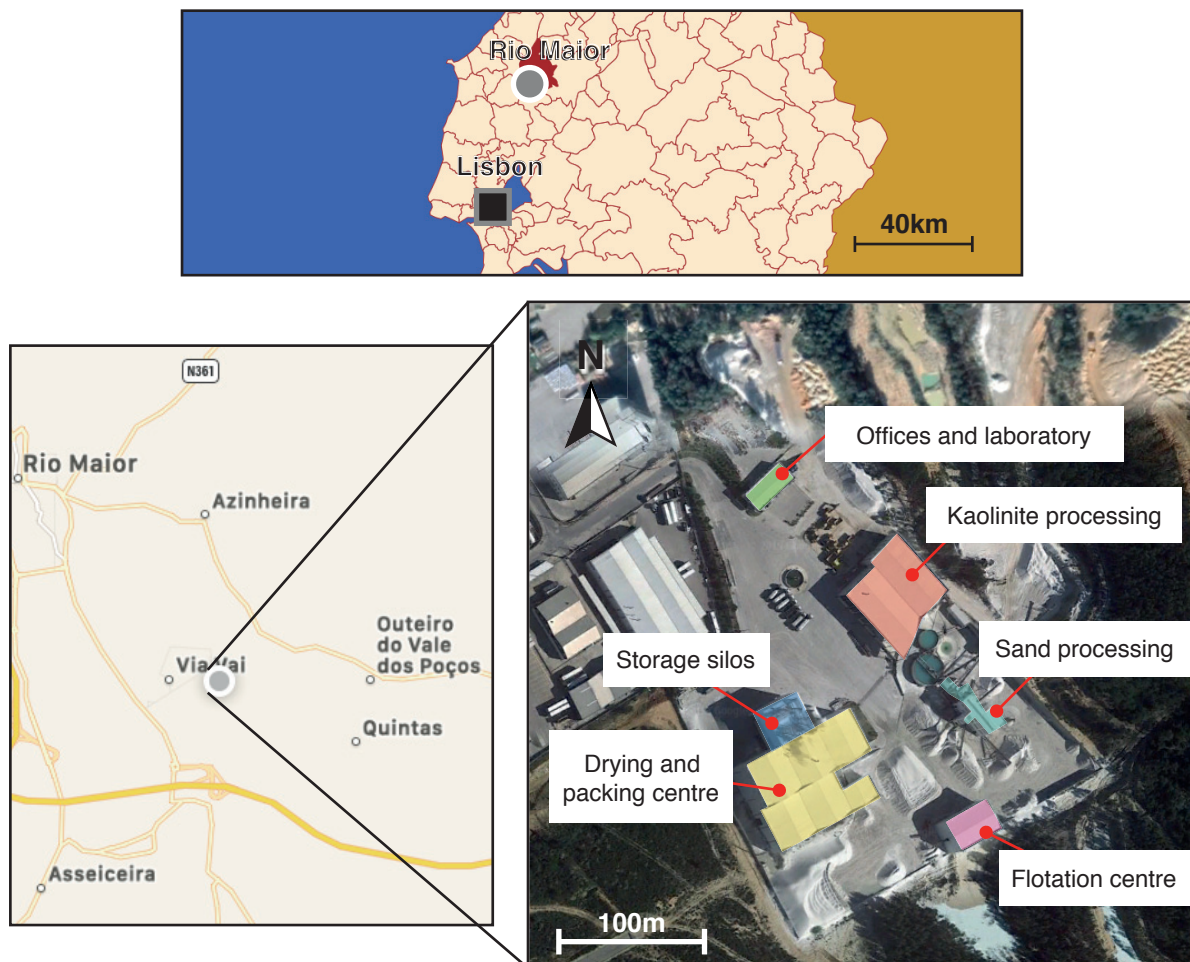


Figure 2.1. Location of Sifucel, Rio Maior and arrangement of buildings on the site. Maps constructed using Google Earth and Apple Maps.

2. Sifucel and the silica market

Using a dredge in the quarry, a pipeline transports the extracted material to the refinement works. The sand is treated and sorted to produce kaolin, refined white sand, silica powder, and washed gravel. Sifucel normally produces about 3 200 tons of sand per day of operation.

2.2. Market and uses

Special sand (also known as silica sand) is characterised by having a high concentration of silica dioxide (SiO_2) up to 99.9% (Moura & Velho, 2012, European Commission, 2014). This sand is desirable for several physical qualities: a hardness of 6 - 7 on Mohs scale; a density of 1.36 - 1.6 g/cm^3 (disaggregated sand rather than sandstone or quartz); and a melting temperature of 1427 - 1760°C. These sands are also usually clear, whiteish, or beige in colour, moderately rounded to angular, with no fractures or coatings of other minerals (Moura & Velho, 2012). These qualities allow them to withstand electronic applications, heat treatment, strong acids, and thermal shock (European Commission, 2014).

While there is extensive data on the international trade on sand, there is no trade data on special sand (European Commission, 2014). While values have increased for some uses of special sand, others have decreased, resulting in a slight, insignificant rise (Figure 2.2, Kelly *et al.*, 2014).

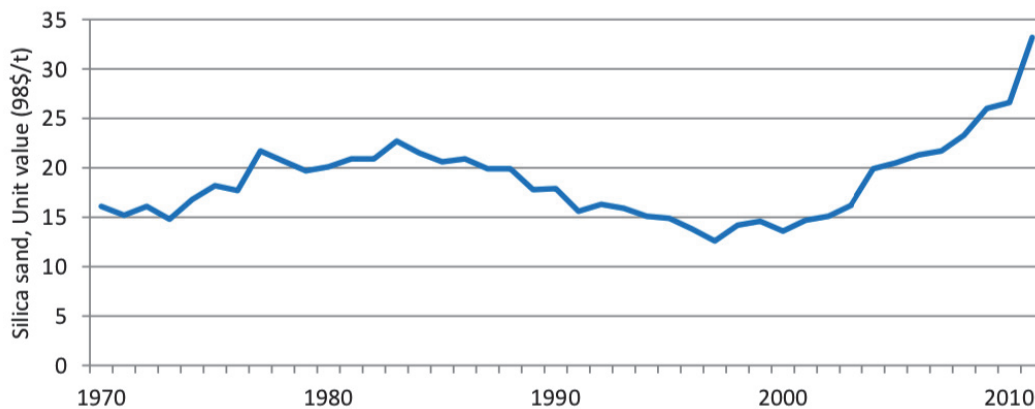


Figure 2.2. Average silica sand historical price volatility (98 US\$/tonne, from Kelly *et al.*, 2014 and modified by European Commission, 2014).

2.2.1. Uses of silica

The European consumption of silica is sorted into seven categories (Figure 2.3).

- **Construction sand and soil:** this is sold in high and low quality. It is used in high-end concrete, composite kitchen tops, equestrian surfaces, sports soils, asphalt, and road

construction (IMA-Europe, 2013). Sifucel is known for producing sand for golf courses, which also falls into this category.

- **Glass (container, flat, and other):** the two main types of glass are container glass (jars, bottles, etc.) and flat glass (windows, mirrors, vehicle windscreens). It also includes tableware, lighting glass for electric bulbs and fluorescent tubes, television tubes and screens (IMA-Europe, 2011). Specialised glass is required for glass fibre, plasma screens, and optics. Impurities are added during manufacture to affect the stability and durability of the glass (SAMSA, 2019) or, in the case of iron and aluminium, add colour to the glass (Mitchell, 2012). All glass manufacture requires a silica dioxide content of above 98.5% and a grain size of 100 - 600 µm (European Commission, 2014).
- **Foundry casting:** the sand is mixed with a binder to make moulds for iron, copper, or aluminium, which have lower melting points than silica dioxide (European Commission, 2014). Silica and cristobalite powder are used for the precision casting of jewellery, dental bridges, golf clubs, and aviation blades (IMA-Europe, 2011).
- **Ceramics:** this includes tableware, sanitary-ware, ornaments, and tiles for floors and walls. Silica sand is also used in the manufacture of refractory bricks, and silica powder is a major component of ceramic glazes (IMA-Europe, 2011).
- **Other uses:** includes paints, plastics, polymer compounds, rubber, sealants and adhesives, filtration, oil field applications, agriculture, chemicals, and production of silicon metal and ferrosilicon in the metallurgical industry (IMA-Europe, 2011). Sifucel is a known supplier of sands for filtration systems to extract waste from water systems.

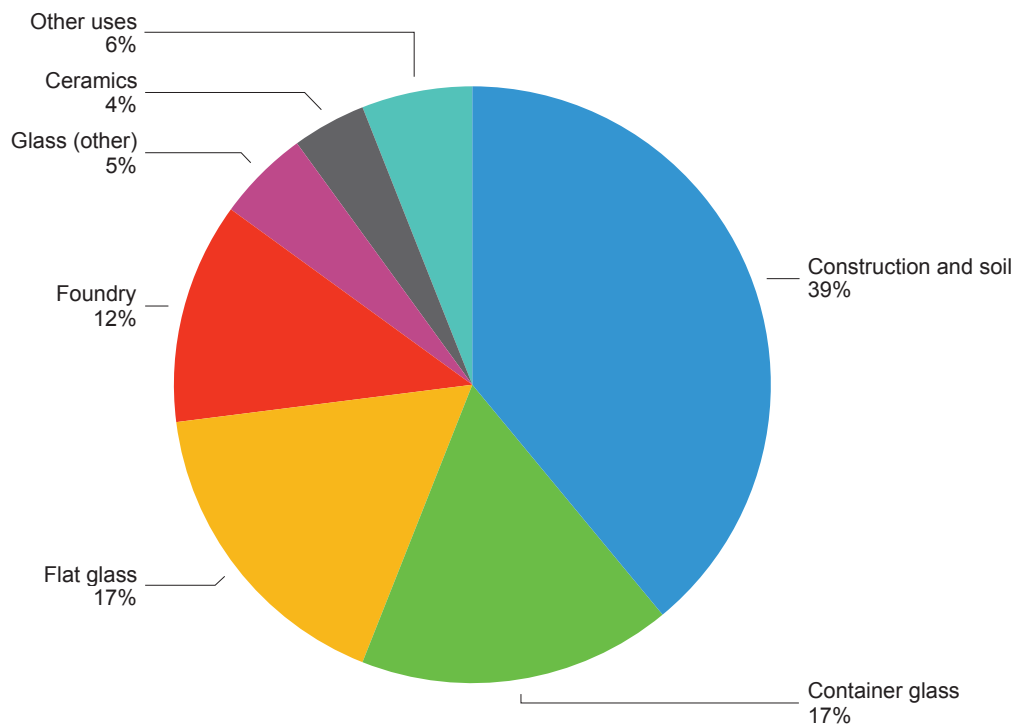


Figure 2.3. European silica consumption by market (industry estimate, modified from IMA-Europe, 2013).

3. Extraction methods and refinement of the Rio Maior sand

3.1. Extraction and processing of sand

The Rio Maior facilities mainly treat material extracted from the Via-Vai quarry. There is much interconnectivity between the Sifucel facilities and Parapedra Group companies, however, they mostly handle their local production sources (Grupo Parapedra, 2013).

The Environmental Impact Study for the Via-Vai Quarry Project (Visa, 2004) estimated the useful amount of sandy mass available to be approximately 3 687 000 m³, or 7 374 000 t. It estimates 5% of this to be low quality sand (184 350 m³, 331 830 t), 12% to be kaolin (420 320 m³, 840 640 t), leaving 83% of special sand (3 080 330 m³, 6 160 660 t). Based on an annual production of 35 000 t of kaolinite, 15 000 t of low quality sand, and 250 000 t of special sand, the study predicted the lifespan of the quarry to be approximately 24.6 years.

All of the special sand produced by Sifucel go through 6 processes to extract them, clean them, separate them from contaminants, and sort them by grade (size). This also separates the kaolin from the material. These processes are: extraction; hopper; trommel; hydrocyclone; vibrating screen; and gravity separation (Dias, 2015). Figure 3.1 shows a flowchart of these processes and how they are involved in producing the various sands.

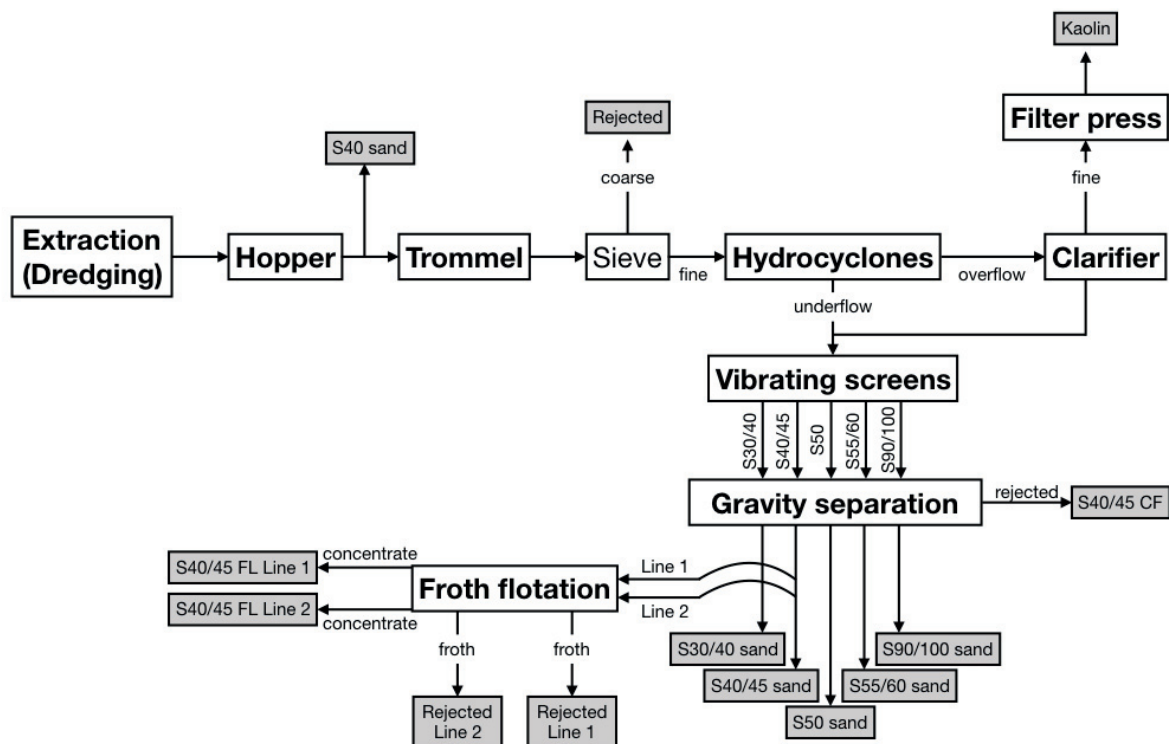


Figure 3.1. Flowchart showing the processes used to produce sand (the sand classifications can be found in Table 3.1).

While the sand has undergone gravity separation to remove heavy minerals in addition to sorting the silica grains, the chemical composition of the product is not sufficient for use in specialised industries, such as glass manufacture. The material designated for this use, undergoes an additional process, froth flotation, to reduce the concentration of heavy metals (particularly iron) to suitably low levels.

3.1.1. Extraction

The exploitation surface in the Via-Vai quarry is currently below the water table, so a floating dredger is used (Figure 3.2). Diggers work around the edges of the quarry, dumping



Figure 3.2. Dredger working inside the Via-Vai quarry (Grupo Parapedra, 2013).

fresh material into the lagoon, adding to the material the dredger extracts. A suction system allows the dredger to excavate sand in a watery suspension and pump it through a pipeline to the Sifucel facility (Figure 3.3).

Significant amounts of red and orange sand are extracted by digger from the quarry. As these contain relatively high levels of iron and other heavy minerals, these will be mixed with rejected material and sold as sand for construction.

3.1.2. Hopper

The material which is transported through the pipeline goes to a reservoir. This reservoir allows for the sand to be separated from the suspension and acts as storage, enabling Sifucel to continue



Figure 3.3. Dredger working inside the Via-Vai quarry and pipeline transporting sand for processing.

3. Extraction methods and refinement of the Rio Maior sand

production if the supply through the pipeline is interrupted. The sand then passes over a vibrating horizontal screen to reduce excess water, and by conveyor belts, into the hopper (Figure 3.4). Here it is stored for further processing. The sand is designated S40 as it is assumed to have an average grain size of 303 μm due to the sorting by the vibrating screen (although the variation is great and this average measure is not routinely tested for).

3.1.3. Trommel

A conveyor belt (from where samples of S40 were obtained) transports the sand from the hopper feed to the trommel (Figure 3.5). The trommel is a large rotating drum. As it rotates, the sand inside is washed and disaggregated into individual grains. This also allows later processes to more easily separate the sand from the clay material.

The output material is passed through a sieve to remove very coarse sand and larger grains. This rejected material is added to the construction sand.



Figure 3.4. Hopper feeding conveyor belt.
Reservoir in the background.



Figure 3.5. Inside trommel.

3.1.4. Hydrocyclone

The disaggregated material in suspension is then pumped into a series of hydrocyclones (Figure 3.6).

Hydrocyclones (also called 'cyclones'), use a combination of centrifugal and centripetal force to separate suspended material (Colman, 1981). A hydrocyclone is made up of an inverted conical cylinder with one inlet in the upper side, and two outlets: one in the top and one in the bottom. The suspension enters under pressure, and so creates a vortex inside. The less dense particles and much of the water are drawn to the centre of the vortex and moved upwards by the accumulation of denser material below it. The finer fraction then exits the hydrocyclone through the top outlet, the overflow. The denser particles achieve a

higher velocity and are drawn to the walls of the cyclone. Gravity, and the accumulation of less dense material above, force the coarse material down to be discharged through the bottom outlet, the underflow (Carrisso & Correira, 2004).

After passing through various hydrocyclones, the final overflow is transported to a clarifier (Figure 3.7). In the clarifier, the fine kaolin clay flocculates (Nichols, 1999) and is deposited on the bottom, separating it from most of the water and any fine quartz particles in suspension. The kaolin is collected and any excess water removed with a filter press (Figure 3.8). The water and any remaining fine sand particles from the clarifier overflow are mixed with the material from the underflows for further processing.

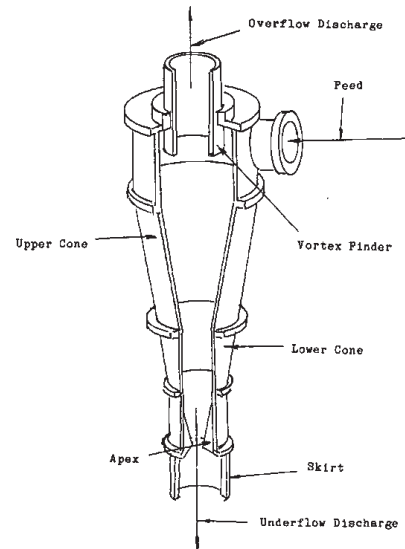


Figure 3.6. Design of a hydrocyclone (Michaud, 2015).



Figure 3.7. Clarifier.



Figure 3.8. Kaolin filter press.

3.1.5. Vibrating screen

The products from the clarifier and hydrocyclone processes are collected and washed using vibrating screens (Figure 3.9) to remove detrital material that might have been accidentally collected by the dredger in the lagoon, and to sort the sand.

The vibrating screens collect material on their surfaces and are washed with water. The pressure of the water is calibrated so that finer material is removed, leaving coarser,

3. Extraction methods and refinement of the Rio Maior sand

denser particles. The overflow is transported to another screen, where the water pressure is lower, allowing finer particles to remain. This process, repeated, allows for the sand to be sorted into different granulometries.



Figure 3.9. Vibrating screen.

3.1.6. Gravity separation

The material has excess heavy minerals removed by gravity separation with the use of spirals (Figures 3.10, 3.11). The material is washed down the spirals with water.

The heavier minerals attain a lower velocity than the quartz and lighter minerals, and remain in the inner part of the spiral. These are then separated out from the quartz, which gathers at the outer part of the spiral. This is carried out for each of the sand designations. The collected rejected heavy mineral rich sand is designated S 40/45 CF.



Figure 3.10. Set of four sorting spirals.



Figure 3.11. Inside of spirals showing separation outlets.

3.1.7 Froth flotation

The above processes produce sand with a purity of usually >95% silica, and >99% in the coarser granulometries. Certain industries, however, require not only a very high percentage of silica, but a very low percentage of other contaminants. This is achieved by flotation, which is applied to the granulometry classification S 40/45 (average grain size of 303 - 250 μm). This designation results in granulometries which are advantageous to various industries for their intended purpose (Moura & Velho, 2012, European Commission, 2014).

There are two lines which operate independently, having their own feeding conveyors, rejected outputs, and product collectors. The purpose of these two lines is to continue production if one fails or does not produce product of sufficient quality.

The previous processes use difference in density to sort out the heavy minerals. Froth flotation uses the difference in the surface properties of the minerals to sort them (Noronha, 2010). Froth flotation is a physical-chemical process where chemical reagents attach to minerals and provide them artificial buoyancy. The reagent adheres to minerals with particular surface characteristics, and, as it is water repellent, causes it to rise to the surface as a froth. As the desired material sinks while the contaminants float, this technique is known as reverse froth flotation (Figure 3.12).

At Sifucel, the reagents attach themselves to the heavy mineral contaminants, making them water repellent. Bubbles released at the bottom of the tank attach to water repellent particles and encourage them to rise to the surface. Here they are scraped off the surface by blades and removed (Figure 3.13). The quartz, not being water repellent, remains in suspension. This, now containing a higher concentration of silica with the removal of the water repellent contaminants, is removed as concentrate.

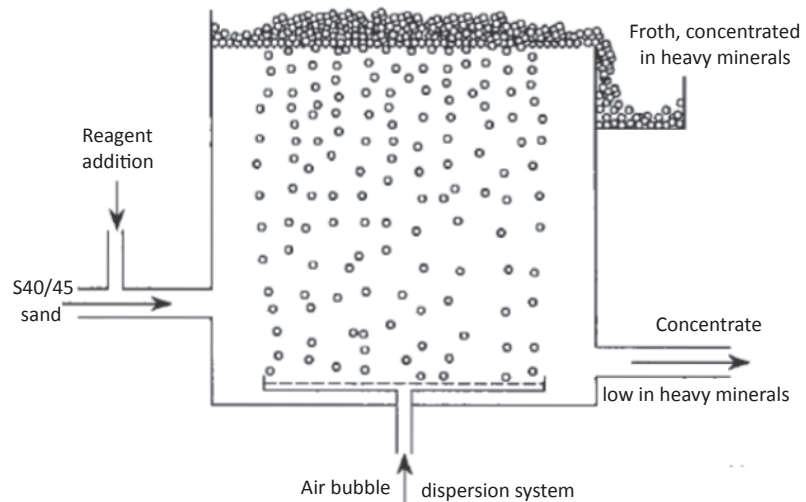


Figure 3.12. Diagram of froth flotation, modified from Michaud (2013).

3.1.8. Stock

The vibrating screen process allows the sand to be separated into different grades according to size. These are then stored as separate batches to be sold (Table 3.1). Each type is assigned a classification based on the average fineness index (American Foundrymen’s Association, A.F.A., Figure 3.14).


Due to the way values are



Figure 3.13. Rejected material concentrated in heavy minerals.

3. Extraction methods and refinement of the Rio Maior sand

Table 3.1. Types of sands produced and sold by Sifucel.

Granulometry / Grain fineness number	Sand designation	Average grain size (µm)
More coarse / smaller number	S 30/40	428 - 303
	S 40	303
	S 40/45	303 - 250
	S 50	227
	S 55/60	203 - 180
	S 90/100	115 - 109
More fine / larger number		

$$\text{Grain fineness number} = \frac{\sum (\text{Retained in sieve} \times \text{Multiplication factor})}{\sum \text{Retained in sieve}}$$

Sieves (µm)	>1000	>710	>500	>355	>250	>180	>125	>90	>63	<63
Multiplication factor	9	15	25	35	45	60	81	118	164	275

Figure 3.14. Grain fineness calculation from Brown (1936).

calculated, the range of sizes in a sample can be considerable. In all cases, Sifucel set limits for the variance in each designation. For S 40/45, there are two products, type 1 (T1) and type 2 (T2). These have the same average grain size, however, type 1 contains a greater range of grain sizes than type 2.

After a grade of sand has been separated, it is then transported by conveyor belt to be stored in a pile of wet sand. A portion of this wet sand is transported into the drying facility (Figures 3.15, 3.16) by loaders and fed into the dryer by conveyor belt. This is then stored in silos (Figures 3.17, 3.18), some to be packed in 'big bags' or packages (whichever form the customer requires).

One of the products produced by Sifucel is silica powder. The sand is fed from the drier into grinders, which breaks the sand down into a powder. This powder is then stored in a silo.

The material stored in silos can be poured into trucks to be transported to their final destination. Parapedra owns a road haulage company, Calcitrans (Soc. Transportes Rodoviários, Lda.), which owns its own fleet of large transport vehicles. This company is the main transporter of Parapedra's product for domestic consumption. Some of the sand is stored in big bags or in packages (Figures 3.19, 3.20), which are preferable for transporting in shipping containers to be transported to other parts of the world.

White Sands of Rio Maior



Figure 3.15. Inside the drying and packing centre.



Figure 3.16. Revolving dryer.



Figure 3.17. Storage silos.



Figure 3.18. Underneath storage silos with outlets labelled with the product.



Figure 3.19. Sifucel 'big bags'.



Figure 3.20. Sifucel packages.

3.2. Quality control

Most Sifucel products are certified with CE markings, and therefore must comply with ISO 9001:2015 standards. To ensure this, Sifucel has an inspection and testing plan for each product. The inspection and testing evaluates the physical and chemical properties of the sand. These tests are carried out in the Sifucel laboratory, daily at least for flotation feed and product, weekly for general product. Flotation products are also sent to an external laboratory for additional testing. Other tests may also be carried out at the request of the customer.

3.2.1. Internal control

In Sifucel, the sand, silica powder, and kaolin are controlled with a standard series of tests. These are listed below, although can be amended to suit the customer's requirements.

Sand

- Dry granulometric analysis
- Fineness index calculation (AFA)
- X-ray fluorescence chemical analysis
- Determination of heavy mineral percentage

Silica powder

- Wet granulometric analysis
- Whiteness index
- Particle count analysis
- Moisture determination

Kaolin

- Wet granulometric analysis
- Moisture determination

a) Dry granulometric analysis is carried out in the laboratory located near the drying and packing facility. It involved feeding the material into a series of sieves, which are shaken by a machine (Figure 3.21). The proportions of material which remains in each sieve is used to assess the granulometry of the sand.

This method is also used in association with average fineness index to confirm the grain classification.

b) X-ray fluorescence (XRF) is a technique used to analyse the chemical composition of a sample. While it does not reveal mineralogy, it is useful for the determination of elements with a high degree of accuracy, able to detect even trace amounts of molecules which might have an effect on the product (such as iron oxides).

This analysis is carried out in the main laboratory on the Sifucel premises (Figure 3.22). The sample is turned into a silica powder using a marble crusher. The resulting powder is added to polyvinyl alcohol to act as a binder. The two are mixed using a mortar and pestle until a fine powder is produced. This powder is poured into a mould and compressed. The disc produced is cleaned of excess dust with compressed air and analysed by XRF in the Malvern Panalytical Zetium machine (Figure 3.23).



Figure 3.21. Sieves used for dry granulometric analysis.



Figure 3.22. Preparation area for chemical analysis discs.

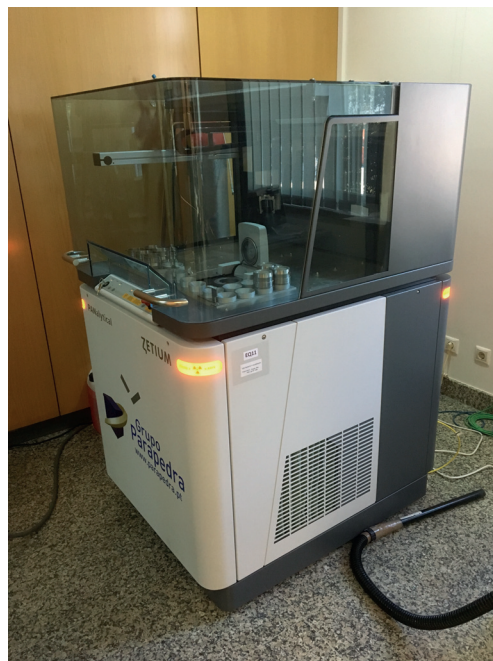


Figure 3.23. Malvern Panalytical Zetium machine.

3. Extraction methods and refinement of the Rio Maior sand

XRF operates using photoelectric absorption. An X-ray beam with known energy and wavelength is emitted at the sample. The chemical elements present in the sample are excited by the beam and emit fluorescent radiation which is picked up by the detector. By measuring the intensity of the radiation emitted, the chemical composition of the sample can be determined.

There are numerous types of analysis which can be carried out by the XRF machine, which vary in precision and range. All of the calibrations used in this work presuppose a silica sand composition, identifying inconclusive material within a certain range as being part of the silica composition. One calibration measures the amount of SiO_2 , Al_2O_3 , TiO_2 , K_2O , Fe_2O_3 , MgO , Na_2O , CaO , and P_2O_5 within the sample. This is a standard calibration analysis called AREIA (used in Tables 4.4 and 4.7). Another calibration also measures Bi_2O_3 , Cd_2O_3 , CeO_2 , Cl , Cr_2O_3 , Ga_2O_3 , HfO_2 , La_2O_3 , MnO , Nb_2O_5 , NiO , PbO , PtO_2 , Rb_2O , SnO_2 , SO_3 , SrO , ThO_2 , Y_2O_3 , ZnO , and ZrO_2 . This calibration is called OMNIAN, more thorough, and takes more time so is only used when a diverse range of contaminants is expected (used in Tables 4.6 and 6.1).

c) To determine the effectiveness of flotation on the removal of heavy minerals from the sand, all flotation samples receive additional analysis. At the end of the day, all flotation samples are collected from the onsite laboratory and transported to an offsite laboratory for density separation and mineralogical analysis through X-ray diffraction.

The density separation method isolates the silica sand from heavy minerals. Due to the toxic nature of the substances used, the process must be carried out in a fume cupboard and protective equipment worn.

The process involves dried sand placed inside a decantation flask containing bromoform (CHBr_3). The bromoform has a density of 2.89 g/cm^3 , greater than that of SiO_2 (2.65 g/cm^3 , Nichols, 1999), causing the silica to float and the heavier minerals to sink, accumulating at the bottom of the flask. These are collected into filter paper, dried, and weighed. This allows the weight percentage of heavy minerals in the sand to be determined.

X-ray diffraction (XRD) is a technique used to identify and quantify the minerals collected from the sample. It works using the the diffraction of X-rays by a mineral crystal's structure for identification.

A monochromatic X-ray beam of known wavelength is emitted at the sample. The beam strikes the crystal lattice and is diffracted. By varying the angle at which the beam strikes the sample, and measuring the diffraction angles and intensities, patterns can be identified. Different angles and intensities (diffractograms) allow for the identification of minerals in the sample (Terroso, 2005, IMR Test Labs, 2019).

d) Wet granulometric analysis is run with the silica powder in suspension in water and also provides a particle count analysis. A small measure of powder is placed into the Sample

White Sands of Rio Maior

Dispersion Unit and is fed into the Optical Bench of the Mastersizer 3000 machine (Figure 3.24). This uses laser diffraction to quantify the size of the particles. Beams of red and blue light are diffracted off the grains from several angles. Measuring the diffractions allow the granulometry to be calculated.

e) The whiteness index is a measure of the colour of the silica powder. It is measured with the use of a colorimeter (Figure 3.25).



Figure 3.24. Mastersizer 3000 machine.



Figure 3.25. Colorimeter.

f) Calculating the moisture content of sand which has not been through the drying process is important to determine the exact weight of product being transported. This is used in the case of the transportation of loose sand and is carried out after a transporting vehicle has been weighed but before leaving the site. A moisture scale is used to calculate the weight percentage of water (Figure 3.26).

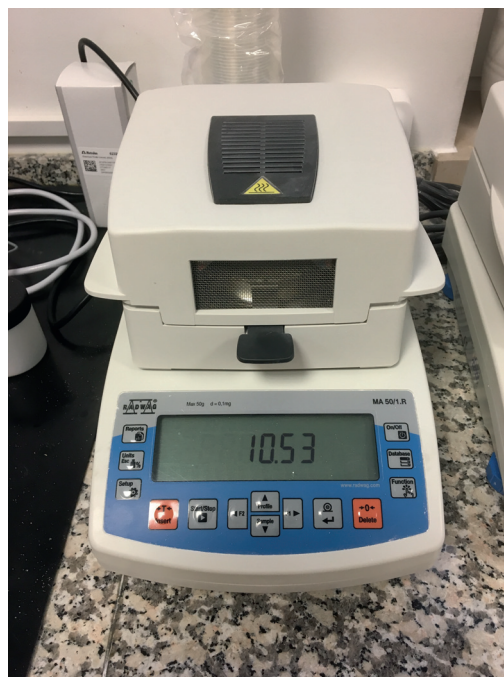


Figure 3.26. Moisture scale.

4. Composition of Sifucel sands

4. Composition of Sifucel sands

Through the various processing methods, a range of compositional differences emerge from the designations of sand. This is mainly due to the granulometry of the contaminants.

4.1. Granulometric analysis

The following are the results of granulometric analyses using sieves. Non-flotation samples have an expected range for each mesh. If a reading is outside the expected range, it is highlighted and corrective procedures are implemented. The sieve matrix used can vary with the designation and expected ranges. Below are examples of granulometric analysis:

Table 4.1. Granulometric compositions of S40/45 sand types 1 and 2 and flotation sand (FL). Type 1 feeds line 1 and type 2 feeds line 2. The samples were collected at 16h on 27/02/2019.

Sample	>0.425 mm	>0.16 mm	<0.16 mm
S40/45 T1	76.34%	23.66%	0
S40/45 T2	13.66%	86.21%	0.13%
S40/45 FL L1	8.75%	90.29%	0.96%
S40/45 FL L2	11.61%	87.95%	0.44%

Table 4.2. Granulometric compositions of S30/40 sand. The sample was collected at 16h on 27/02/2019.

	>0.25 mm	<0.25 mm
S30/40	99.69%	0.31%

Table 4.3. Granulometric compositions of S55/60 sand. The sample was collected at 16h on 27/02/2019.

	>0.4 mm	>0.315 mm	<0.315 mm
S55/60	3.46%	24.07%	72.47%

4.2. Chemical composition

The following are sand samples analysed using the above technique for chemical analysis. Samples were collected and tested on site at Sifucel.

4.2.1. Non-flotation sand designations

Table 4.4. shows the chemical composition of the sands produced by Sifucel that have not gone through the flotation process. The construction sand is the most contaminated as it has not undergone any sorting apart from washing during its extraction. The highest level of contamination of processed sand is of the S90/100 designation (Figures 4.1, 4.2). This is due to the high proportion of fine contaminated minerals in the deposit, which concentrate in this fine grade of sand (Carvalho & Pereira, 1973).

Table 4.4. Chemical compositions of various sands produced by Sifucel. All samples were measured using the AREIRA calibration (3.2.1(b)). SiO₂ values are estimated. The construction sand was measured at 14h on 01/11/2018, while the other samples were collected at 16h on 27/02/2019.

Molecule	Construction sand	S40	S30/40	S40/45	S55/60	S90/100
SiO ₂	95.17%	99.54%	99.58%	99.69%	99.51%	97.25%
Al ₂ O ₃	3.88%	0.19%	0.16%	0.08%	0.2%	1.12%
TiO ₂	0.29%	0.021%	0.014%	0.007%	0.033%	0.78%
MgO	0.098%	0.01%	0.01%	-	0.01%	0.02%
Fe ₂ O ₃	0.36%	0.03%	0.032%	0.011%	0.026%	0.26%
K ₂ O	0.12%	0.005%	0.001%	0.001%	0.011%	0.32%
P ₂ O ₅	0.014%	0.001%	0.001%	0.001%	0.001%	0.001%
CaO	0.019%	-	-	-	-	0.01%
Na ₂ O	-	-	-	-	-	0.03%

Among the various applications of sand which Sifucel supplies, the most demanding in terms of chemical composition is glass production. According to Moura and Velho (2012), S40 (Figures 4.3, 4.4), S30/40 (Figures 4.5, 4.6), S40/45 (Figures 4.7, 4.8), and S55/60 all possess the expected chemical requirements for the production of glass for containers and

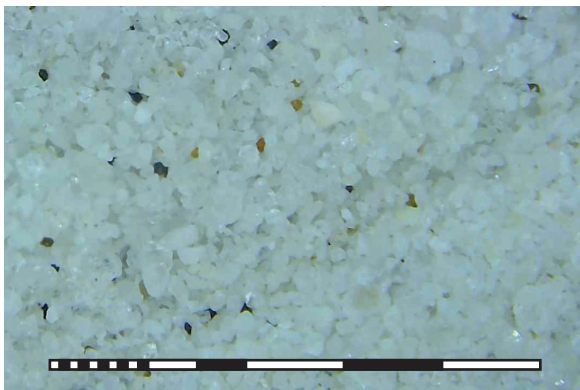


Figure 4.1. S90/100 sand. Scale is 5 mm.

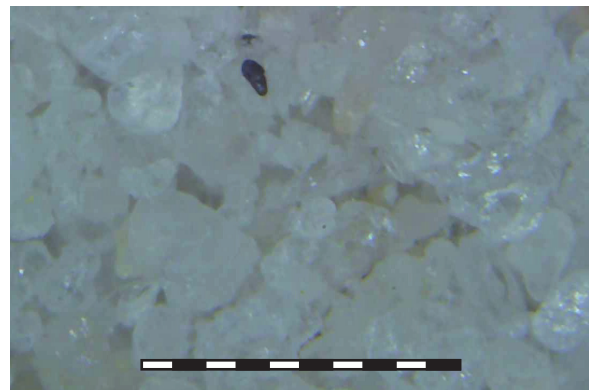


Figure 4.2. S90/100 sand. Scale is 1 mm.

4. Composition of Sifucel sands



Figure 4.3. S40 sand. Scale is 5 mm.

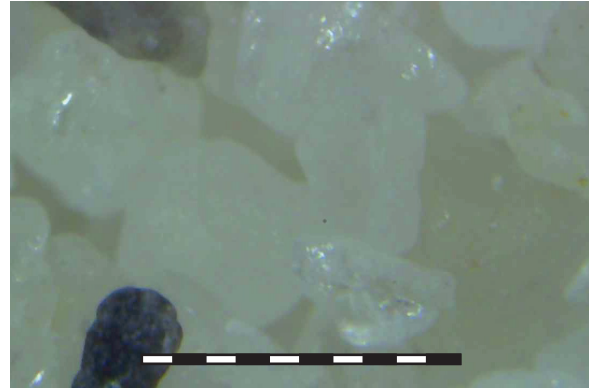


Figure 4.4. S40 sand. Scale is 1 mm.

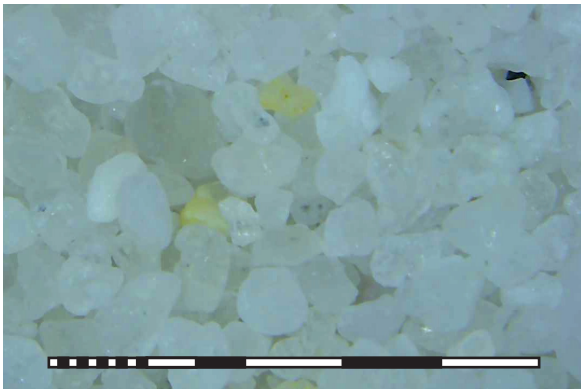


Figure 4.5. S30/40 sand. Scale is 5 mm.

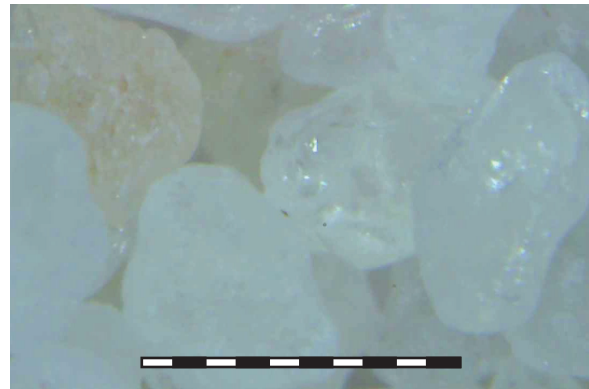


Figure 4.6. S30/40 sand. Scale is 1 mm.

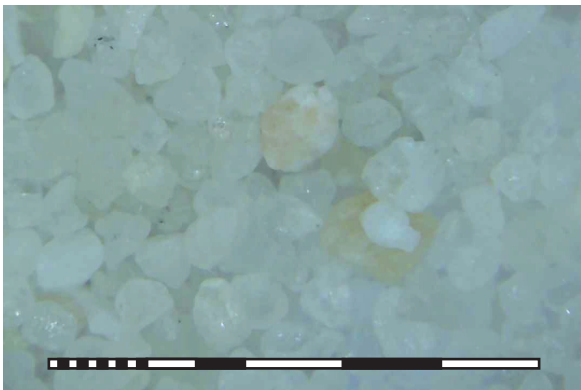


Figure 4.7. S40/45 sand. Scale is 5 mm.

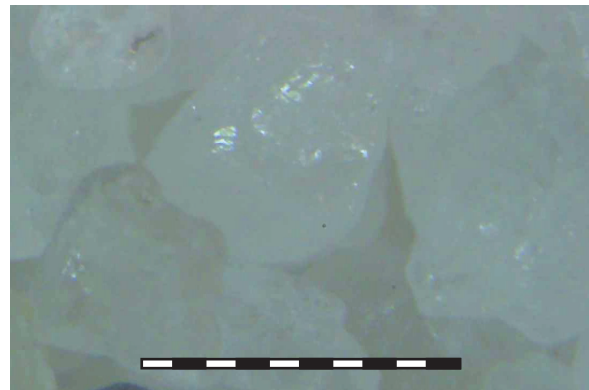


Figure 4.8. S40/45 sand. Scale is 1 mm.

packaging. Only S40/45 possesses the important $<0.013\%$ of Fe_2O_3 required for colourless glass, and none that contain the $<0.01\%$ which is desirable for clear glass (Table 4.5).

Table 4.5. Typical chemical composition of sand for clear glass (Moura & Velho, 2012).

Molecule	Typical results of sand for glass.
SiO_2	99.45%
Al_2O_3	0.30%
TiO_2	0.07%
$\text{MgO} + \text{CaO}$	0.01%
Fe_2O_3	0.01%
$\text{K}_2\text{O} + \text{Na}_2\text{O}$	0.06%

4.2.2. Chemical composition of rejected sand

The chemical composition of the sand rejected from the refinement process (S40/45 CF, Figures 4.9, 4.10) and from the flotation process (Line 1 rejected and Line 2 rejected, Figures 4.11 to 4.14) are sold for various purposes. The comprehensive chemical analysis can be seen in Table 4.6.

While the general process removes a significant amount of iron, titanium makes up the majority of the contaminating elements removed. This is due to the dense nature of titanium and its mineral rutile (Klein & Hurlbut, 1985). The rejected samples from the flotation

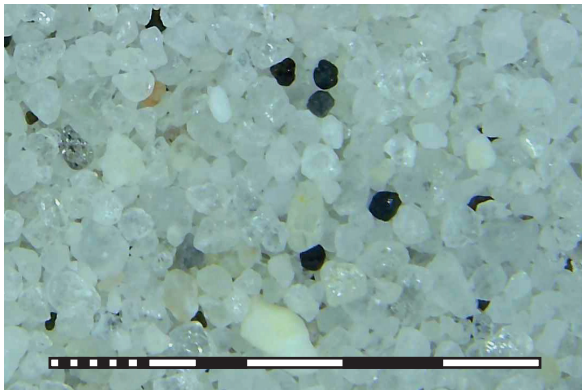


Figure 4.9. S40/45 CF sand. Scale is 5 mm.

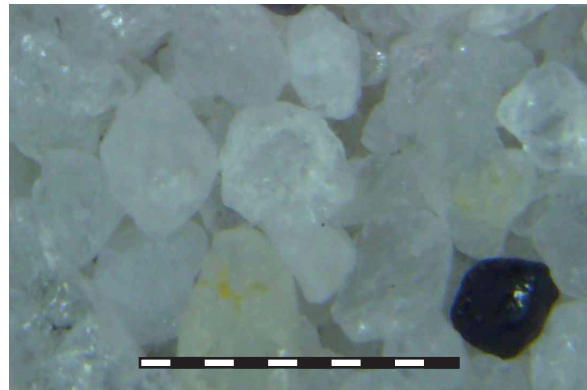


Figure 4.10. S40/45 CF sand. Scale is 1 mm.

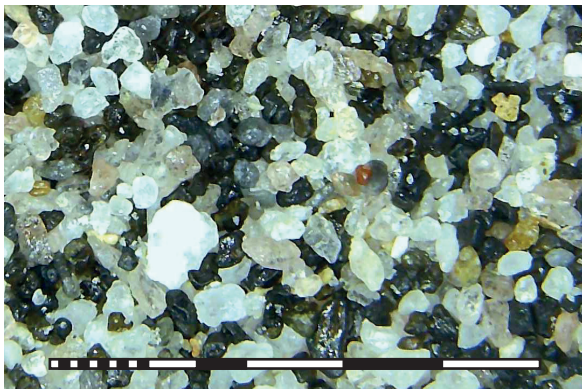


Figure 4.11. Line 1 rejected sand. Scale is 5 mm.



Figure 4.12. Line 1 rejected sand. Scale is 1 mm.



Figure 4.13. Line 2 rejected sand. Scale is 5 mm.



Figure 4.14. Line 2 rejected sand. Scale is 1 mm.

4. Composition of Sifucel sands

Table 4.6. Chemical compositions of construction sand, material rejected by hydraulic separation (S40/45 CF), and material rejected by flotation (Line 1 & Line 2 rejected). All samples were measured using the OMNIAN calibration (3.2.1(b)). SiO₂ values are estimated. The construction sand was measured at 14h on 01/11/2018, while the other samples were collected at 16h on 27/02/2019.

Molecule	Construction sand	S40/45 CF	Line 1 rejected	Line 2 rejected
SiO ₂	95.17%	94.26%	64.71%	87.99%
Al ₂ O ₃	3.88%	1.53%	25.52%	8.35%
TiO ₂	0.29%	2.36%	2.4%	0.94%
MgO	0.098%	0.096%	1.1%	0.37%
Fe ₂ O ₃	0.36%	1.15%	5.12%	1.82%
K ₂ O	0.12%	0.048%	0.12%	0.086%
P ₂ O ₅	0.014%	0.021%	0.04%	0.018%
CaO	0.019%	0.016%	0.18%	0.11%
Na ₂ O	-	0.043%	0.55%	0.17%
CeO ₂	-	0.032%	-	-
Cr ₂ O ₃	-	0.024%	0.009%	-
Ga ₂ O ₃	-	-	0.008%	0.002%
HfO ₂	-	0.007%	-	-
MnO	-	0.054%	0.088%	0.032%
Nb ₂ O ₅	-	0.007%	0.004%	0.002%
NiO	-	0.005%	-	0.006%
PbO	-	0.003%	0.007%	-
Rb ₂ O	0.001%	-	-	-
SnO ₂	-	0.015%	-	-
SO ₃	0.009%	-	0.035%	0.016%
SrO	0.001%	-	0.008%	0.003%
ThO ₂	-	0.004%	-	-
Y ₂ O ₃	0.003%	0.008%	0.005%	0.004%
ZnO	-	0.005%	0.039%	0.013%
ZrO ₂	0.043%	0.31%	0.065%	0.064%

process show that the technique successfully removes a significant amount of iron, but the contaminating element which is removed the most is aluminium. This is not unexpected

considering the relatively high concentration of aluminium present in all sands produced by Sifucel.

A not insignificant amount of the rejected samples contain SiO_2 , while a proportion is due to unavoidable margins of error in the processes, the rest is probably due to the considerable silica content in contaminating minerals. While the construction sand analysis shows a lack of many elements such as manganese, these should not be considered as absent, but too low for them to be detectable by the analysis.

4.2.3. Chemical analysis of flotation sand

The two flotation lines operate independently and are regularly analysed to maintain the low amount of iron they contain. S40/45 FL sand (Figures 4.15 to 4.18) has an extremely high level of purity, fulfils all the typical chemical expectations for clear glass production (Table 4.7), and has a sufficiently low percentage of iron that it can be used for high quality glass including optics (<0.008%, Moura & Velho, 2012).



Figure 4.15. S40/45 FL Line 1 sand. Scale is 5 mm.

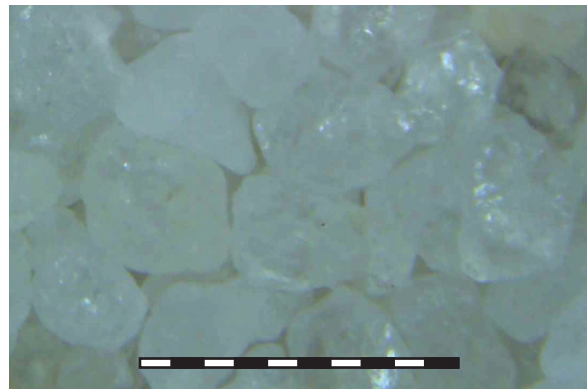


Figure 4.16. S40/45 FL Line 1 sand. Scale is 1 mm.



Figure 4.17. S40/45 FL Line 2 sand. Scale is 5 mm.

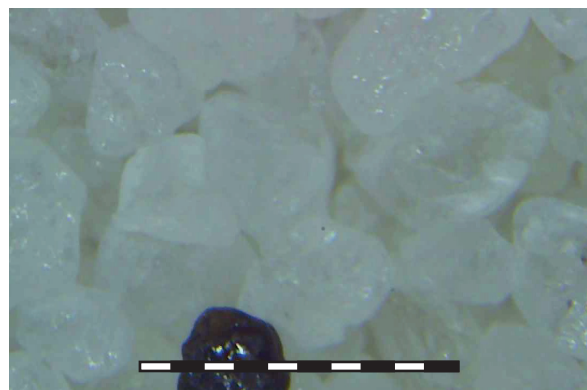


Figure 4.18. S40/45 FL Line 2 sand. Scale is 1 mm.

4. Composition of Sifucel sands

Table 4.7. Chemical compositions of sand entering flotation (Entrada) and leaving flotation (S40/45 FL). All sample were measured using the AREIA calibration (3.2.1(b)). SiO₂ values are estimated.

The samples were collected at 16h on 27/02/2019.

Molecule	Entrada Line 1	S40/45 FL Line 1	Entrada Line 2	S40/45 FL Line 2
SiO ₂	99.55%	99.63%	99.49%	99.67%
Al ₂ O ₃	0.18%	0.12%	0.23%	0.1%
TiO ₂	0.02%	0.014%	0.025%	0.014%
MgO	0.01%	0.01%	0.01%	-
Fe ₂ O ₃	0.024%	0.008%	0.035%	0.008%
K ₂ O	0.011%	0.016%	0.01%	0.008%
P ₂ O ₅	0.001%	0.001%	0.001%	0.001%
CaO	-	-	-	-
Na ₂ O	-	-	-	-

4.3. Mineralogical analysis

The following are the results of numerous analyses carried out on white sand from the Rio Maior area concerning its mineralogical make up.

The results show which minerals are present and that the vast majority of heavy minerals are small (<250µm). For Table 4.8, two slides were create from each size fraction to produce the range of percentages. The percentage of heavy minerals in Table 4.9 is a result of the density separation method described above.

Table 4.8. Approximate values for the percentage of heavy minerals in various granulometric fractions (Carvalho & Pereira, 1973).

	1000-500µm	500-250µm	250-125µm	125-62µm
Percentage of heavy minerals	-	0.1-0.5%	1-5%	4-12%

The minerals above were identified through QEMSCAN, and so cannot differentiate between minerals of the same chemical structure but different arrangement (Serpa, 2018). Minerals that were identified through X-Ray diffraction but not included above are:

- Anatase - TiO₂
- Goethite - FeO(OH)
- Siderite - FeCO₃
- Sillimanite - Al₂SiO₅

White Sands of Rio Maior

- Galena - PbS
- Opal - SiO₂ · nH₂O
- Magnetite-maghemite - Fe₂O₃
- Other phyllosilicates

This is from data collected by Dias (2015).

Table 4.9. Identification of minerals from different granulometric sizes of samples of S 40 designation (Serpa, 2018).

Minerals	Composition	S 40 250µm	S 40 125µm	S 40 63µm
Quartz	SiO ₂	99.52%	96.31%	85.67%
Tourmaline	(Ca,K,Na,_) (Al,Fe,Li,Mg,Mn) ₃ (Al,Cr,Fe,V) ₆ (BO ₃) ₃ (Si,Al,B) ₆ O ₁₈ (OH,F) ₄	0.00%	0.91%	0.64%
Andalusite	Al ₂ SiO ₅	0.00%	0.75%	1.12%
Haematite	Fe ₂ O ₃	0.00%	0.42%	4.68%
Staurolite	Fe ²⁺ ₂ Al ₉ O ₆ (SiO ₄) ₄ (O,OH) ₂	0.00%	0.12%	0.30%
Kaolinite	Al ₂ Si ₂ O ₅ (OH) ₄	0.03%	0.15%	0.24%
Feldspar	(K,Na,CaAl)AlSi ₃ O ₈	0.00%	0.17%	2.44%
Rutile	TiO ₂	0.00%	0.28%	2.17%
Zircon	ZrSiO ₄	0.00%	0.02%	1.06%
Quartz clay	SiO ₂	0.23%	0.60%	0.89%
Muscovite	KAl ₂ (AlSi ₃ O ₁₀)(F,OH) ₂	0.04%	0.05%	0.19%
Other clays	various	0.02%	0.04%	0.14%
Cr Spinel	(Mg,Fe)Cr ₂ O ₄	0.00%	0.01%	0.08%
Illite	(K,H ₃ O)(Al,Mg,Fe) ₂ (Si,Al) ₄ O ₁₀ [(OH) ₂ , (H ₂ O)]	0.01%	0.01%	0.08%
Monazite	(Ce,La)PO ₄	0.00%	0.00%	0.06%
Smectite	various	0.01%	0.03%	0.04%
Albite	NaAlSi ₃ O ₈	0.01%	0.01%	0.00%
Unidentified	n/a	0.01%	0.04%	0.12%

5. Geology and palaeoenvironment of the Rio Maior basin

5.1. Description of the Rio Maior basin

The Rio Maior basin occupies the SE end of Sheet 26D - Caldas da Rainha (Zbyszewski, 1960) and the NE end of Sheet 30B - Bombarral (Zbyszewski, 1966), both 1/50 000 scale. These studies, and subsequent analysis from Carvalho and Pereira (1973), identify this material as Plio-Pleistocene material topped by more recent deposits and alluvium. It is bordered to the north and north-east by Mesozoic material, and elsewhere by Miocene sedimentary deposits which extend to the southeast.

The basin is elongated in a NNW-SSE direction and measures 7.5 km long and 3 km wide. It is mostly made up of a thick layer of sand topped by generally alternating layers of diatomite and lignite (Carvalho & Pereira, 1973). These formations are sunk between two major faults which are orientated 40°NW. There is another fault orientation which confines the basin that is 30°NE, although Antunes *et al.* (1992) adds 50°NW also. Along the edges of the basin, in contact with the boundary faults, the sand is typically 20 to 60 m thick. This increases towards the centre, where the upper horizon is over 120 m below the surface and it extends to a depth of about 240 m (Carvalho & Pereira, 1973).

The diatomite and lignite make up the “lignite basin” along the same orientation of the Rio Maior basin, but only 3 km long and 1 km wide (Carvalho & Pereira, 1973, Flores, 1996). It lies above the deepest part of the basin, bordered by sand to the west and south, between Fonte da Bica and Azinheira. Here it forms a small asymmetrical syncline with the western sand layers dipping 10° to 15° towards the NE (Flores, 1996). On the eastern edge, a contact is created by the Cidral fault (Carvalho & Pereira, 1973) between the diatomite and lignite group and the Mesozoic limestone of the Extremadura massif.

The following is a summary of the formations present from top to bottom by Carvalho and Pereira (1973):

1. Recent coverage of sands with intercalations of clay and sub-rolled quartz-quartzite calcareous rocks. The group presents intense rubefaction.
2. Lignite and diatomite complex:
 - a) Thick layers of diatomite with sand and clay beds intercalations.
 - b) Main layer of lignite.
 - c) Dark diatomite, lignite, in alternating layers with lignites and levels of sand and clay.
3. Fine, well-sorted, slightly clayey, kaolinite, white and yellowish sand.

In Figure 5.1, Formation 1 is represented by Pleistocene deposits. Formations 2 and 3 are grouped into Plio-pleistocene deposits.

White Sands of Rio Maior

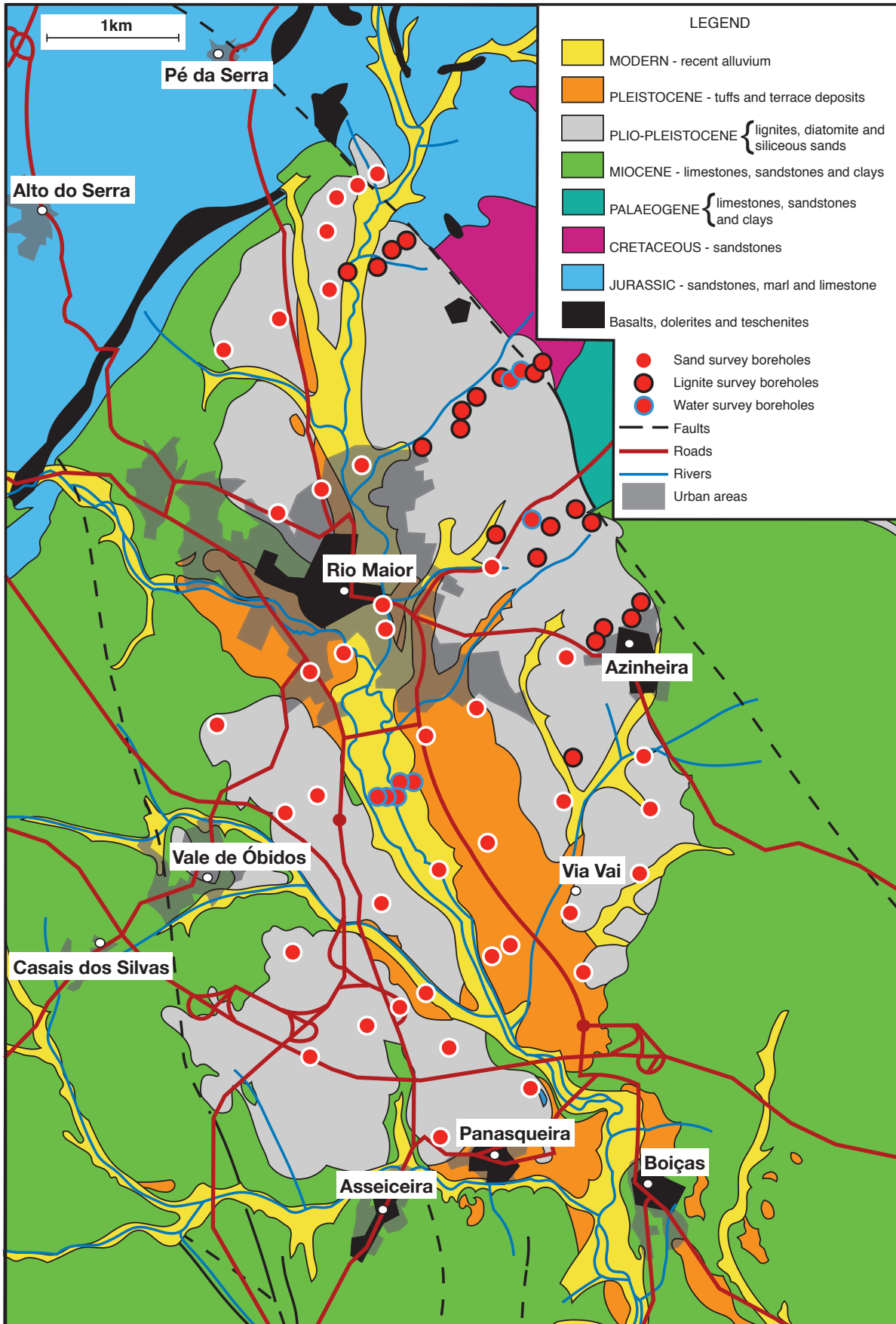


Figure 5.1. Geological map of the area of interest showing the location of relevant boreholes (modified from Zbyszewski & Almeida, 1960 and Carvalho & Pereira, 1973).

5.2. Previous studies

There have been multiple studies carried out on the Rio Maior basin, however, these have mostly been characterisations of the lignite basin of Rio Maior (Flores, 1996, LNEG, 2019). The first exploration surveys began in 1916 with the main objective to define the lignite deposit. This study corresponds with the boreholes carried out between 1916 and 1948 attributed to the SFM (Serviço de Fomento Mineiro) identified as F- and S- (Carvalho & Pereira, 1973, LNEG, 2019). Zbyszewski (1943) carried out one of the first detailed geological surveys of the area, characterising many features of the basin and the surrounding area using information from these boreholes (Zbyszewski & Almeida, 1960). More boreholes were created for water prospection in 1949 by Empresa de Sondagens e Fundações Teixeira Duarte, identified as A- and B- (Carvalho & Pereira, 1973, LNEG, 2019). In 1968, Sondagens e Fundações A. Cavaco, L.da. created five boreholes in the area focussing on lignite in ACF- holes and water in ACO- and ACB- holes (Carvalho & Pereira, 1973, LNEG, 2019). Carvalho and Pereira (1973) carried out an exhaustive study on the extent of the white sand deposits in the area. The boreholes carried out for this study in 1970 and 1971 (AF-) are the only ones in the area focussing on sand (LNEG, 2019). Later significant studies which rely on borehole data of the Rio Maior basin have used information from the Carvalho and Pereira (1973) study or the earlier boreholes (Zbyszewski, 1967, Flores, 1996, Vieira, 2009). Several boreholes have been created since, five in 1981 by Alfonso (1981), twenty by SFM between 1968 and 1976, and six by LNEG in 1991. All surveys were for prospection and focussed on the layers of lignite (LNEG, 2019).

Since, there have been numerous studies to more precisely characterise the lignites (Zbyszewski, 1967, Flores, 1987, LNEG, 2019) and identify the plants and diatoms (Silva, 1946, Diniz, 1984a, Pais, 1987). The main work to identify the pollen assemblages, date the basin, and determine climatic conditions was carried out by Diniz (1984b). This was the first important contribution to biostratigraphically characterising the Plio-Quaternary on the southern Europe Atlantic margin, and the locality has been used as a reference section for the Portuguese Pliocene since, due to its abundance of data (Vieira *et al.*, 2011).

Diniz (1984b) concluded that the Rio Maior deposits encompass the whole Pliocene based on correlation with synthetic pollen diagrams from northern Europe (Zagwijn, 1960) and the Mediterranean (Suc, 1984). This theory stated that the most basal parts of the Rio Maior basin are of Zanclean age and reach Gelasian at the top (Diniz, 1984b, Suc *et al.*, 1995, Fauquette *et al.*, 1999). The top being placed at the Piacenzian-Gelasian boundary was secure (Diniz & Mörner, 1995), however, the placement of the base was not. No representation could be found at the base of the succession for the Zanclean-Piacenzian marine incursion, casting doubt on the placement (Cunha *et al.*, 1993, Pais, 2012).

The most significant recent development regarding the Rio Maior basin was carried out by Vieira (2009). He studied the F98 borehole, which contains a record of almost the

entire sedimentary succession, and compared it to other studies. More information was recovered from the bottom of the core than previous studies, allowing Vieira (2009) to consider the succession being of Piacenzian age to Gelasian.

5.3. Geological history of the basin

Since the formation of the Rio Maior basin, it has been subject to multiple stages of tectonic disturbance and climatic change (Pais, 2012). These alterations can be seen in the facies around Rio Maior and correlated to other geological events in other parts of Portugal and Western Europe.

5.3.1. Mesozoic

Since the opening of the Atlantic ocean in the Triassic, Iberia had been moving eastward between the Eurasian and African plates. During much of the Mesozoic, this created an extensional regime, creating faults trending north-northeast (mainly N20°, Montenat *et al.*, 1988).

During the Late Triassic to the Lower Jurassic, a period of evaporite deposition left salt deposits around the area which is now the Rio Maior basin (Uphoff *et al.*, 2002, Calado & Brandão, 2009). From the Lower Jurassic, possibly as early as the Hettangian or lower Sinemurian (Montenat *et al.*, 1988), open-marine influences began to encroach on the Lusitanian Basin, and spread across it by the Middle Jurassic (Mouterde, 1971, Mouterde *et al.*, 1979), depositing the limestones which presently surround Rio Maior. With this sedimentation came halokinetic movements of the underlying evaporite deposits of Rio Maior along the nearby fault, at least as early as the Toarcian (Montenat *et al.*, 1988).

After the Late Cretaceous, a compressive regime replaced the extensional tectonic phase. This led to intense intraplate deformation with lithospheric folding (Cloetingh *et al.*, 2002, Tejero *et al.*, 2010) and the development of sedimentary basins (Pais, 2012). The maximum compression was along a N-S orientation (Vegas, 2006) which is seen now as NW-SE after the Late Miocene Iberian rotation (Ribeiro *et al.*, 1996, De Vicente *et al.*, 2008, Kullberg *et al.*, 2011).

The Rio Maior basin began to develop as part of the larger Lower Tejo basin at this point. The tectonic inversion encouraged salt withdrawal, extrusion, and welding, causing sagging and the creation of several new basins, including the Rio Maior basin (Terrinha *et al.*, 1996, Figure 5.2).

5. Geology and palaeoenvironment of the Rio Maior basin

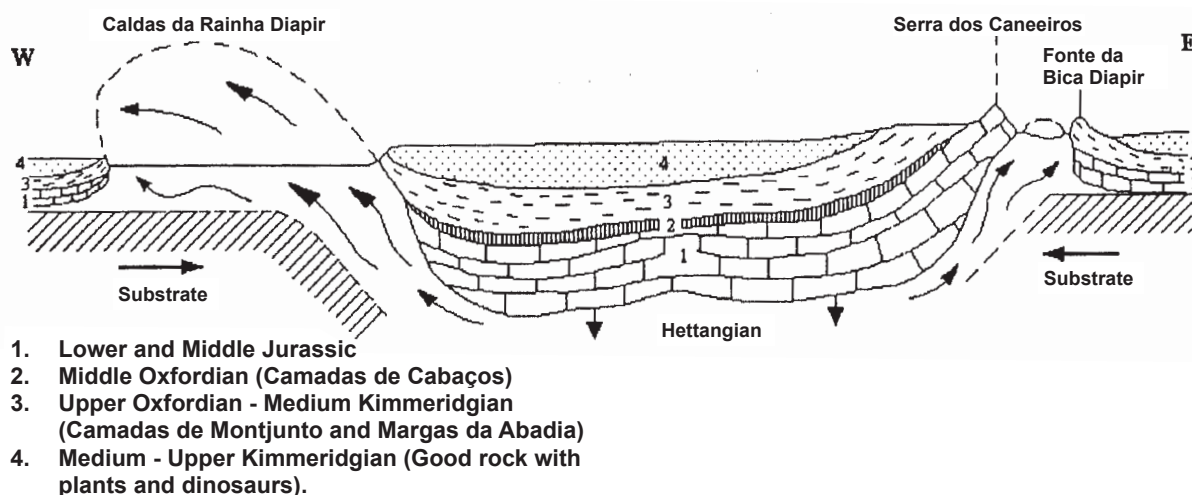


Figure 5.2. Diagram showing the position of the Caldas da Rainha and Fonte da Bica diapirs (modified from Zbyszewski, 1959).

5.3.2. Paleogene and Miocene

The Portuguese Cenozoic basins (Mondego, Lower Tejo, Guadiana, Alvalade, and Moura) began to be filled in the Middle Eocene with the erosion of the Hesperian Massif. This continued until the middle Tortonian (Pais, 2012).

The environment of much of the Paleogene was semi-arid to subtropical with a long dry season (Pais, 2012), but by the Aquitanian, tropical to subtropical plants dominate the Iberian record (Pais, 2010). It is also about this time that the Lower Tejo basin had given way to the Tagus basin. The deposits of this basin provides a rich geological and palaeontological record for much of the Miocene in the area around Rio Maior (Antunes & Pais, 1993).

The Aquitanian was a time of tropical conditions with coralline barrier reefs and a marine transgression reaching Almeirim (Antunes & Pais, 1993). During the Burdigalian, there was a regression, rising temperatures, and lower humidity (Pais, 2010) comparable to present day Guinea (Antunes & Pais, 1993). This was the case until about 19 Ma. with a marine transgression and a change to subtropical and temperate forms of vegetation. This grew wetter and hotter towards the end of the Burdigalian (Pais, 2010).

As the Burdigalian gave way to the Langhain, there were two brief oscillations of sea level (Antunes & Pais, 1993). Fossilised traumatic structures indicate that there were abrupt environmental changes also, although subtropical and temperate plants prevail (Pais, 2010).

There was an abrupt change in the Serravallian with wet tropical plants associated with aquatic and/or riverine types (Pais, 2010), probably indicative of the Serravallian transgression. This marine incursion spread marine influences past Santarém and further inland, before retreating in the Tortonian (Antunes & Pais, 1993).

During the Tortonian, there are indications of a temperate climate with contrasting seasons, very different to the climatic optimum of the upper Burdigalian and Langhain (Pais, 2010). This is the beginning of the Monterey Cooling Event which lasted into the lower

Pliocene (Jimenez-Moreno *et al.*, 2005). The contrasting seasons are due to a growing Atlantic rather than Mediterranean influence over the west coast of Iberia (Pais, 1986, Antunes & Pais, 1984, Antunes *et al.*, 1992). There is no plant data, and therefore no climatic data, from the Messinian (7.246 - 5.333 Ma.) in Portugal (Pais, 2010).

The average variation in temperature and humidity of the Iberian Peninsula through the majority of the Miocene can be seen in Figure 5.3 based on fossilised plant data (Pais, 2010).

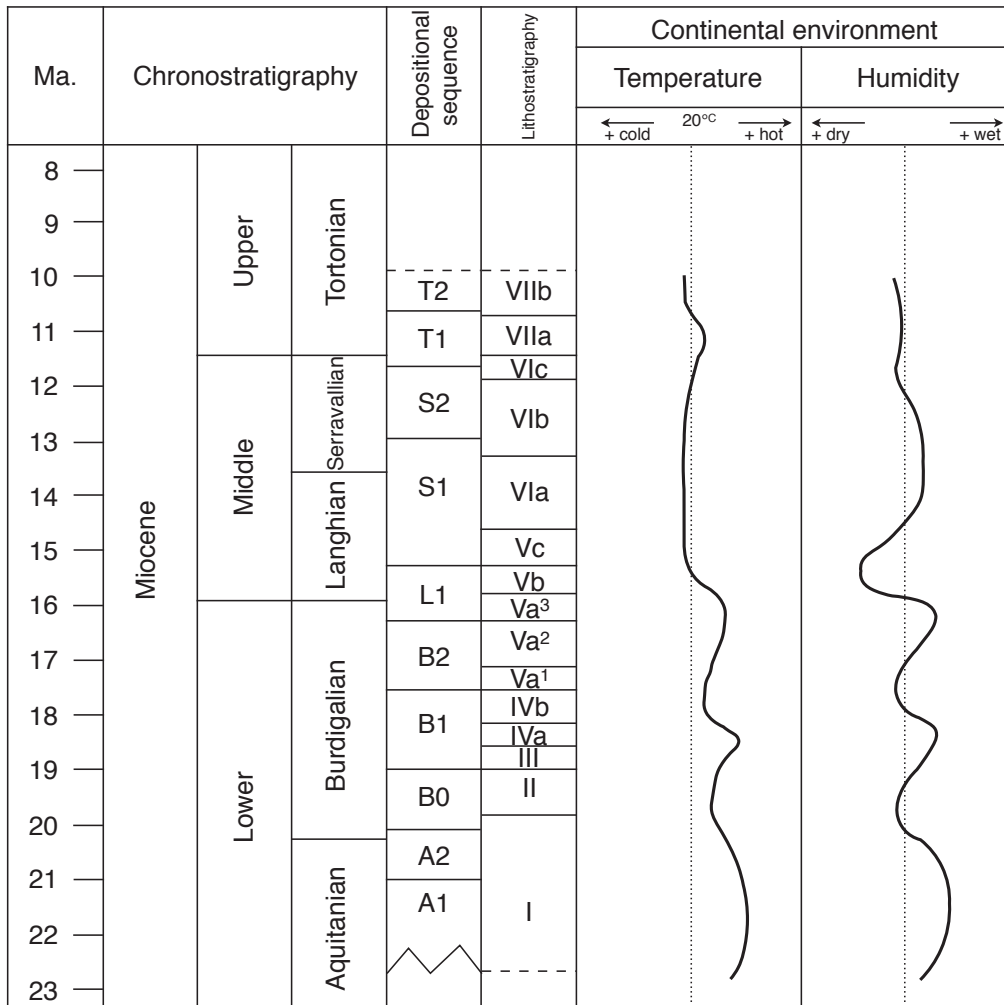


Figure 5.3. Mean variation of temperature and humidity in the Miocene of the Lower Tejo basin (modified from Pais, 2010, using data from Antunes & Pais, 1984, Antunes *et al.*, 2000).

5.3.3. Pliocene

The study by Vieira (2009) dated the lower deposits of the Rio Maior basin to the Piacenzian, leaving no deposits in Portugal of Zanclean age (Teixeira & Gonçalves, 1980, Ramos, 2008, Pais, 2012). The sands which make up the lower layer of the basin infilling have correlations to the sands of Coia (Setúbal), Roussa (Leiria-Pombal), Alhadas (F. Foz),

5. Geology and palaeoenvironment of the Rio Maior basin

and Agueira (Águeda) (Antunes & Pais, 1993, Barbosa, 1995), and have been ascribed to the Ulme Formation (Pais, 2012). The Ulme Formation are late Pliocene quartz-feldspathic sands. They are yellowish to reddish in colour and have a medium to coarse texture with a high amount of kaolinite and illite clay (Azevêdo, 1997, Barbosa, 1995, Barbosa & Reis, 1996).

There are indications that the Ulme Formation (particularly in Rio Maior) is evidence of a Piacenzian marine ingressión, one not as large as the Lower Pliocene, but with greater consequences for Portugal (Antunes & Pais, 1993). The sands in the Rio Maior basin are unusual for the Ulme Formation due to their high silica content and low granulometric distribution which classify them as special sands (Carvalho & Pereira, 1973, Pereira, 1991). This high degree of sorting and the rolled, unpolished nature of the quartz grains, indicate aeolian transport (Carvalho, 1968, Carvalho & Pereira, 1973). Carvalho (1968) proposed that these sands originated from the west, specifically the Aljubarrota platform. This was a vast sandy littoral abrasion platform that was 200m long (Antunes & Pais, 1993, Flores, 1996). The sand moved east through dune progression, passing between Serra de Candeeiros and Serra de Montejunto, encouraged by a marine transgression. Later studies confirmed this scenario (Magalhães & Carvalho, 1984). The Rio Maior basin has been interpreted as being a lacustrine environment based primarily on the conditions best suited to precede the overlying lignite complex (Carvalho & Pereira, 1973).

The lignite and diatomite complex located stratigraphically above the sand provides much more environmental data. The diatoms are not indicative of much, however, there is a coexistence of freshwater and saltwater species (Silva, 1946). Flores (1996) identified six distinct layers of lignite and carried out exhaustive geochemical analyses on each. There have also been numerous studies on pollen, which have led to a confident reconstruction of the environment (Vieira *et al.*, 2011). The first layers indicate a warm, humid climate with temperatures of around 20°C and annual precipitation between 1 300 and 2 000 mm (Diniz, 1984b, Vieira *et al.*, 2011). Vieira (2009) provides evidence of a diverse mixed forest, dominated by evergreen vegetation and some temperate elements. This is indicative of a moist, subtropical environment associated with swamps, similar to modern Southeast Asia and Florida (USA) (Vieira *et al.*, 2010) and is due to the proximity to the Atlantic ocean, while eastern Iberia experienced the spread of Mediterranean-type vegetation (Barrón *et al.*, 2010). The swamp environment explains the presence of mostly aquatic taxa (Diniz, 1984b) during a regression episode (Teixeira, 1973). The water table was always above the topographic surface of the basin, but varied in its height (Flores, 1996) as there was a move from a river dominated marshy swamp to a lagoon or upper deltaic forest swamp (Pais, 1989, Cunha *et al.*, 1993, Flores, 1996). This change can also be seen in the surrounding vegetation with progressive cooling becoming more intense (Lisiecki & Raymo, 2005) and paratropical elements being substituted by temperate species (Vieira, 2009). This change through the Pliocene can be seen in Figure 5.4 (Pais, 2010). There is evidence that the top

layers of lignite might have experienced saltwater influences. This is unclear, and it is not known whether a minor marine transgression or influence from the Fonte da Bica evaporites could be the cause (Flores, 1996).

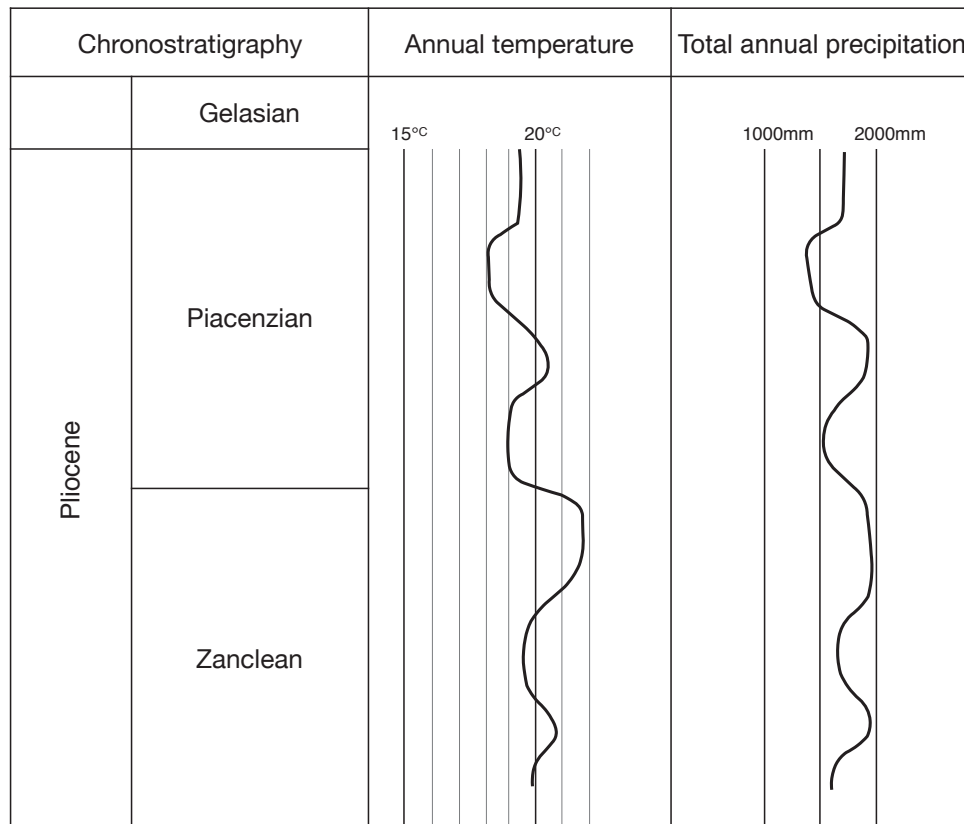


Figure 5.4. Mean variation of temperature and humidity in the Pliocene of the Rio Maior basin (modified from Pais, 2010, using data from Diniz, 1984, 2003).

Towards the end of the Piacenzian, there was an increase in fluvial energy, resulting in the deposition of the Almeirim Formation in the basin (Pais, 2012). This formation is made up of gravels, some channel structures, and illite clay dominating over kaolinite (Barbosa, 1995, Barra *et al.*, 2000), again indicative of a more temperate environment (Nichols, 1999). These deposits are from the upper most Piacenzian, passing into the Gelasian (Pais, 2012).

5.4. Utility

The geological and environmental history of a deposit are important considerations in analysing and interpreting data. Depositional models rely on this kind of information on which to build, giving the data context.

The faults interpreted by Carvalho and Pereira (1973) and used by Flores (1996) confine the Rio Maior depositional basin (Figure 5.5), and so attempts to extend sand data trends beyond these limits would be invalid. The work carried out by Carvalho (1968), and Magalhães and Carvalho (1984) confirm the sand's origin and therefore give context to

5. Geology and palaeoenvironment of the Rio Maior basin

changes in granulometry and chemical composition across the basin. Also, while not the case in this instance, the geological history could be important for interactions and features that are apart from the main area of interest, but could have a significant affect on it.

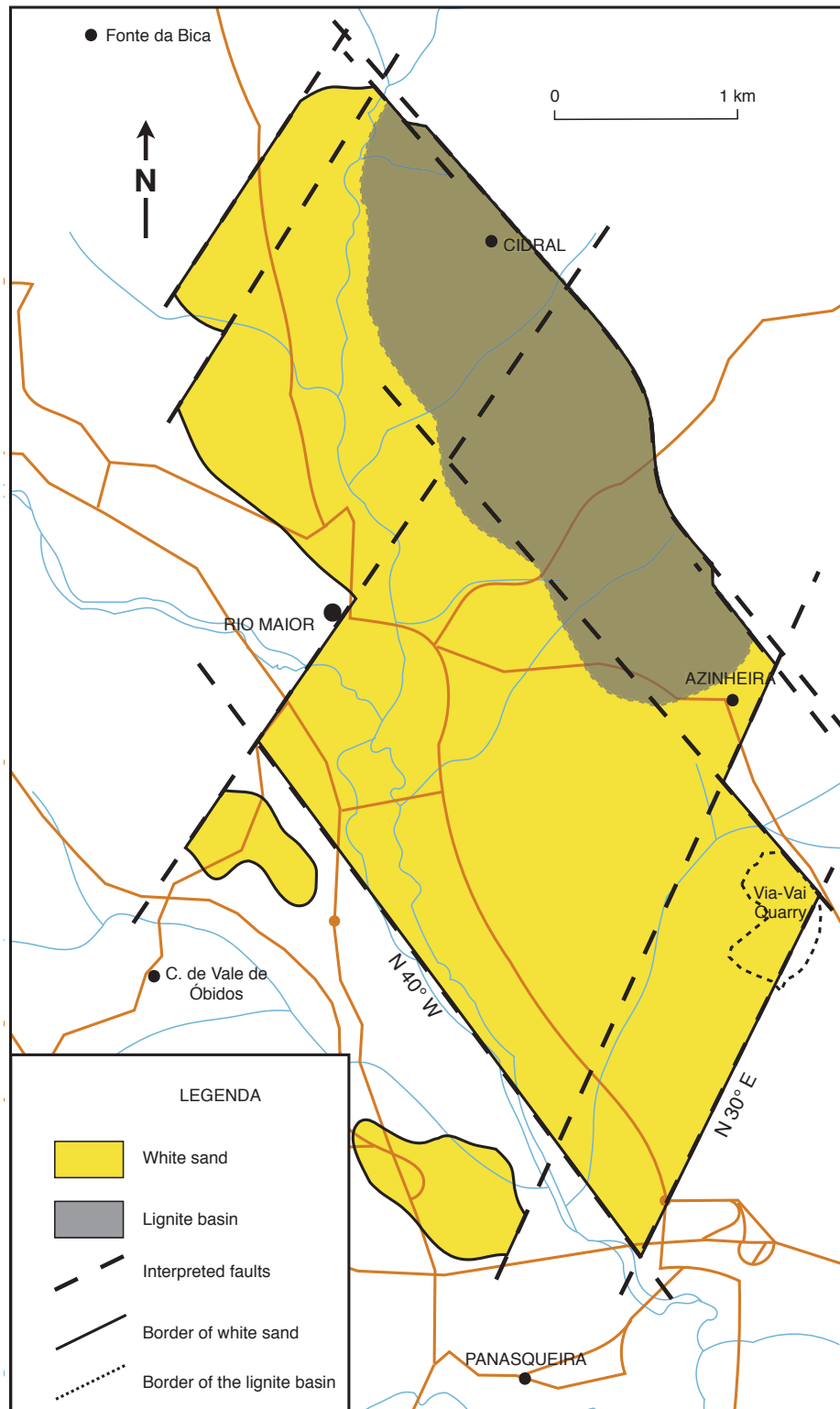


Figure 5.5. Map of the area showing the extent of the sand in the Rio Maior basin (modified from Carvalho & Pereira, 1973), the lignite basin (modified from Flores, 1996), and the location of the Via-Vai quarry.

6. Analysis of white sand and interpretation

6.1. Sand analysis

The following is an analysis of the white sand present in the Rio Maior basin. This is limited due to the sparse exposures of the deposit. Much of the work on the basin as a whole comes from the study of Carvalho and Pereira (1973). This was a thorough study with a consistent methodology, and as such, is used as the main source of data for granulometric and chemical analysis of the basin as a whole.

However, the Via-Vai quarry allows a portion of the deposit to be directly observed and features examined which are not easily identified from the cores used by previous surveys. During this study, visible features were described and samples taken to be analysed in the Sifucel laboratory. These samples are not compared directly to those analysed by Carvalho and Pereira (1973), due to differences in equipment and methodology, but are used to interpret features observed in the sand deposit.

6.1.1. Granulometry

The sand is well sorted (according to the parameters of Harrell, 1984) in all the samples examined from the Via-Vai quarry, with grains which are sub-rounded to sub angular with a medium to low sphericity (according to Pettijohn *et al.*, 1987). This agrees with the description of white sand in other parts of the basin carried out by Carvalho and Pereira (1973). That study used two different sieve matrices to determine the granulometric distributions, resulting in frequency curves A and B in Figure 6.1 (what same sieve matrices were used are shown on the x axes). The curves show a well sorted deposit with the greatest

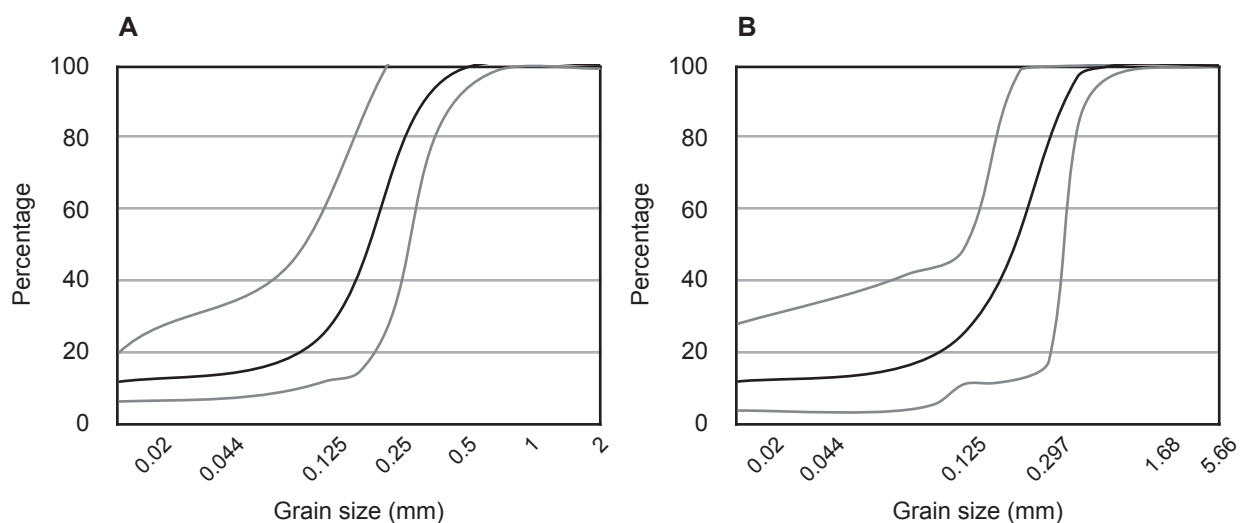


Figure 6.1. Cumulative frequency curves showing average, maximum, and minimum percentages for each grade measured. **A:** Sieve matrix from >2 to <0.02 mm. **B:** Sieve matrix from >5.66 to <0.02 mm.

6. Analysis of white sand and interpretation

variation towards fine granulometries (Pettijohn, 1975, Lewis & McConchie, 1994). This degree of sorting is usually an indication of aeolian or beach transport and distribution, the former being more likely due to the high percentage of fine grains. However, this may be different than the final depositional environment (Nichols, 1999).

Carvalho and Pereira (1973) also discovered a difference in roundness according to size: grains larger than 1 mm were rounded; grains between 1 and 0.5 mm were rounded to sub-rounded; and grains below 0.5 mm were sub-rounded to angular. This might be indicative of the larger grains having been transported further than the finer grains, or larger grains being of sufficient mass to affect their sphericity (Nichols, 1999).

The variation across the basin can be seen in Figure 6.2. In this, the average A.F.A. Fineness number has been calculated, with the average grain size ranging between 164 and

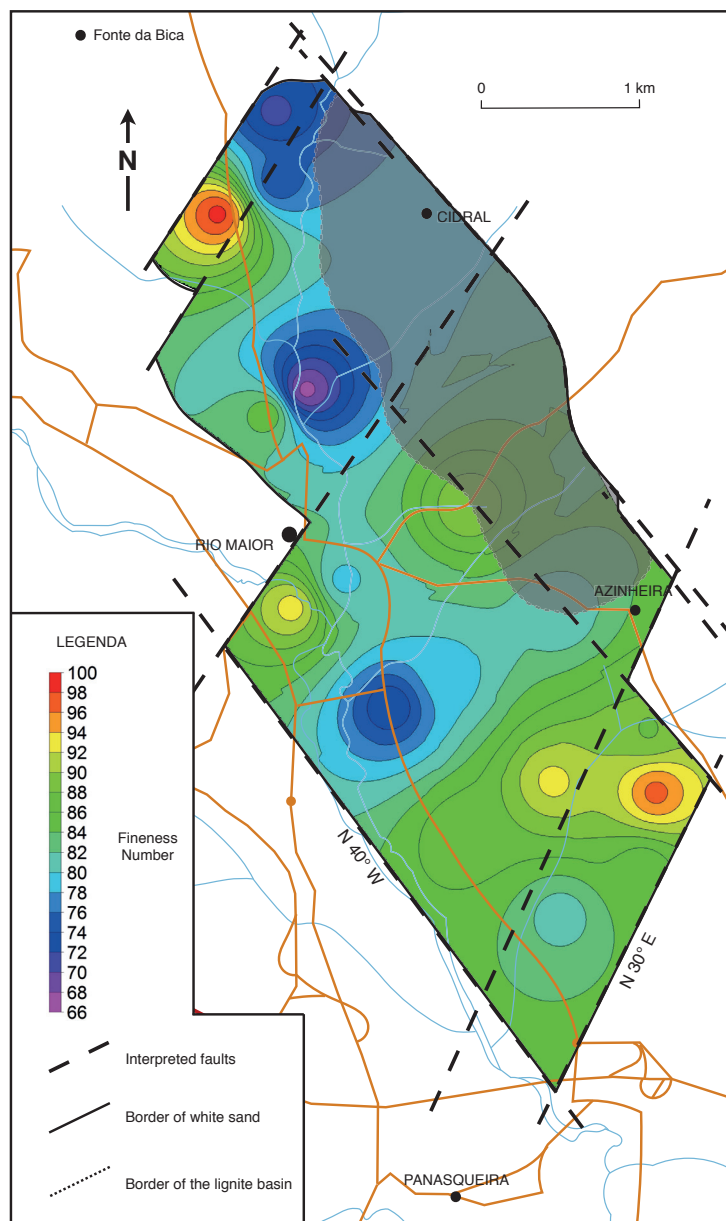


Figure 6.2. Average A.F.A. Fineness Number across basin. Map modified from Carvalho and Pereira (1973) data using RockWorks.

109 μm . While results from beneath the lignite basin are lacking, the main concentrations of the finest sand are in the northwest, the middle west, and the southeast. While the differences appear stark in Figure 6.2, the actual results show more conformity, grain size varying greatest in those areas with high average fineness numbers. The well sorted nature of the original sediment may obscure features that would be more obvious with a source of greater size variation, and the sampled depths may be too sparse to detect changes in depositional facies. However, there do seem to be some visible patterns.

There seems to be little circulation as there are marked differences between close points. This can sometimes occur with the rapid reduction of energy when a fluvial system meets a lacustrine environment. The coarser sand seems focused to areas north and west in the basin, with the coarsest sediment in the southern part having an average grain size of $<125\mu\text{m}$ (Fineness number of >80). This sand could be transported by wind across the basin, coarser and heavier sediment coming out of suspension over the northern and western areas of basin.

6.1.2. Chemistry

Being white special sand, the majority mineral is quartz, making up more than 91% of all samples tested. 97% of samples tested across the basin by Carvalho and Pereira (1973) are made up of over 95% quartz (Figure 6.3), classifying the material as a quartz arenite (Pettijohn, 1975). Other chemical signatures which are significant are, in order of average abundance: aluminium, potassium, titanium, iron, magnesium, and sodium (Carvalho and Pereira, 1973, also measure calcium, but there is only one occurrence outside samples of $<44\ \mu\text{m}$). Remaining Unidentified minerals are classified as 'other'. Below potassium, sodium, and calcium are grouped together as they are all associated with element-specific types of feldspar.

The samples chosen for chemical and mineralogical analysis by Carvalho and Pereira (1973) were sorted using a 325 mesh screen ($44\ \mu\text{m}$). The sandy residue retained by this screen was analysed chemically and mineralogically, the results of which are used to create the cumulative frequency curves below. The finer grains are of interest as they demonstrate relationships between chemical elements and minerals could indicate the mineralogical composition of samples. All analyses used from Carvalho and Pereira (1973) were carried out by Divisão de Química do Serviço de Formento Mineiro. All graphs below have an x axis of samples arranged in rising percentage order of the chemical oxide being discussed.

6.1.2.1. Silicon dioxide

In addition to quartz, there are many other minerals which are found among the Rio Maior sands which contain silicon: andalusite, staurolite, muscovite, feldspar, kaolinite,

6. Analysis of white sand and interpretation

sillimanite, zircon, and opal. There are also tourmaline and illite which may contain silicon. The <44 µm fraction analysed by Carvalho and Pereira (1973) shows a strong positive correlation between silicon and quartz, a negative correlation with kaolin, and little to no correlation with feldspar (the three most abundant silica minerals, Figure 6.4). The negative correlation to kaolin is probably due to aluminium increasing in proportion considering the strong correlation shown in Figure 6.6.

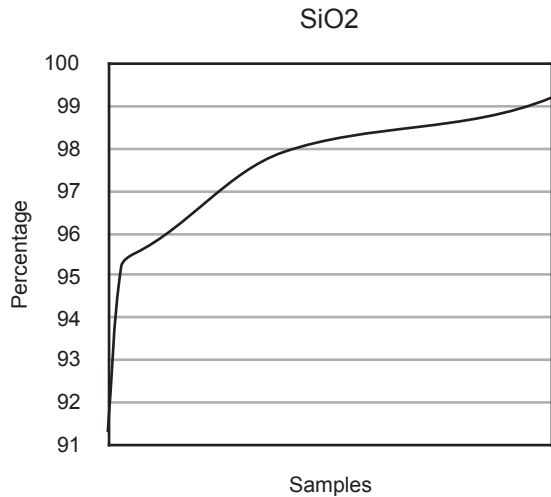


Figure 6.3. Cumulative frequency curve of SiO₂ (data from Carvalho & Pereira, 1973).

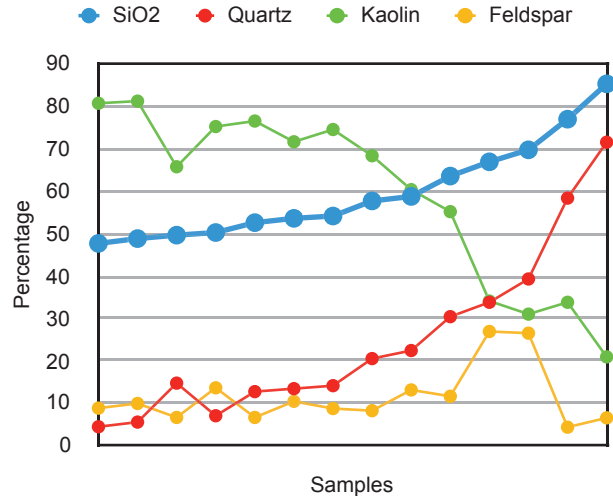


Figure 6.4. Concentrations in <44 µm fraction (data from Carvalho & Pereira, 1973).

In analysing the abundance of silicon dioxide across the basin (Figure 6.18), it should be noted that this does not demonstrate changes in the deposition of quartz grains, but the deposition of contaminants. Large areas of the basin are around 99% silica, with particularly high areas around the west and south east. The lowest areas are in the centre of the basin. The range of average values, however, is about 1.6%.

6.1.2.2. Aluminium oxide

The aluminium content is the most variable mineral in the Rio Maior sands, ranging from 0.22 to 3.14 %. The extent of the variation can be seen in the frequency curve of Figure 6.5 with a range of almost 3%. Aluminium is also the most abundant element apart from silicon in over 90% of samples tested. This is probably partly due to the wealth of minerals which can contain aluminium, but also because of the presence of kaolin in the sand. As Figure 6.6 shows, there is a marked correlation between the aluminium content in sediment smaller than 44 µm and that of kaolin. Discrepancies in this and the element's presence in coarser sand may be explained by the occurrence of, in general order of abundance: feldspar, tourmaline, andalusite, staurolite, muscovite, illite, and sillimanite (Carvalho & Pereira, 1973, Dias, 2015).

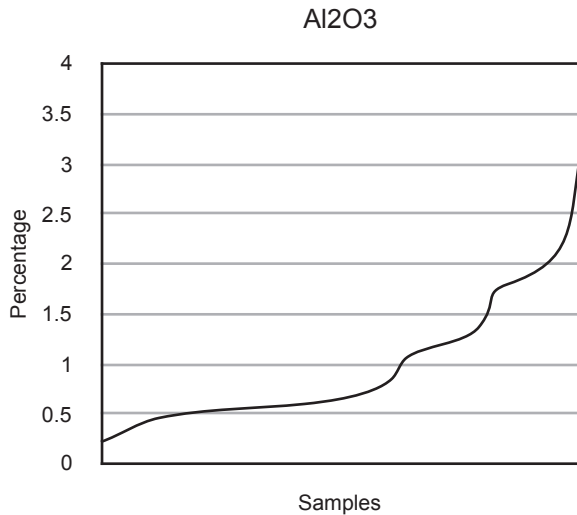


Figure 6.5. Cumulative frequency curve of Al_2O_3 (data from Carvalho & Pereira, 1973).

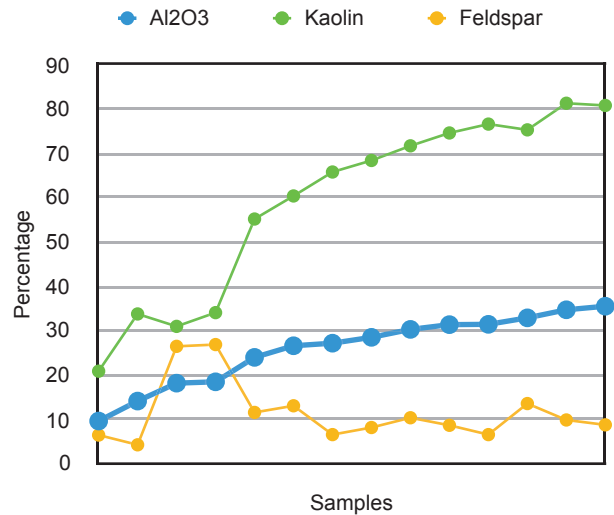


Figure 6.6. Concentrations in $<44 \mu\text{m}$ fraction (data from Carvalho & Pereira, 1973).

Aluminium oxide concentrations are high in the northern part of the basin and rise to their highest levels in the centre of the basin (Figure 6.19). Areas to the west, and particularly the south east, are where the aluminium content is low.

6.1.2.3. Potassium, sodium, and calcium oxides

Potassium, sodium, and calcium are present in the Rio Maior sands to different extents. Potassium is the most abundant with 74% of samples containing 0 to 0.33% of the element (Figure 6.7). Sodium is the most consistent with 97% of samples containing 0.05 to 0.15% of the element (Figure 6.9). Calcium is the least abundant element measured individually by Carvalho and Pereira (1973), with only 3% of the samples containing a measurable quantity (Figure 6.11). This rises to 43% when examining the $<44 \mu\text{m}$ fraction. It is also in this fraction that there is a correlation between these elements and minerals. While tourmaline can contain any of these three elements, and illite can contain potassium (both minerals present in the sands according to Dias, 2015) the fine fraction shows a distinct correlation to feldspars containing these elements (Figures 6.8, 6.10, 6.12). This indicates that a majority of these elements in $<44 \mu\text{m}$ fractions of the sand make up feldspar minerals. Potassium is associated with alkali feldspars, calcium with plagioclase feldspars, and sodium with both types (Bishop *et al.*, 1999). The small size of the feldspar minerals suggest heavy weathering and transport of the sediment, also indicated by 39 to 91% of the feldspar being potassium feldspar, the more durable variety (Nichols, 1999).

In general, both potassium and sodium oxides (the two molecules for which there is continuous distribution data) show a similar distribution throughout the basin (Figures 6.20, 6.21). Both show a significant concentration in the northern part of the basin, increasing to the highest levels in the centre of the basin. The southern area of the basin has the lowest

6. Analysis of white sand and interpretation

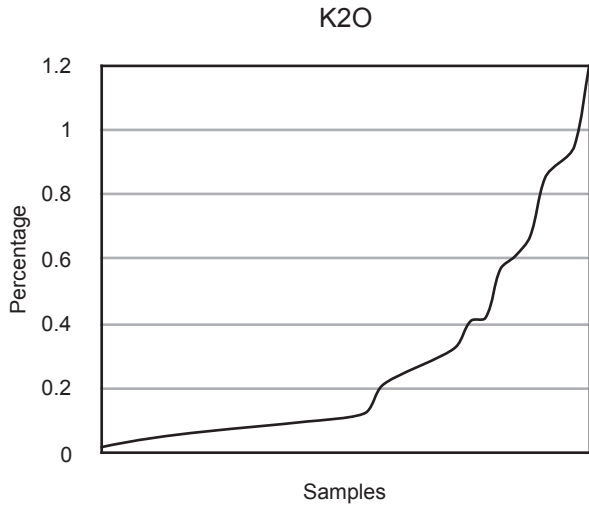


Figure 6.7. Cumulative frequency curve of K_2O (data from Carvalho & Pereira, 1973).

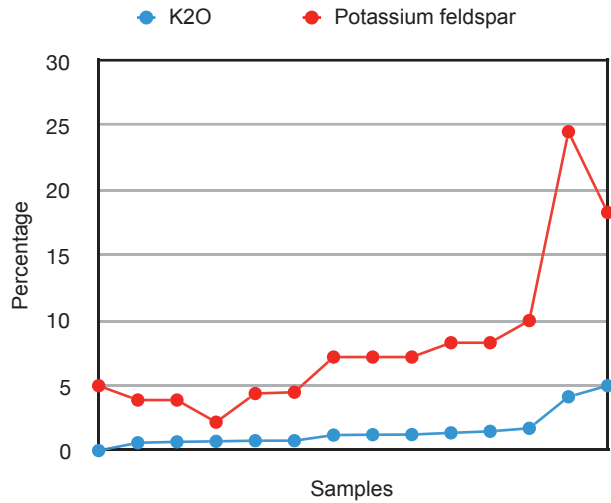


Figure 6.8. Concentrations in $<44 \mu m$ fraction (data from Carvalho & Pereira, 1973).

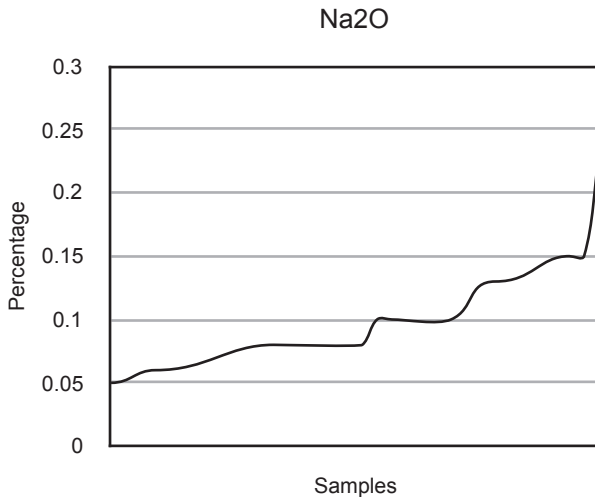


Figure 6.9. Cumulative frequency curve of Na_2O (data from Carvalho & Pereira, 1973).

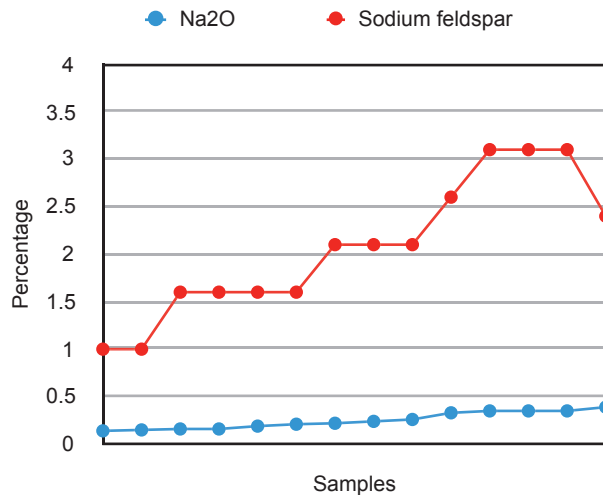


Figure 6.10. Concentrations in $<44 \mu m$ fraction (data from Carvalho & Pereira, 1973).

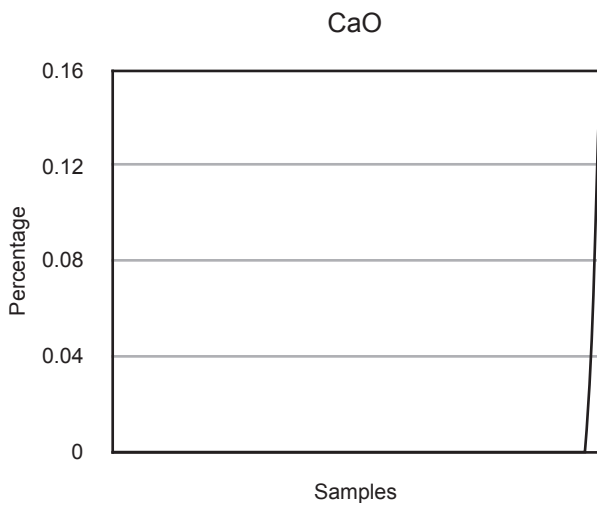


Figure 6.11. Cumulative frequency curve of CaO (data from Carvalho & Pereira, 1973).

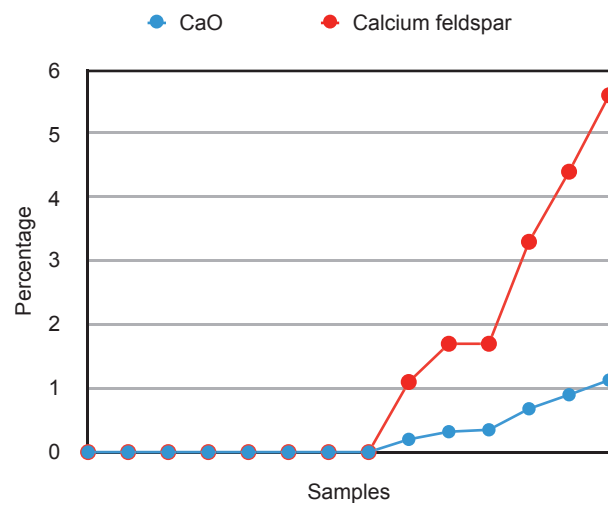


Figure 6.12. Concentrations in $<44 \mu m$ fraction (data from Carvalho & Pereira, 1973).

concentrations of the molecules. Notable differences include a high spike of potassium in the northern part of the basin, and a spike of sodium in the south east area. It is this sodium anomaly which contains the only measurable amount of calcium.

6.1.2.4. Titanium dioxide

Titanium has a generally low abundance in the Rio Maior sands, 88% of samples containing <0.5% of the element (Figure 6.13). The minerals found in the sands containing titanium are rutile and anatase (Dias, 2015), both consisting of titanium and oxygen, making it possible to equate the occurrence of this element directly with the occurrence of these minerals. This is indicated by the close correlation between titanium and rutile in the <44 μm fraction (Figure 6.14). Rutile, due to its density and resistance, is often associated with mature sediments, particularly those of beaches owing to its ability to resist weathering and transport by high energy environments (Hubert, 1962). While anatase is not as dense or resistant as rutile, its presence is probably due to its traits being closer to those of quartz (Bishop *et al.*, 1999).

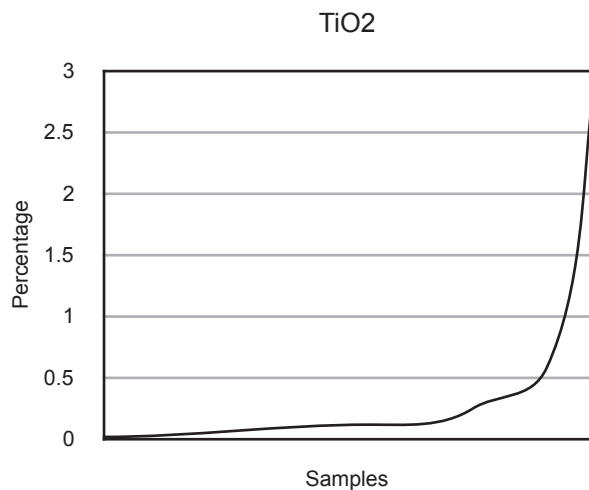


Figure 6.13. Cumulative frequency curve of TiO_2 (data from Carvalho & Pereira, 1973).

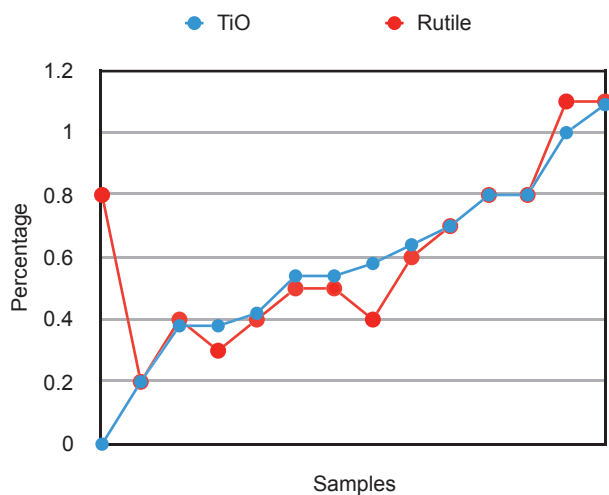


Figure 6.14. Concentrations in <44 μm fraction (data from Carvalho & Pereira, 1973).

In distribution, titanium oxide is generally split into two NE-SW bands with the highest concentration being in the centre of the basin (Figure 6.22). The distribution appears to be restrictive, with areas in the north, middle, and south exhibiting the lowest concentrations, limiting titanium to the bands described.

6.1.2.5. Iron oxide

Iron has a low abundance in the Rio Maior sands, 85% of samples containing <0.2% of the element (Figure 6.15). It is this low level of iron which makes the sands here so desirable for exploitation as iron is common in many sands and detrimental to many uses of

6. Analysis of white sand and interpretation

sand. It is a component of many minerals found in these sands: staurolite, goethite, siderite, magnetite/maghematite, and hematite. It is also a possible component of tourmaline and illite (also present). While it seems that much of this iron comes from goethite and hematite, it is unclear which of these is more abundant in unprocessed sand. After gravity separation, but before flotation in the Sifucel facility (see 3.1.6. and 3.1.7. respectively), the concentration of goethite is greater than that of hematite (Dias, 2015), but this might be a result of hematite's higher density (Bishop *et al.*, 1999). In the <44 μm fraction, however, the strong correlation between iron and hematite indicates that this is the origin mineral, at least in the fine fraction (Figure 6.16). This analysis is corroborated by iron contents being 5 to 9 times higher in more red sands (indicative of hematite) than white sands in samples analysed from the Via-Vai quarry (Table 6.1). This differentiation is important for palaeoenvironmental interpretations and for high fidelity processing considering the differences between goethite and hematite.

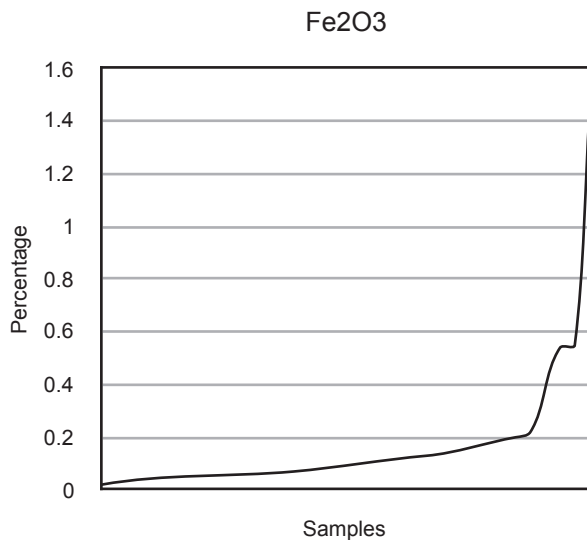


Figure 6.15. Cumulative frequency curve of Fe₂O₃ (data from Carvalho & Pereira, 1973).

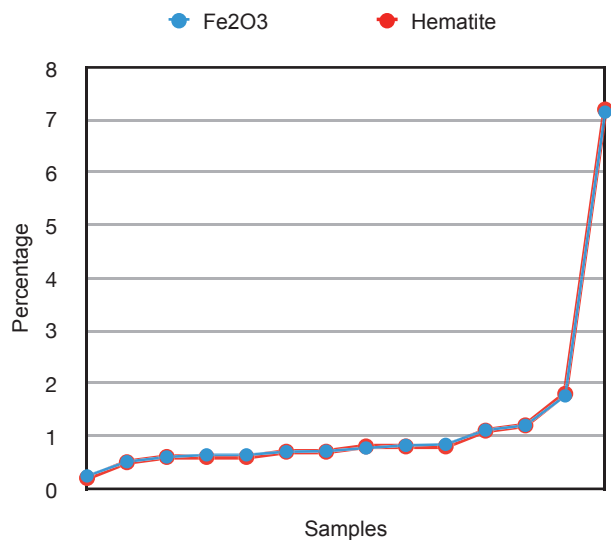


Figure 6.16. Concentrations in <44 μm fraction (data from Carvalho & Pereira, 1973).

Iron is concentrated in an E-W band across the basin north of its greatest occurrence in the centre. The areas of low concentration are in the north, middle east and west margins, with the southern part being the lowest (Figure 6.23). Like titanium dioxide, this seems to be a restrictive pattern.

6.1.2.6. Magnesium oxide

Magnesium has a very low abundance in the Rio Maior sands, 91% of samples containing <0.16% of the element (Figure 6.17). There are only two minerals present which have magnesium as a possible component: tourmaline and illite. It is probably a combination of these which make up the magnesium content of the sands.

The distribution of magnesium oxide is patchy across the basin (Figure 6.24). Unusually, the highest concentrations are located on the middle west margin. The north and south most distant points have low concentrations.

6.1.2.7. Other contaminants

The distribution of other elements are highest around the centre with the lowest being to the north and, particularly, the south (Figure 6.25). This may be due to finer, heavier minerals collecting in the centre of the basin. The general distributions described above and show in Figures 6.18 to 6.25 are difficult to make sweeping judgements on as there is considerable variance in mineral content in the same borehole (e.g. Figure 6.26). This is why the average concentration ranges on distribution maps do not always reflect the distribution of point data.

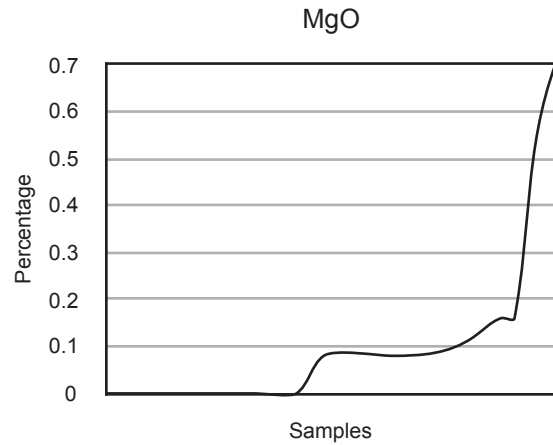


Figure 6.17. Cumulative frequency curve of MgO (data from Carvalho & Pereira, 1973).

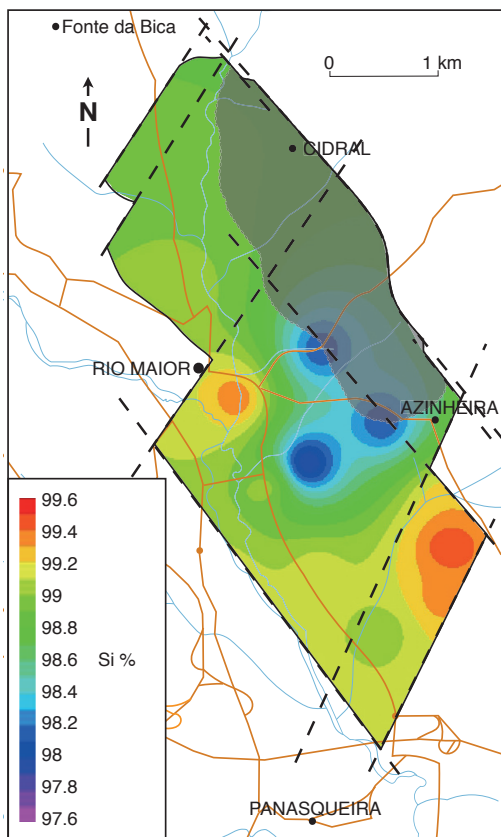


Figure 6.18. Distribution of SiO₂ throughout basin. Made using RockWorks.

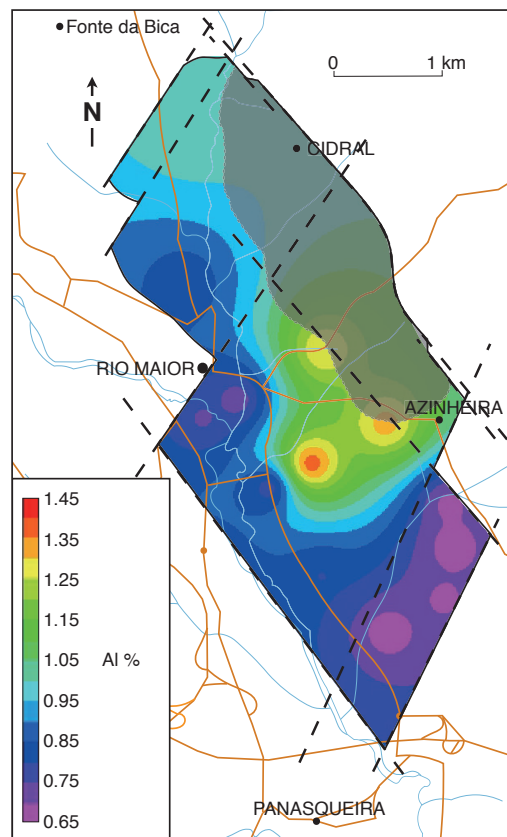


Figure 6.19. Distribution of Al₂O₃ throughout basin. Made using RockWorks.

6. Analysis of white sand and interpretation

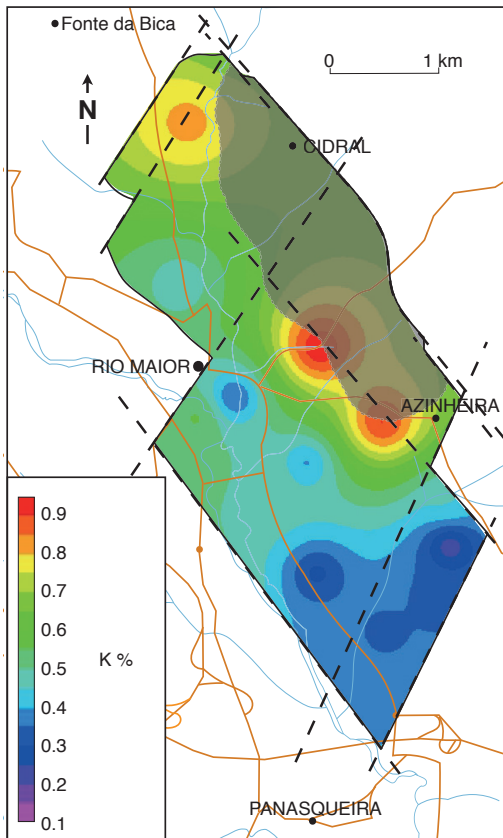


Figure 6.20. Distribution of K₂O throughout basin. Made using RockWorks.

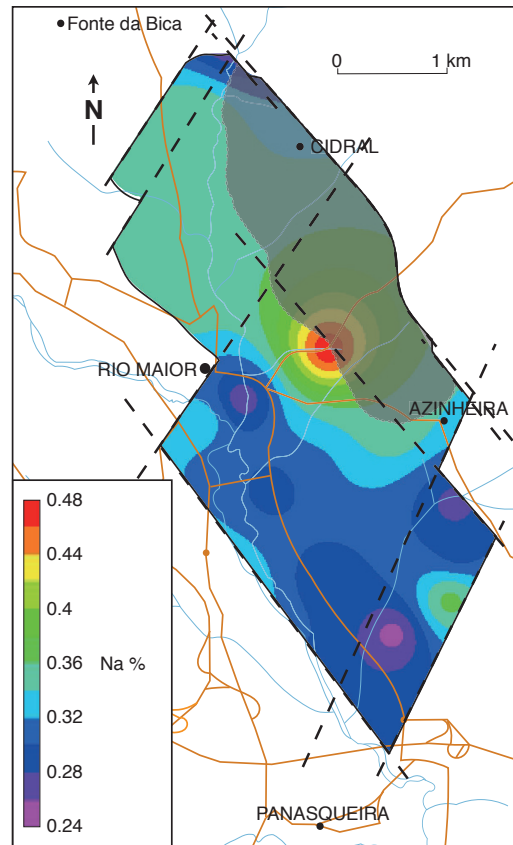


Figure 6.21. Distribution of Na₂O throughout basin. Made using RockWorks.

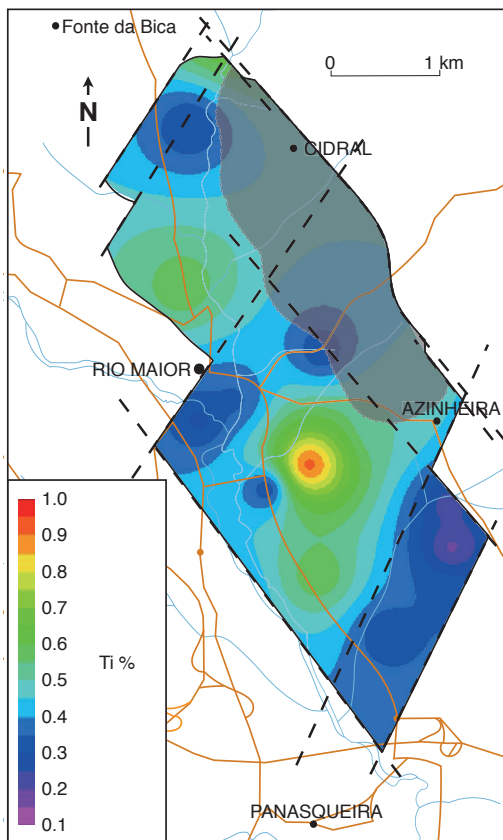


Figure 6.22. Distribution of TiO₂ throughout basin. Made using RockWorks.

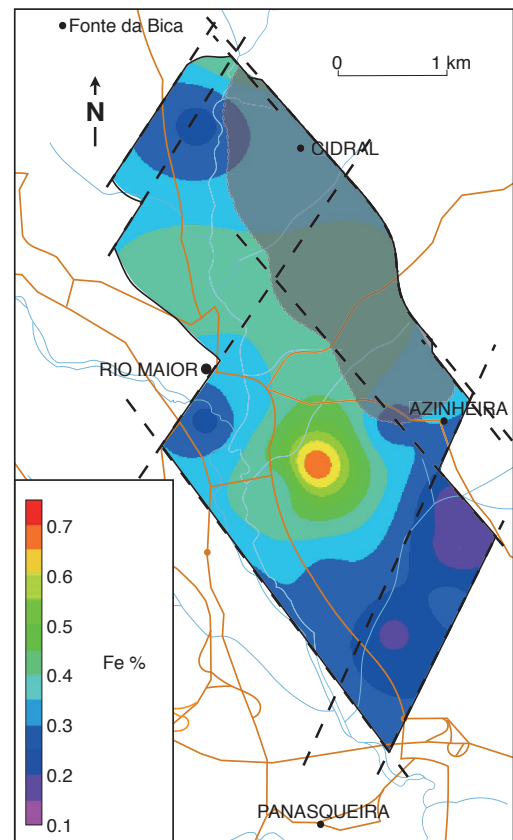


Figure 6.23. Distribution of Fe₂O₃ throughout basin. Made using RockWorks.

White Sands of Rio Maior

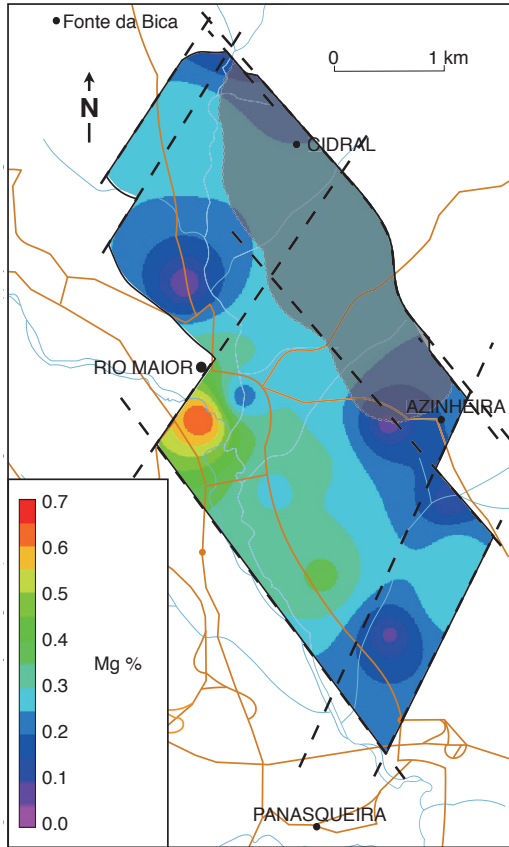


Figure 6.24. Distribution of MgO throughout basin. Made using RockWorks.

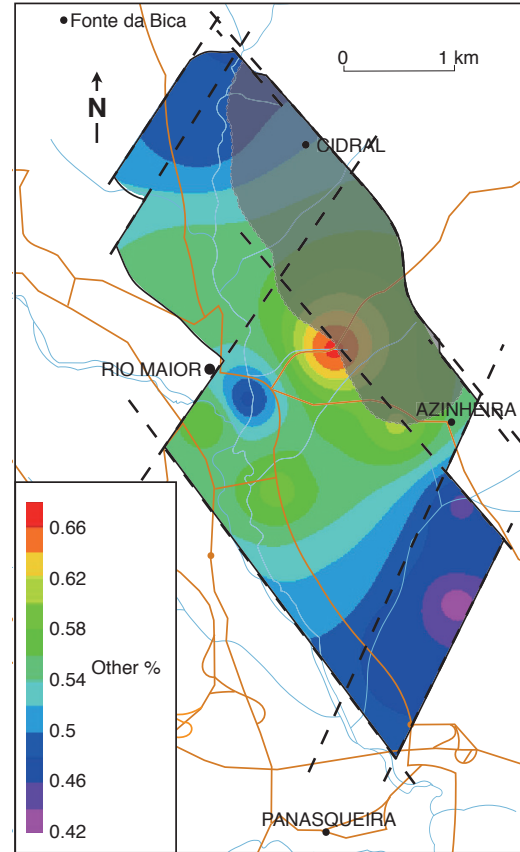


Figure 6.25. Distribution of other contaminants throughout basin. Made using RockWorks.

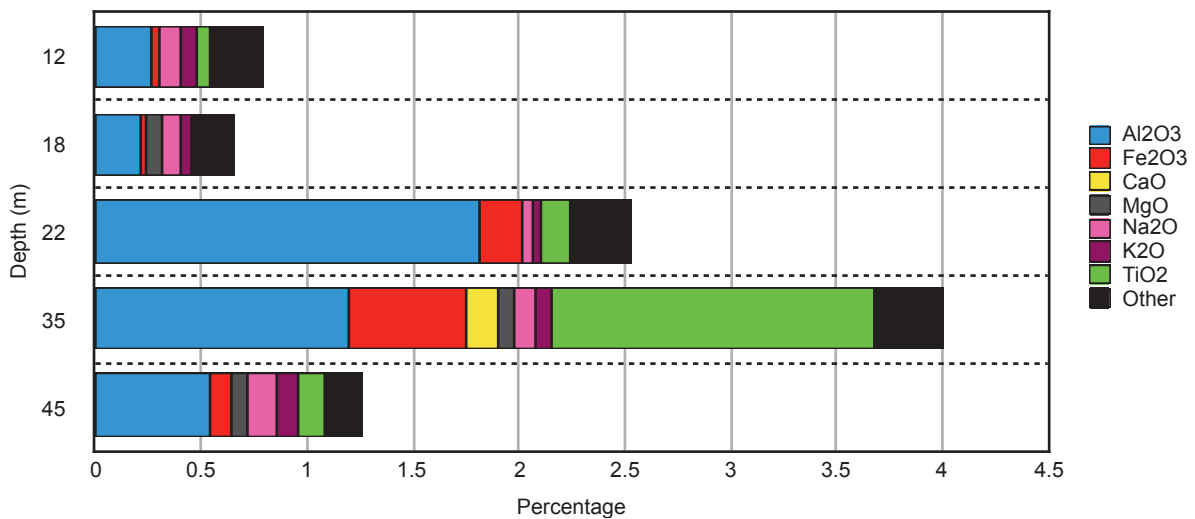


Figure 6.26. Variation of chemical composition of sand samples according to depth in borehole AF 28 (data from Carvalho & Perreira, 1973).

6.1.2.8. Mineralogical indications

The presence of kaolinite and, lesser, muscovite, are probably from the breakup of feldspars (Nichols, 1999). Although this does not affect the chemical composition, it does point towards a more mature sediment where aluminium oxide is present.

6. Analysis of white sand and interpretation

Iron oxide in the form of hematite or goethite is generally precipitated from the water. The former forms in well-oxygenated environments, while the latter is formed in poor-oxygenated environments, particularly bogs and lagoons. In areas such as the Via-Vai quarry, the high iron content can be seen in red sand, indicative of hematite. This is to be expected around the shallow edge of the basin. The high iron sands in the centre of the basin are likely goethite, being deposited in a poor-oxygenated environment.

Rutile, zircon, spinel, and monazite all show concentrations in very mature sediments, particularly alluvial and beach sands due to their density and hardness (Bishop *et al.*, 1999).

The detectable presence of opal might indicate life in the basin (sponges, radiolaria, diatoms) which use dissolved silicon to create their exoskeletons (Bishop *et al.*, 1999).

6.1.3. Structures

The Via-Vai quarry offers the opportunity to observe more structural evidence than can be reliably observed from borehole evidence. Locations of samples and features are marked on Figure 6.27.

Visible on the sides of the quarry are bedding planes which curve, becoming steeper to the south and shallower to the north (Figure 6.28). While easily observable on a macro



Figure 6.27. Via-Vai quarry showing sample points. Created using GoogleEarth.



Figure 6.28. South west side of the Via-Vai quarry with bedding planes highlighted. Whole view is 350m.

scale, these planes are difficult to identify up close. By measuring more clear bedding above the white sand at point γ , dips ranging from 20° to 36° (28° average) were recorded with an average direction between north and north-northwest (348° , and marked on Figure 6.27). This is consistent with the dips seen in the underlying white sand.

In the quarry, there are numerous instances where red and white lenses of sand can be seen (e.g. Figure 6.29). These lenses are irregular and vary in their colour intensity. I have analysed these bands and found that the white bands are more pure, having a lower aluminium and iron content (35% less Al_2O_3 and 80% less Fe_2O_3 , α samples Table 6.1). These lenses are indicative of a braided river system, the thinness of the lenses suggesting either slow sedimentation or rapid abandonment and overlapping of channels. These channels, the shallow slope, and termination at a large body of water are characteristic of a river-dominated delta (Nichols, 1999). Instability of major and minor channels might explain the high aluminium and iron content. As channels are abandoned, the aluminium-rich kaolinite clays are deposited as flow dissipates, along with iron oxides being precipitated. These iron oxides may have either formed light coloured goethite or more vibrant hematite based on post-depositional processes. In an anoxic watery environment forming goethite, and hematite in the oxygenated abandoned river channel (Berner, 1971, Nichols, 1999).

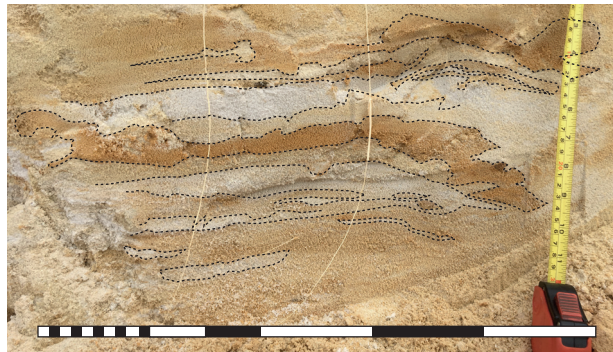


Figure 6.29. Red and white sand lenses located in point α . Scale is 50cm.

There is more evidence of a delta at point $\delta 1$. Here sloping beds are cut and topped by near horizontal beds (Figure 6.30). This is indicative of the progradation of a delta, the sloped beds of the distributary delta channel or mouth bar, overlain by the horizontal beds of an advancing delta plain (Nichols, 1999). The sandy nature of this sequence would usually classify this as a fan delta (Wescott & Ethridge, 1990). However, this is also normally accompanied by changes in granulometry, this change is largely absent probably due to the well sorted source of the sediment, making determinations based on such evidence difficult.

In these more shallow areas of the quarry, orange-brown sands dominate with a similar appearance to the lenses of point α . At points $\delta 1-5$ the chemical composition is largely

6. Analysis of white sand and interpretation

Table 6.1. Chemical compositions of samples from the Via-Vai quarry. All samples were measured using the OMNIAN calibration (3.2.1(b)). SiO₂ values are estimated. The samples were collected between 27/02/2019 and 16/05/2019.

	α white (%)	α red (%)	β red (%)	β dark (%)	δ 1 (%)	δ 2 (%)	δ 3 (%)	δ 4 (%)	δ 5 (%)	Purple nodule (%)
SiO ₂	96.89	95.09	95.06	95.54	97.79	98.61	96.74	96.55	96.82	91.2
Al ₂ O ₃	2.76	4.19	4.03	3.55	1.24	0.99	2.61	2.95	2.64	7.15
K ₂ O	0.092	0.19	0.13	0.13	0.024	0.022	0.12	0.15	0.13	0.17
Na ₂ O	0.041	-	-	-	-	-	-	-	-	-
Fe ₂ O ₃	0.054	0.26	0.47	0.44	0.36	0.14	0.25	0.14	0.14	0.27
TiO ₂	0.028	0.083	0.11	0.11	0.43	0.14	0.11	0.094	0.13	0.82
MgO	0.082	0.084	0.083	0.091	0.084	0.059	0.072	0.063	0.06	0.095
ZrO ₂	0.033	0.034	0.035	0.073	0.06	0.043	0.044	0.04	0.046	0.064
Y ₂ O ₃	0.0022	0.0026	0.0026	0.0065	0.0033	0.0024	0.0033	0.0033	0.0042	0.027
MnO	-	-	-	0.0062	-	-	-	-	-	0.022
P ₂ O ₅	-	0.011	0.015	0.012	-	-	0.011	0.009	0.0089	0.016
SO ₃	-	0.0085	0.0092	0.011	-	-	0.012	-	0.012	0.013
CaO	0.011	0.033	0.026	0.027	-	0.0077	0.021	-	0.015	0.011
Rb ₂ O	0.0013	0.013	0.013	0.0015	-	-	-	-	-	0.0017
Nb ₂ O ₃	-	-	-	-	-	-	-	-	-	0.062
La ₂ O ₃	-	-	-	-	-	-	-	-	-	0.031
Cd ₂ O ₃	-	-	-	-	-	-	-	-	-	0.017
Cr ₂ O ₃	-	-	-	-	-	-	-	-	-	0.017
Bi ₂ O ₃	-	-	-	-	0.0026	-	-	-	-	-
Cl	-	-	-	-	-	-	-	-	-	0.0051
Nb ₂ O ₅	-	-	-	-	0.0016	-	-	-	-	-
NiO	-	0.0056	-	-	-	-	-	-	-	0.0081
PbO	-	-	0.0026	-	-	-	-	0.0018	-	0.0049
PtO ₂	-	-	0.0026	-	-	-	-	-	-	-
SrO	-	-	-	-	-	-	-	-	-	0.0024
ThO ₂	-	-	-	-	-	-	-	-	-	0.0026
ZnO	-	-	-	-	0.0031	-	-	-	-	0.0021

similar to the white sand, but contain >2.5 times the proportion of iron oxide. At point β , the iron content is 9 times the white sand level and other molecules making it similar to the red sand. There are some white spots and elongated vertical forms with signs of carbonised plant material (Figure 6.31). This is consistent with the development of a delta plain, with plant growth and a greater proportion of fine grain (in this case clay) minerals being

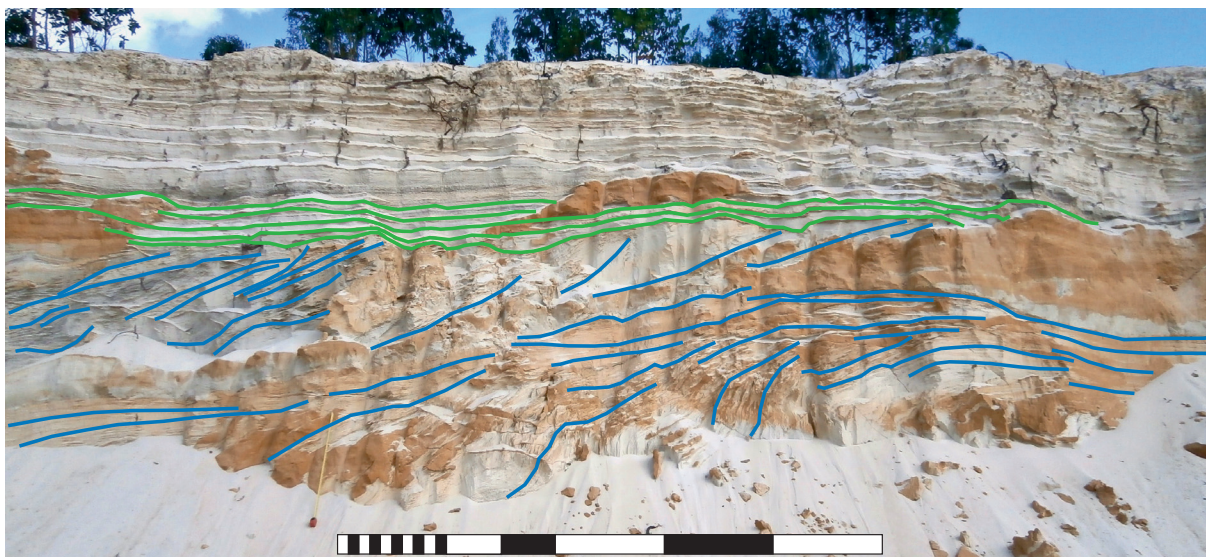


Figure 6.30. Sample point $\delta 1$. Sloping delta beds are highlighted in blue, near-horizontal beds are highlighted in green. Scale is 10m.

deposited (Nichols, 1999). This sort of texture is observed by Carvalho and Pereira (1973) in numerous cores taken in other areas of the basin, particularly in the northern area.

These signs of plant material are the only remains of life persevered in the sediment. Material is found above (Diniz, 1984b, Flores, 1996) and stratigraphically below (Antunes *et al.*, 1992), but not within the white sand. This is probably due to the low amount of fine clay and cementation material with which to take and preserve impressions. At point β , in the clayey material where measurable slope data was taken, two fossils were also recorded (Figures 6.32 and 6.33). These include a gastropod identified as *Planorbarius* sp. and a shell which does not exhibit

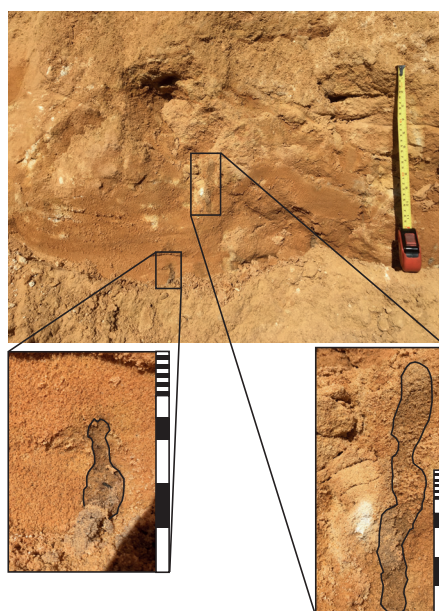


Figure 6.31. Signs of black plant material in red sand located in point β . Scale is 5cm.

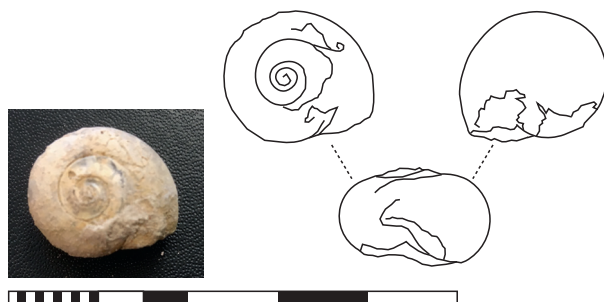


Figure 6.32. *Planorbarius* sp. Scale is 5cm.



Figure 6.33. Unidentified bivalve or brachiopod. Scale is 5cm.

6. Analysis of white sand and interpretation

enough detail to positively identify it beyond a bivalve or brachiopod. These sediments, however, are representative of a different depositional environment than that in which the white sand was deposited (Flores, 1996).

In the analysis of boreholes by Carvalho and Pereira (1973), there are multiple mentions of purple clay or purple nodules being found in various sedimentary layers (including white sand) past the western edge of the basin. In the Via-Vai quarry, several purple fragments were found among disaggregated sand near point $\delta 1$ (Figure 6.34). When analysed, this nodule was made up of silty grains (62-4 μm) and contained a relatively high proportion of contaminants (8.8%). 81% of these contaminants were aluminium oxide and 9% were titanium oxides. These levels are far higher and include numerous other contaminant oxides which are too rare to be measured in other samples. There are also laminae visible indicative of seasonal changes of sedimentation. Although this fragment and others like it in the quarry are probably from the formation above the sand layer with a large proportion of kaolin. Most other instances around the basin are above or below the sand, or in shallow sand deposits separate from the main basin.



Figure 6.34. Fragment of purple siltstone. Scale is 10cm.

6.2. Interpretations

There is no definitive link between the proportion of heavy mineral contaminants and the overall fineness of the sample, while there is a greater abundance of contaminants in the finer grains. Difficulty in this area is due to the aeolian transport commented on in Carvalho and Pereira (1973), which sorted out many heavy minerals and coarse sand, leaving little differentiation possible. The quality of this deposit lies in the sorted nature of the quartz grains from its form of transport, and its maturity, which left some contaminants during transport and broke down many that remained (hence minerals such as kaolin).

Most of the heavy minerals have their highest concentration around the middle of the basin. While these are not necessarily the deepest areas, it is difficult to ascertain the effects of depth on the heavy mineral content as the deepest parts remain underneath the thick

lignite basin. Although boreholes were created in this area, chemical analyses of the sand were not carried out (Carvalho & Pereira, 1973, Flores, 1996). However, the placement of minerals in a lacustrine basin have less to do with depth and more to do with distance from the source.

The patterns of aluminium and potassium oxides show a significant correlation, displaying high concentrations in the northern end of the basin and decreasing around the western edge and reaching its lowest levels around the south. This northwest skew implies a northwestern source for the most likely minerals for these chemical signals: feldspar and kaolinite. This agrees with the evidence of progressing dunes passing between Sierras de Candeeiros and Montejunto being the source of the sand (Magalhães & Carvalho, 1984). Evidence of feldspar and (particularly) kaolinite being present in <44 µm fractions indicates that these minerals could easily be part of an aeolian sand. A fluvial system likely introduced the sand and associated minerals into the basin, along with possible aeolian influences associated with the dunes' progression, producing the relatively high concentration of aluminium and potassium oxides along the northern edge of the basin.

The north was not the only input direction as iron, titanium, and other oxides each have three areas of abnormally low concentration: the northern end, the western midpoint, and the southern end. These three areas all have low concentrations of the above oxides, and moderate concentrations of sodium and magnesium oxides. The sodium concentration shows little variation in the western midpoint, but skews markedly to the north with a high concentration anomaly in the south. For magnesium, the north and south avoid low concentrations with a very high concentration in the western midpoint. This indicates three sites of input, causing many heavy minerals to settle around the centre where energy was low, being equidistant from the three flows (Sturm & Matter, 1978). These three interpreted inputs are represented in Figure 6.35.

The northern input was heavily charged with aluminium and potassium minerals from the sand dunes. The western midpoint input shows low aluminium, moderate levels of potassium, and the highest levels of magnesium. The southern input shows low aluminium and potassium. High levels of sodium and at least moderate levels of magnesium are present in all three input areas. The southern input has the greatest amount of evidence of its fluvio-deltaic features due to the Via-Vai quarry. As discussed above, the southern input was probably a shallow, river-dominated deltaic system. While structural evidence is less substantial for the western and northern inputs, being based on boreholes, Carvalho and Pereira (1973) reported intercalations and possible lenses in these areas, suggestive of other deltaic systems. The input from the north was heavily influenced by the dune deposits, with the other two affected by aeolian sediment. This can be seen in the silicon oxide distribution as sand deposited around the western and southern inputs had fewer heavy contaminants such as aluminium, which would have come out of suspension over the basin. The sodium and potassium seems to have been transported further, being distributed along the northwest

6. Analysis of white sand and interpretation

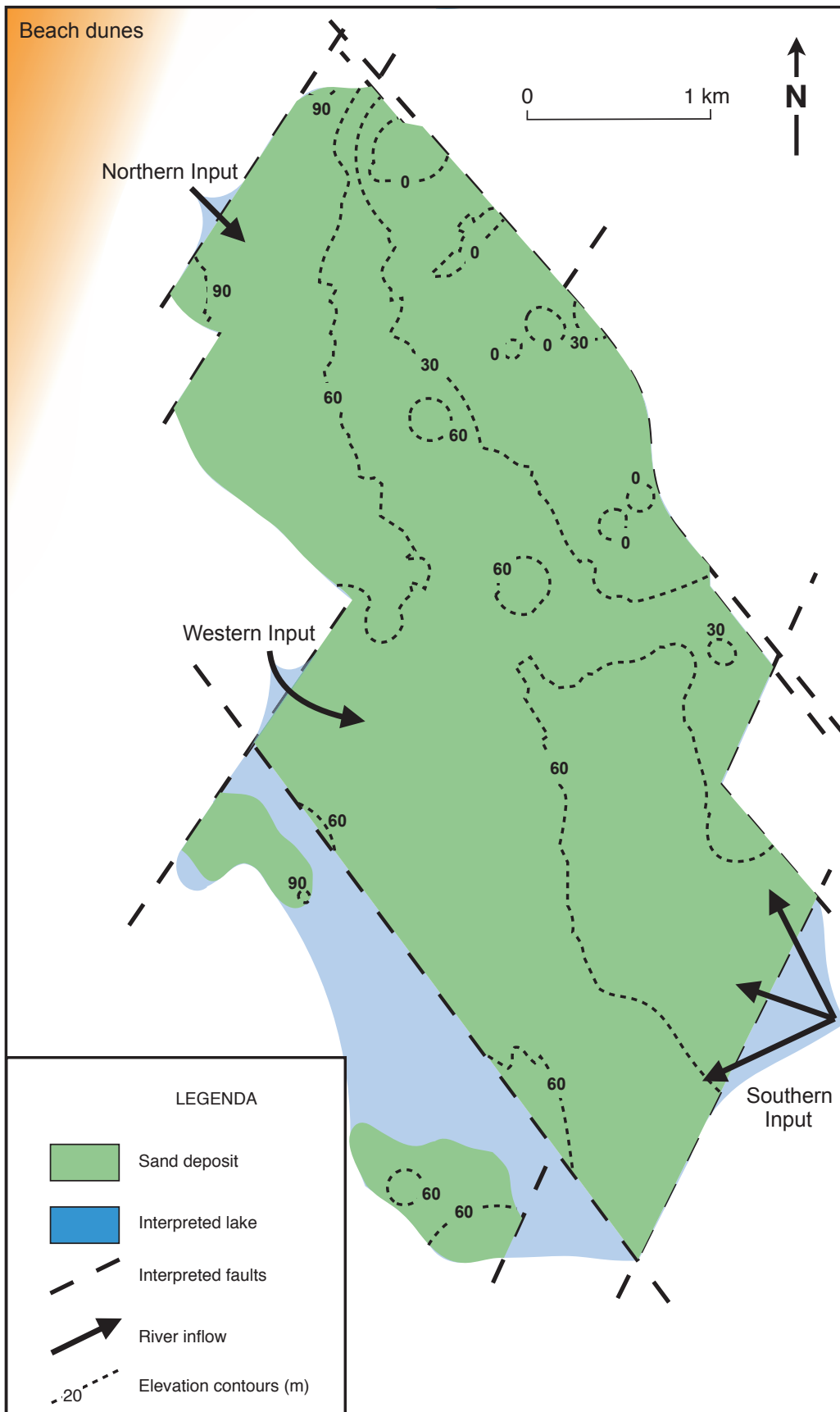


Figure 6.35. Reconstruction of the Rio Maior basin during sand deposition. Map based on current sand deposits and elevations based on the upper horizon of the deposit. The source of the sand is the beach dunes, and three interpreted inputs are marked.

edge of the basin, being present in the north and west inputs. The sodium minerals appear to have been blown across the basin to be returned in the southern input. Although it is also possible that the less robust calcium and sodium feldspars were removed from the dune sand as it matured and brought by the western and southern inputs from other sources. Magnesium minerals seem to have been transported by all three inputs, but highest from the western input, indicating this was also from an independent source.

The basin lake displays few notable structural features. No features such as turbidites and a lack of thick, restricted delta lobes suggest a relatively shallow lacustrine environment, dominated by delta front influences (Elliott, 1989, Nichols, 1999). In addition to the above mineralogical signifiers, the three input areas are also marked by particularly fine sediment (Figure 6.2). These are probably signs of fine prodeltas, subaqueous bars of fine material deposited as the deltaic material comes from a fluvial system into the standing water of a lacustrine system. The northern and western inputs would have had their material heavily influenced by the beach dunes. Winds, likely funnelled by the Serra de Candeeiros and Serra de Montejunto, could have blown finer sand across the basin to be captured and redeposited by the southern input.

The lack of biological information hinders much further interpretation of environment, however, the presence of sulphur in reddish sands of the Via-Vai quarry (85 - 118 ppm) suggest plant material. While sulphur may be produced by bacteria under anaerobic conditions (Casagrande, 1987), the presence of oxidised hematite and carbonised organic matter in the highest sulphur samples, indicates the source to be sulphates assimilated by plant material (Casagrande, 1985). This is probably vegetation which grew on mid-channel bars exposed long enough for vegetation to take hold (Bridge, 1993).

While there is evidence of not inconsiderable plant material close to the top of the deposit (close to the eventual change into a marshy swamp, Flores, 1996), there is little evidence beyond elevated sulphur levels deeper in the Via-Vai quarry. It is suggestive of a generally north flowing delta in this area, feeding the basin with frequent avulsion of its channels. While this may have been affected by changes in rainfall and evaporation, the shallow dip and apparent lack of vegetation would have increased the instability (Nichols, 1999). The extent of the deltaic formation is not clear due to the changing nature of the lobes and homogeneity of the sediment hiding sorting that would have been due to delta facies. This is the case for the southern input, but is unknown whether this is also applicable for one or both of the other inputs.

7. Areas of further exploitation

7.1. Need for further excavation

To maintain production, Sifucel has to have a source of special sand that can, with minimum processing, satisfy market demands and maintain the currently produced characteristics.

While the Via-Vai quarry contained an estimated 7.374 million tonnes when excavations began, the lifespan of the quarry was calculated as 24.6 years (Visa, 2004). It is necessary, therefore, for Sifucel to investigate other sources of special sand. The most readily available course of action is to continue exploitation of the Rio Maior basin.

The Rio Maior basin contains approximately 919 million cubic metres of sand (based on RockWorks model), containing two large working quarries, one small working quarry, and one abandoned quarry, none of which have made a significant impact to this amount. The basin also contains sand of a similar quality to that already exploited in the Via-Vai quarry. The sand is of a very high purity and the basin is the most important national producer of special sand (Moura & Velho, 2012), making it the obvious choice for further exploitation.

7.2. Virtual modelling

The virtual models used to calculate the various conditions of the sand deposit were created using RockWorks. RockWorks is a geological modelling software developed by RockWare. It used borehole data from the work carried out by Carvalho and Pereira (1973). This work uses 68 boreholes, 40 of which were carried out by the authors and have detailed descriptions of the material recovered. Many of these samples were chemically and mineralogically analysed, with 29 from the 'white sand' deposit. The reports of the previous boreholes do not contain information on, or chemical or mineralogical analysis of, the sand apart from its upper horizon as they were focussed on the diatomite and lignite complex (Zbyszewski, 1967, Flores, 1996).

All cores were unavailable for analysis as the LNEG (Laboratório Nacional de Energia e Geologia) database on cores listed all cores as non-existent or lost ("Inexistente/perdida", LNEG, 2019). Testing samples in Sifucel would have allowed for chemicals labelled 'other' to be identified and for comparisons with other samples collected to be made, eliminating procedural and equipment bias.

In the data produced by Carvalho and Pereira (1973), only 21 of the boreholes met the lower horizon of the sand deposit. Of the other 19 which crossed sand, the projections included in the cross sections were used as the lower horizon in the RockWorks model. These projections were based on the work carried out by Carvalho and Pereira (1973), and data collected by Zbyszewski (1960). This was required for accurate modelling of the sand deposit.

During the modelling process, the Inverse Distance (IDW) method was used for interpolation. This is standard in some countries (RockWare, 2017) but was used here rather than Kriging, due to the statistical noise produced by the latter method. This was probably due to the relatively few data points. During the analysis of chemical concentrations, all interval data was transferred into point data to be used collectively with the other chemical data, recorded as point data. In these models, isotropic modelling was used to create the voxels, as it is the preferred method for point data (RockWare, 2017).

The first problem encountered was calculating the coordinates of the boreholes used. Carvalho and Pereira (1973) recorded their positions based on a 1:2000 scale map produced by the Instituto Geográfico e Cadastral. Unable to use the same coordinate system and convert it into UTM projected coordinates for Zone 29S, a series of cartographical overlays were used to connect known points and use those as a basis for conversion equations. This method proved effective when incorporating RockWorks models with Carvalho and Pereira (1973) maps and data.

One problem exhibited by the model is the pervasive nature of the diatomite and lignite complex, and the lithology underlying the sand deposit identified as 'clays, sandstones, loams, and limestones' ("argilas, arenitos, margas e calcários", Carvalho & Pereira, 1973). The diatomite and lignite complex spreads outside the area defined as the lignite basin and the clays, sandstones, loams, and limestones layer intrudes into the sand deposit (Figure 7.1). Both are flaws in the three dimensional interpolations and do not appear in sections based on borehole data alone (fence diagrams do show this as they are based on 3D interpolations).

The lignite basin provides several problems for chemical concentration interpolations. Chemical analysis of the sands were not carried out by surveys before Carvalho and Pereira (1973), so the only data points are around the edges where there are AF boreholes. While the results are reliable, the projections underneath the diatomite and lignite complex have dubious validity due to the lack of data points.

7.3. Area determination

After creating a geological model, the basin can now be assessed on a range of criteria to determine worthwhile areas of exploitation. This can inform Sifucel regarding areas of expansion and assess the worth of doing so.

7.3.1. Owned area

Sifucel already owns two areas to the north of the Via-Vai quarry, both generally quadrilateral in shape (Figures 7.2, 7.3). Area 1 covers an area of 2.12 hectares and contains approximately 3.994 million tonnes of sand. Area 2 covers an area of 10.3 hectares and contains approximately 17.387 million tonnes of sand. Of the two areas, Area 2 is likely to

7. Areas of further exploitation

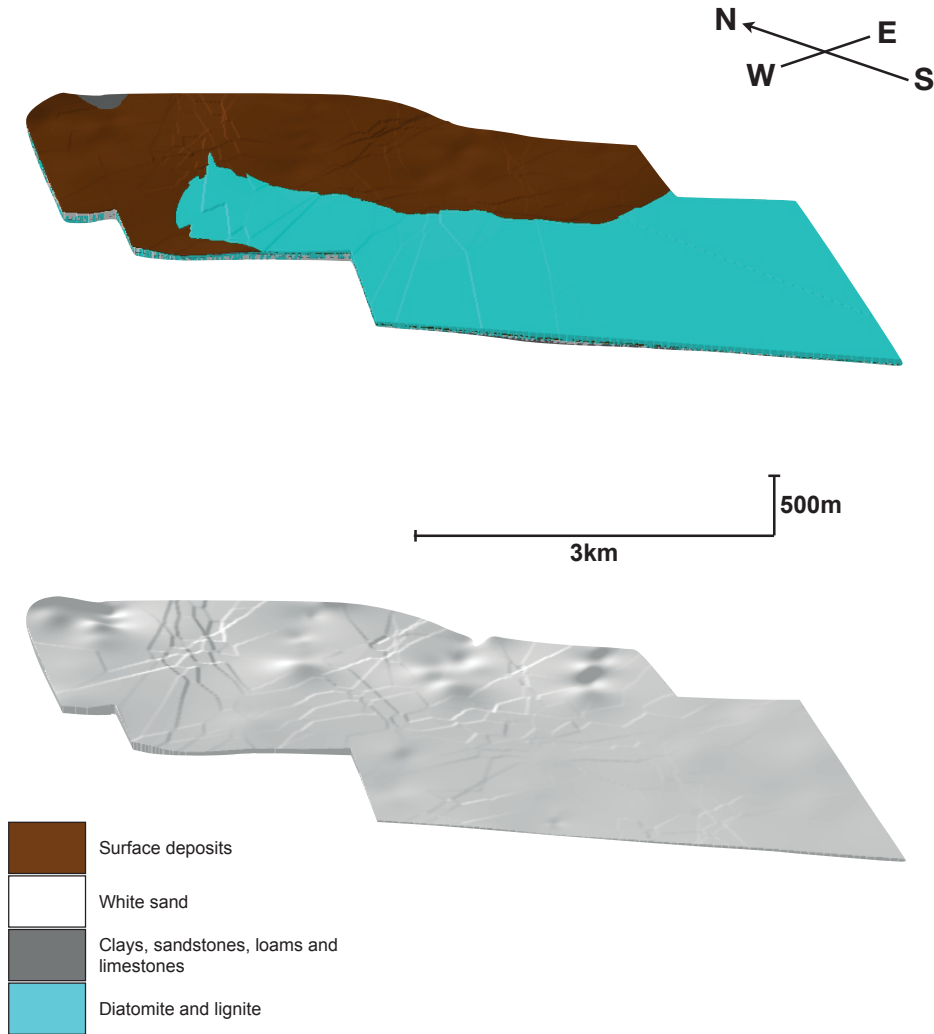


Figure 7.1. RockWorks stratigraphic model of the Rio Maior basin. Above model shows all stratigraphic units. Below model shows only white sand stratigraphic unit.

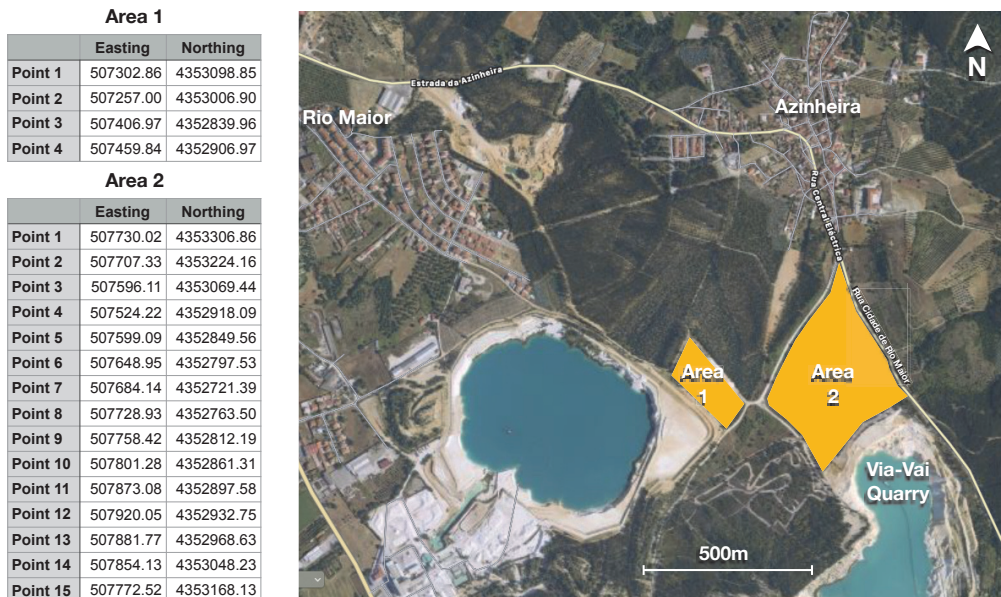


Figure 7.2. Map showing areas, and related approximate coordinates, owned by Sifucel. Map was created using GoogleEarth and AppleMaps.

White Sands of Rio Maior

contain the purer sand by every measurement, however, it is neither as near the surface, or as thick as Area 1 (Figures 7.4, 7.5).

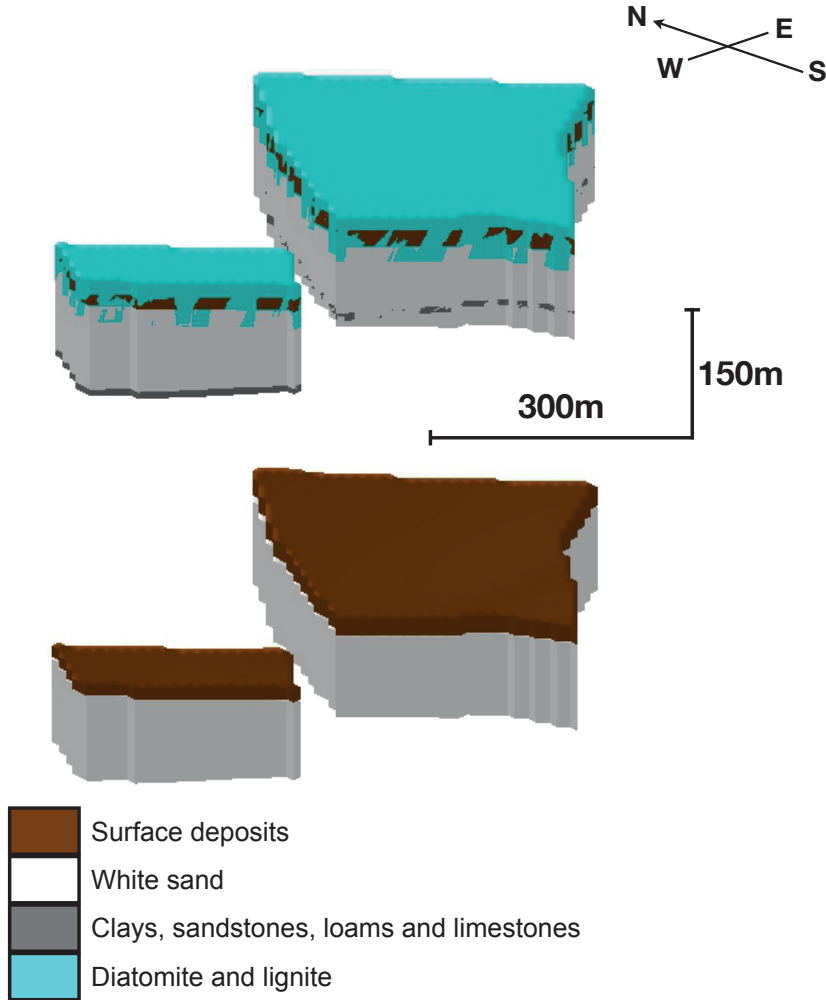


Figure 7.3. RockWorks stratigraphic model of the Areas 1 and 2.

Above model shows all stratigraphic units. Below model shows only surface deposits and white sand stratigraphic units.

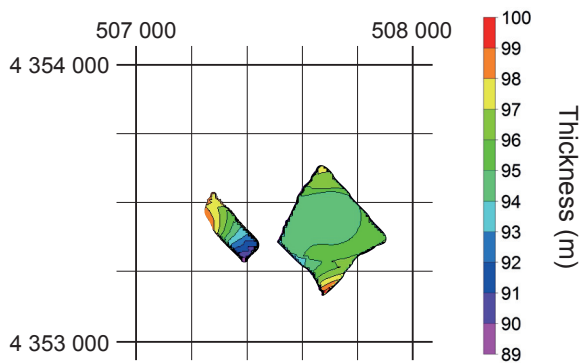


Figure 7.4. Thickness of sand deposit in the Areas 1 and 2. Made using RockWorks.

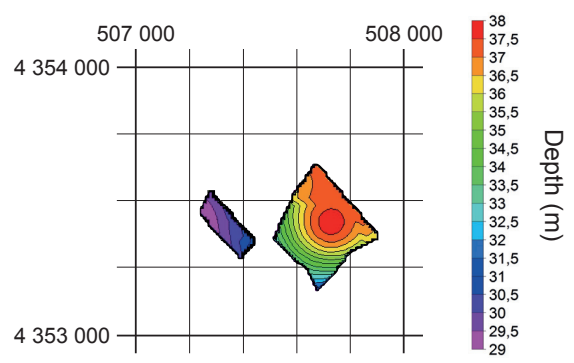


Figure 7.5. Depth of the sand upper horizon in the Areas 1 and 2. Made using RockWorks.

7. Areas of further exploitation

Area 2's chief benefit is that it meets the Via-Vai quarry, allowing for extraction and exploitation to continue on their current course. There is also a reduction of waste from a new pit being excavated.

Using the 300 000 tonnes per year production rate used by Visa (2004), the reserves of Area 1 could extend the life of quarrying in this area by 13.3 years, and Area 2 by 58 years.

7.3.2. Factors for expansion

The areas currently owned by Sifucel provide a starting point with the possibility to join the two if the intervening land can be obtained and excavation permitted. There is also the possibility of further expansion if similar conditions are met. However, there are other factors to consider: land use; thickness of the deposit; depth of the deposit; and the contamination of the sand.

Land use is the most restrictive factor within the Rio Maior basin. This is due to the extensive urban development. For a site of quarrying, the land must be free of important use, as there are associated legal and social issues with different types of land.

Much of the land covering the Rio Maior basin is taken up by urban development. This is complicated by the presence of lone buildings and dwellings apart from more confined built up areas. This complicates the creation of simple exclusion zones when planning excavations. Much of the non-urbanised area is covered with agricultural and forested areas. The former consists mainly of privately rented allotments for farming.

The land surrounding Areas 1 and 2 consists of groves of pinewood, eucalyptus, and olive trees, and what is classified as uncultivated land (Visa, 2004).

Other confining features in the area include the land owned by Sibelco Portuguesa Lda., which consists of their quarry, processing plant, and the forested land to the east of the quarry. The village of Azinheira, the Chainça suburb of Rio Maior, and a small-scale quarry also inhibit planned works. The two main roads in the area are Estrada da Azinheira and Rua Cidade de Rio Maior. There is also a public road, Rua Central Eléctrica, which runs to the southeast of Area 1 and northwest of Area 2.

The presence of groves, uncultivated land, and minor access routes were similar issues with the area used for the Via-Vai quarry, and yet did not prevent its construction.

The thickness of the deposit is a basic, but essential consideration. A deposit must have a sufficient amount of a resource to make it profitable for exploitation.

The thickness of the sand deposit in the Rio Maior basin increases to the northeast, closer to the lignite basin (Figure 7.6). The majority of the contours run in a general NW-SE direction. There are two main areas with a thickness of over 100m that is not capped by the diatomite and lignite complex. There is one area in the north, and one around the middle of the basin.

White Sands of Rio Maior

An attempt to excavate a thick section of the sand deposit would stay far from the west and remain close to the border of the diatomite lignite boundary.

The depth of the deposit is important as a shallower deposit will reduce excavation costs and the amount of material necessary to be moved before the extraction of profitable material. With the inverse cone shape of open cast pits, it is also possible for the depth to be excessive for a given area of an excavation.

In general, the upper horizon of the sand deposit gets deeper towards the northeast of the basin (Figure 7.7). The thickness of the cover increases significantly within the boundary of the lignite basin, creating the most substantial covering unit.

There is a band where the sand is 20-40m deep running in a NW-SE direction. There are some points within this band where the depth of the sand is <10m. Although these areas are small, they might be used as the starting point for an excavation to more easily extract material and build up capital for further, more costly excavation.

Contamination is an issue with every deposit (Kreiter, 1968), but especially important when considering a source of siliceous sand (Moura & Velho, 2012). However, this is less of

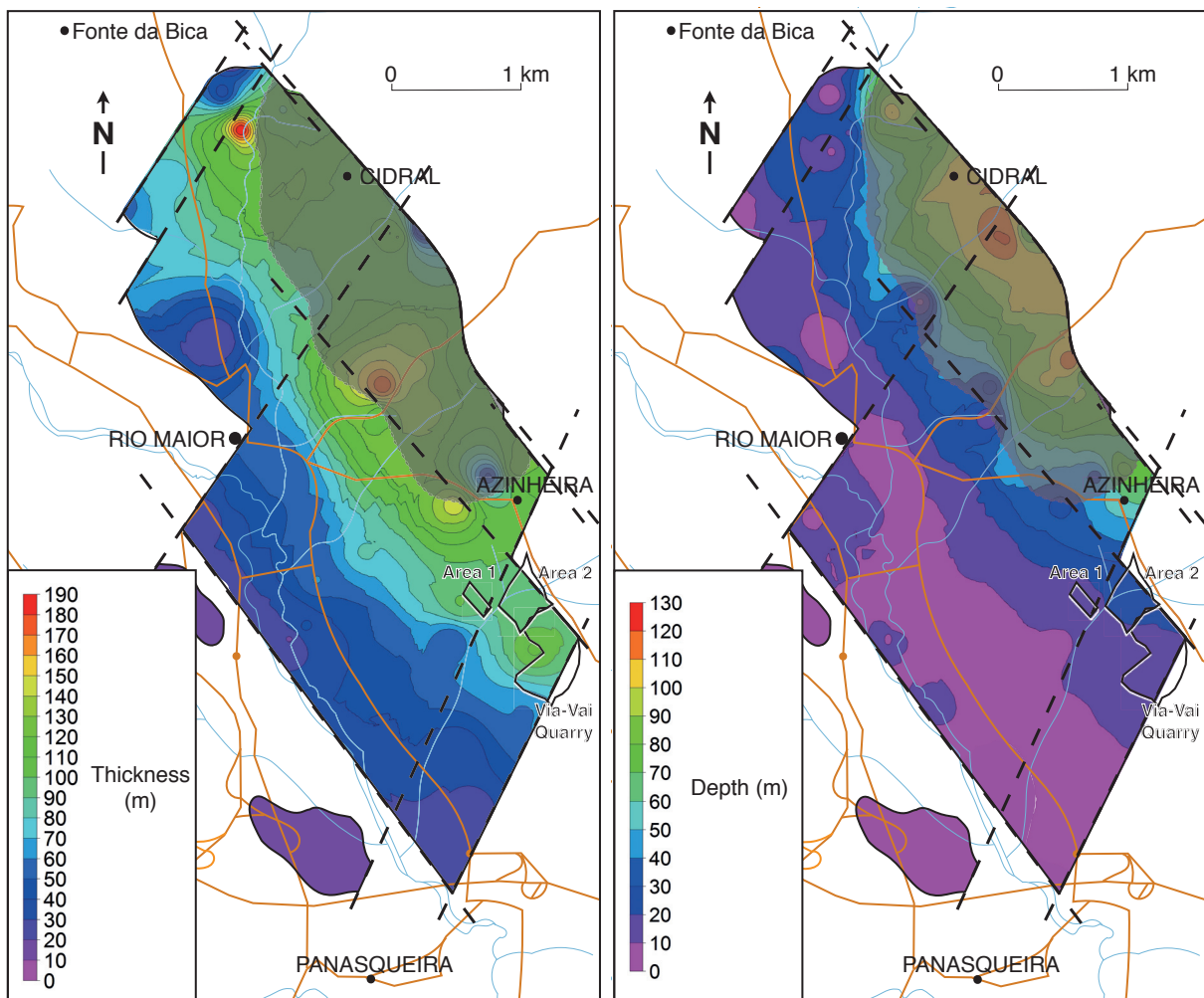


Figure 7.6. Thickness of sand deposit in the Rio Maior basin. Made using RockWorks.

Figure 7.7. Depth of the sand upper horizon in the Rio Maior basin. Made using RockWorks.

7. Areas of further exploitation

an issue with regards to the Rio Maior basin. Coima, the most important Portuguese source for siliceous sand after Rio Maior, has a general SiO₂ content of 96.5% (Moura & Velho, 2012). Some samples from the Rio Maior sands have dipped below this, however, when each borehole is given an average value, the SiO₂ content does not fall below 97%.

Contamination within the Rio Maior basin is minor compared with other sources of siliceous sand (Moura & Velho, 2012). Using averaging to mute outliers and Inverse distance (IDW) extrapolation, the contamination of the sand ranges from 2.1 to 0.5%. The individual measured contamination rates measured range from 8.69 to 0.81%.

This demonstrates the variation within the basin according to locality. While this does depend on the contaminant, they were generally lowest towards the southeast, around borehole AF28. The highest concentrations of contaminants occurs around the centre of the basin, in the vicinity of borehole AF17. This point has the highest measured proportion of contaminants, including aluminium and iron oxides (3.14% and 1.44% respectively) which provide problems for many siliceous sand uses (Mitchell, 2012, Moura & Velho, 2012).

As stated above, the contamination of the sand beneath the deeper parts of the diatomite and lignite complex is unknown as no drilling operations have sampled and tested the sand (Flores, 1996, LNEG, 2019). This raises concerns regarding any proposal to exploit the underlying sand in addition to the problematic depth of any excavation.

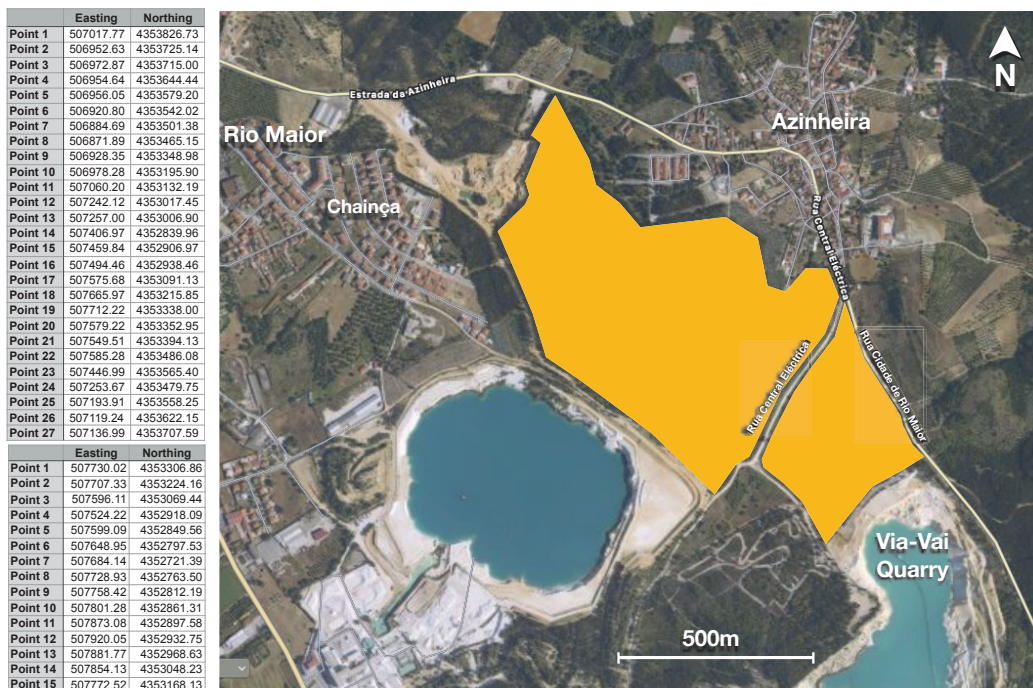


Figure 7.8. Map showing areas, and related approximate coordinates, of proposed excavation location. Rua Central Eléctrica picked out. Map was created using GoogleEarth and AppleMaps.

7.3.3. Proposed excavation location

The area chosen as the most beneficial for further exploitation of siliceous sand by Sifucel is defined in Figure 7.8. It has a total area of 47 ha and is bordered by Azinheira, the Chainça suburban development of Rio Maior, and land owned by Sibelco Portuguesa Lda., separated by the municipal road Rua Central Eléctrica.

For comparison, the data from borehole AF28 has been used as a proxy to the Via-Vai quarry. This borehole has passed through the whole of the sand deposit, has been fully analysed at multiple depths, and was carried out very close to the current quarry. The analysis was carried out by Carvalho and Pereira (1973), making it suitable for comparisons with other analyses in the same study.

The land use is the same as that in the area of the Via-Vai quarry when its creation was proposed (Visa, 2004). This provides precedent for the creation of a quarry site in the proposed area. The main issue is the location of the public road Rua Central Eléctrica (Figure 7.8). This cuts through the area, creating a loss of material due to a larger exclusion zone, and the increased sloped perimeter of the quarry. This is justified by benefits of extending the Via-Vai quarry northwards into Area 2, and the large amount of product that would be available from the remaining area. Subsequent analyses do not include this road for simplicity.

The thickness of the sand in this area increases to the northwest, from 56 to 74m (Figure 7.9). This is an improvement on the Via-Vai quarry where the thickness does not exceed 59.2m. This means an estimated potential of 49.886 million m³ (99.772 million tonnes) of material (Figure 7.10). In proportion to the area of land, this is over 7 times that of the Via-Vai quarry, making this new area potentially highly profitable. This is enough to maintain a production of 300 000 tonnes per year (used in Visa, 2004) for 332.6 years.

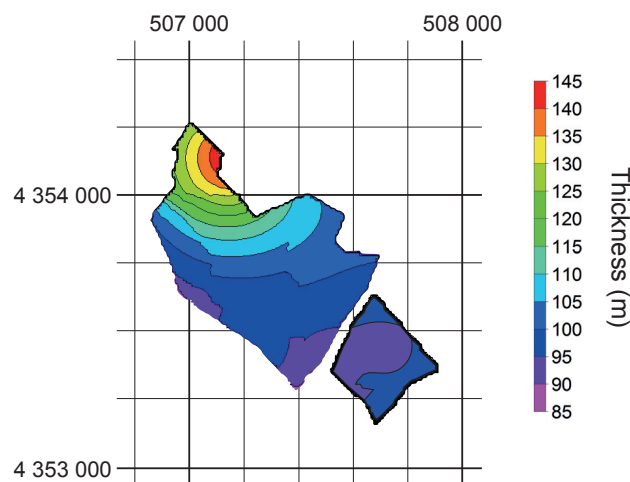


Figure 7.9. Thickness of sand deposit in the proposed excavation location. Made using RockWorks.

7. Areas of further exploitation

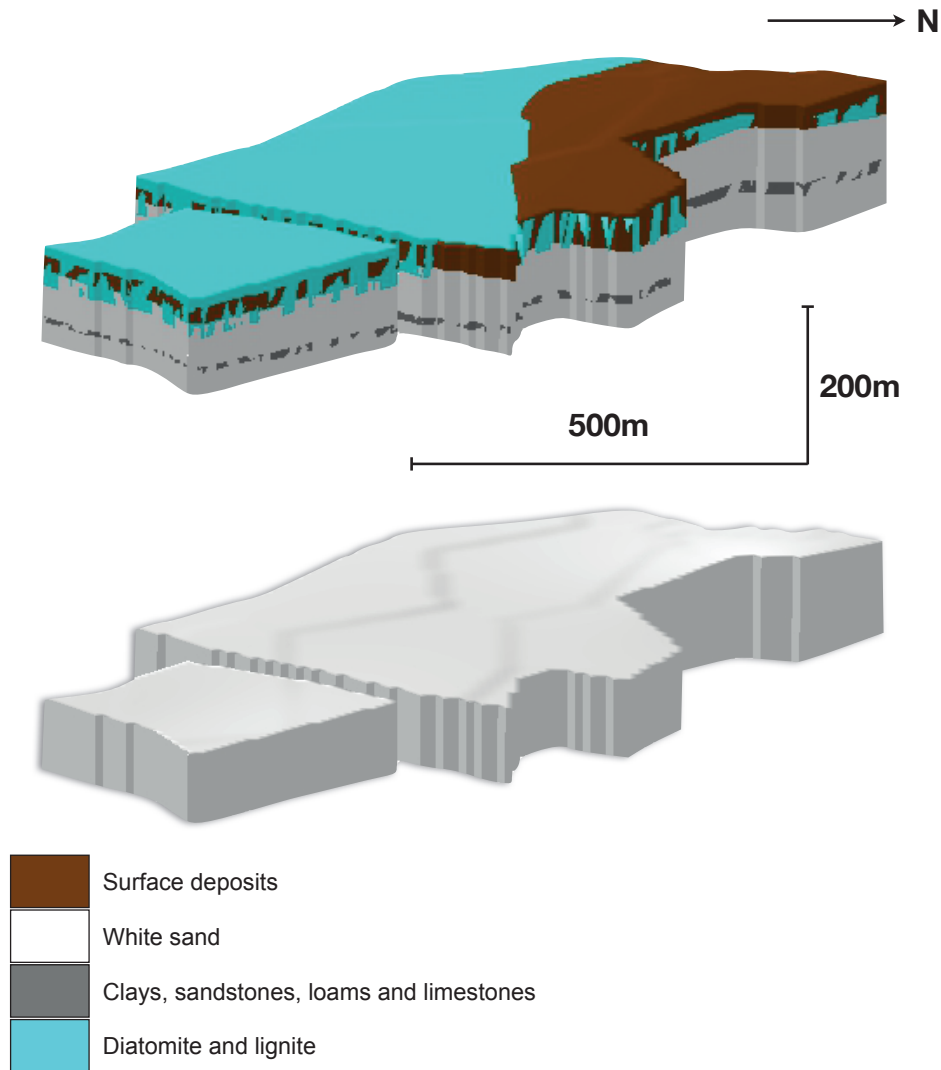


Figure 7.10. RockWorks stratigraphic model of the proposed excavation location. Above model shows all stratigraphic units. Below model shows only the white sand stratigraphic unit.

The depth of the upper horizon of the sand varies between 10 and 55m, increasing in a north-northeast direction (Figure 7.11). This aspect is less favourable compared to the Via-Vai quarry, which had a cover of <30m, measuring 11.8m at borehole AF28, which might not be its shallowest point. This means that the overburden for the Via-Vai quarry is in excess of 65% of the extracted material (there is not sufficient data for exact calculations on this issue). In the prospective area, the overburden would be larger, but an estimated 15% of the extracted material. Sufficient initial capital to remove this overburden would be recouped from the amount of exploitable material.

The concentration of contaminants generally increases from the southeast to the northwest (exceptions include iron, magnesium, and titanium oxides). The most important oxides of aluminium (Figure 7.12) and iron (Figure 7.13) have a range of 0.5-1.8% and

White Sands of Rio Maior

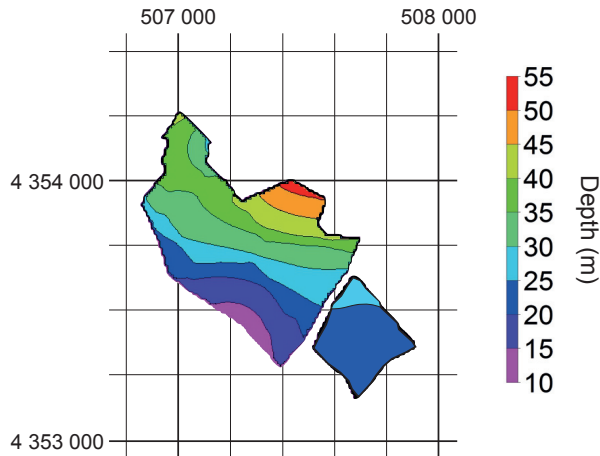


Figure 7.11. Depth of the sand upper horizon in the Rio Maior basin. Made using RockWorks.

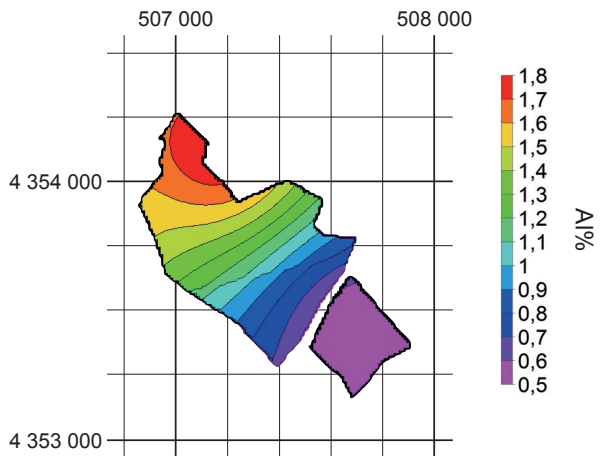


Figure 7.12. Distribution of Al_2O_3 throughout proposed excavation location. Made using RockWorks.

0.04-0.26% respectively. These values cover a range of values within the basin, the concentration of aluminium being in-between the 24th and 90th percentiles, while iron is between the 10th and 87th percentiles. The contaminants in the Via-Vai quarry are generally lower, but with an upper level of iron oxide of 0.55%. The exact influence of these contaminants on the useful amount of sand that can be extracted is unknown, however, if the 62% increase in average aluminium oxide content is consistent with an increase in kaolin content, it would result in approximately 19.4% of the extractable material being kaolin. This would be 9.678 million m³ (19.356 million tonnes) of kaolin.

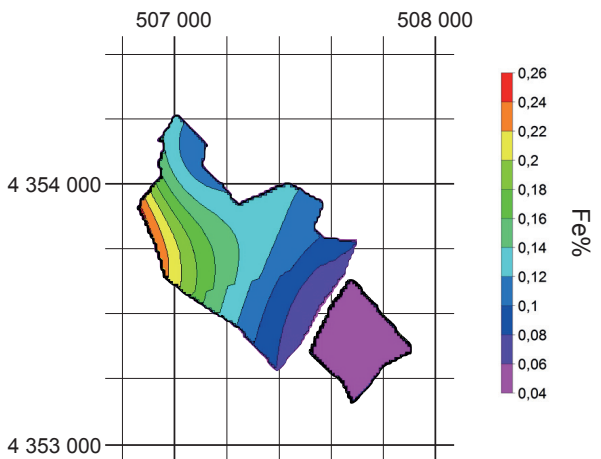


Figure 7.13. Distribution of Fe_2O_3 throughout proposed excavation location. Made using RockWorks.

The amount of the diatomite and lignite complex that overlies the northern portion of the prospective area has not been accurately reconstructed in the geological models used (Figures 7.10, 7.14). Although the amount is unknown, the work of Carvalho and Pereira (1973), and Flores (1996) agree that there will be a portion of diatomite, and possibly lignite, encountered in the northern part of this area. While this material could be removed and stored in the same way as the other overburden material, diatomite could be used in a similar manner to kaolin to produce a product from waste material. Diatomite (also known as diatomaceous earth) is mostly ground up and sold as a silica powder (Crangle, 2016). The diatomite is not suitable as a complete substitute for Sifucel's silica powder production, as diatomite cannot be refined into specific purities as easily as sand. Sifucel usually sells silica

7. Areas of further exploitation

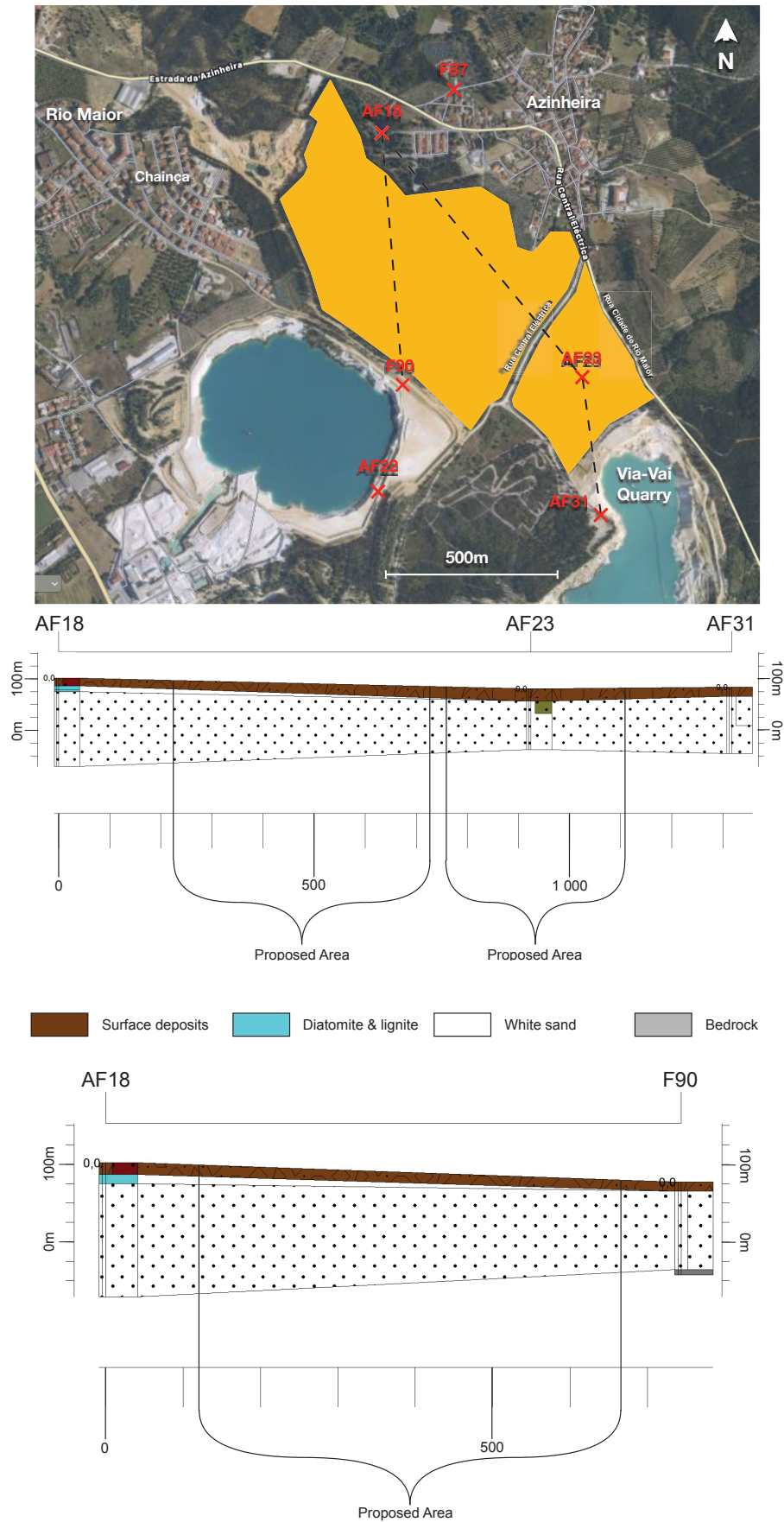


Figure 7.14. RockWorks stratigraphic sections of the proposed excavation location. Above map was created using GoogleEarth and Applemaps, and shows section lines.

powder with well defined characteristics, however using the diatomite as a source for low quality silica powder might offset some costs for its removal and is worthy of evaluation.

7.4. Legal requirements

The primary area for expansion is into Area 2 as it is already purchased and borders the currently operating Via-Vai quarry. As Area 2 is less than 25 hectares, according to Article 36, paragraph 4 of Decreto-Lei n.º 340/2007 of 12th of October, the extension of the quarry could be approved with a notification to the City Council with a favourable Avaliação de Impacte Ambiental (AIA) as part of the Declaração de Impacte Ambiental (DIA). If nothing is received regarding the matter in the next 20 days, the expansion plan has been approved. A certificate deeming it a favourable location would still be needed, however, for the Direção Geral de Energia e Geologia (DGEG). Before quarry work begins, the area should be geologically researched so more detailed mining plans can be made. Research licensing would be granted by the DGEG.

Any work to the northwest of the Rua Central Eléctrica would constitute a separate quarry. Despite not being well defined currently, it would be intended to have a depth of >10m and therefore would be classified as Class 2. This would mean providing the Municipal Council with a plano diretor municipal (PDM) for the approval of a plano ambiental e de recuperação paisagística (PARP) and a favourable DIA for a certificate of location in accordance with Article 9 of Decreto-Lei n.º 340/2007 of 12th of October.

8. Conclusion and recommendations

The Rio Maior basin maintains significant areas for further study in relation to excavating the sand, and for geological exploration and analysis.

8.1. Further excavation of sand

After acquiring the desired land and the rights of preselection, regular cores should be taken of the area. Sand from these samples would be tested and compared with the projected data represented above. This allows for informed evaluation and preparations for any changes in production to be made.

A progressive rather than holistic operation is advised based on current data. This would involve a creeping advancement into the Area 2 as part of the current Via-Vai quarry operations. As work commences on the new excavation, production can continue in the current quarry to maintain profitability. When excavation changes to the new location, the Via-Vai quarry can be recovered in accordance to the Plano de Lavra.

It is important to note that the measurements put forward in this study are for a holistic excavation of the area which is not feasible. This study does not take into account exclusion zones and quarry geometry, both of which would reduce the actual amount of sand able to be excavated. Both of these issues, and their impact involve legal requirements and excavation plans based on production evaluations. Also not considered here is the possible advances in excavation potential and production rate which might affect this project during its predicted lifespan.

8.2. Further geological exploration

The tools and methods used in this study, while sufficient for its intended purpose, did not accurately model the diatomite and lignite complex. Despite the extensive analysis of this minor basin (Zbyszewski, 1967, Diniz, 1984b, Flores, 1996), there are still some inconsistencies regarding its volume and border. It is this latter which is of relevance to this study, which used the most recent Flores (1996) border, but found some examples of diatomite outside this (e.g. AF18). Finding the true extent of the lignite basin would require accumulating data from all previous boreholes in the area and creating more where it appears readings are required for clarity.

The model of the Rio Maior basin produced in this study calculates a total volume of sand of 918 969 989 m³. Using the estimated density of the in-situ sand as 1.8 g/cm³ (Carvalho & Pereira, 1973), this would be 1 654 145 980.2 tonnes. This is 27% greater than the estimate calculated by Carvalho and Pereira (1973) of 722 800 000 m³ and 1 301 040 000 tonnes. This is the case despite using Carvalho and Pereira's model for the lower horizon of the sand layer. This study's model also includes an overly extensive diatomite and

White Sands of Rio Maior

lignite layer, which shares a poorly defined contact with the sand deposit. The problems regarding the contact may be cleared by comparing the modelled contact with the actual contact encountered during prospection and excavation. The most accurate models for the volume of the sand deposit, however, would require more boreholes which transfix the sand deposit, particularly underneath the lignite basin. Chemical analyses of these sands would also allow for accurate maps of contaminant distribution throughout the whole basin. A thorough mineralogical analysis would also allow future works to be prepared for the amounts of kaolin and other minerals likely to be encountered. This is problematic as such an undertaking would require significant funds, which the unprofitable nature of excavating the deepest parts of the basin do not justify.

Bibliography

- Afonso, R. S., 1981. Report of the preliminary project of Rio Maior lignite Opencast Mine. Vol. I - Mining geological study of the Rio Maior lignite basin. *Engineering Consortium Reinbraun*.
- Antunes, M. T. & Pais, J., 1993. The Neogene of Portugal. *Ciências da Terra (UNL)*, **12**, p. 7-22.
- Antunes, M. T. & Pais, J., 1984. Climate during Miocene in Portugal and its evolution. *Paléobiologie continentale*, **14** (2), p. 75-89.
- Antunes, M. T., Legoinha, P., Cunha, P. & Pais, J., 2000. High resolution stratigraphy and Miocene facies correlation in Lisbon and Setúbal Peninsula (Lower Tagus basin, Portugal). *Ciências da Terra*, **14**, p. 183-190.
- Antunes, M. T., Soulié-Märsche, I., Mein, P. & Pais, J., 1992. Le gisement de Asseiceira, Portugal (Miocène supérieur). Données complémentaires sur Freiria de Rio Maior. *Ciências da Terra (UNL)*, **11**, p. 219-253.
- Azevêdo, M. T., 1997. *Depositional Architecture of the sedimentary infilling of the Pre-Tejo river in the upper Pliocene. ECSA Meeting 1997 Estuarine and Coastal Sciences Assoc. Inst. Oceanografia*. Lisboa: FCUL.
- Barbosa, B., 1995. *Alostratigrafia e litostratigrafia das unidades continentais da Bacia terciária do baixo tejo. Relações com o eustatismo e a tectónica*. PhD thesis Universidade de Lisboa.
- Barbosa, B. & Reis, R. P., 1996. Geometrias de enchimento, sistemas deposicionais e organização estratigráfica do pliocénico continental da Bacia Terciária do Baixo Tejo (Portugal). *Com. Serv. Geol. Portugal*, **82**, p. 51-86.
- Barra, A. P., Barbosa, B., Martins, A. A. & Reis, R. P., 2000. Significado regional dos depósitos neogénicos continentais da área de Vila de Rei (Portugal Central). *Ciências da Terra (UNL)*, **14**, p. 163-170.
- Barrón, E., Rivas-Carballo, R., Postigo, M. J., Alcal-de-Olivares, C., Vieira, M., Castro, L., Pais, J. & Valle-Hernandez, M. F., 2010. The Cenozoic vegetation of the Iberian Peninsula. A synthesis. *Review of Palaeobotany and Palynology*, **162**, p. 382-402.
- Berner, R. A., 1971. *Principles of Chemical Sedimentology*. New York: McGraw-Hill.
- Bishop, A. C., Woolley, A. R. & Hamilton, W. R., 1999. *Philip's Guide to Minerals, Rocks and Fossils*. 2nd ed. London: Octopus Publishing Group.
- Bridge, J. S., 1993. The interaction between channel geometry, water flow, sediment transport and deposition in braided rivers. In Best, J. L. & Bristow, C. S., ed. *Braided Rivers*. Geological Society Special Publication.
- Brown, G. G., 1936. Chemical and physical properties of, and cause of bond in sands. *Molding Sands Of Michigan And Their Uses*, **41** (Geological Series 35), p. 1-71.
- Calado, C. & Brandão, J. M., 2009. Salinas interiores em Portugal: o caso das marinhas de Rio Maior. *Geonovas*, **22**, p. 45-54.
- Carriso, R. & Correira, J., 2004. *Classificação e Peneiramento*. 4a ed. Rio de Janeiro: Centro de Tecnologia Mineral.
- Carvalho, A. M. G., 1968. *Contribuição para o conhecimento geológico da Bacia Terciária do Tejo*. Lisboa: Serviços Geológicos de Portugal.
- Carvalho, A. M. G. & Pereira, V. B., 1973. Areias brancas de Rio Maior. Aspectos geológico-económicos. *Estudos, Notas e Trabalhos do Serviço de Fomento Mineiro*, **XXII** (1-2), p. 5-88.

White Sands of Rio Maior

- Casagrande, D. J., 1987. Sulphur in peat and coal. In Scott, A. C., ed. *Coal and Coal-bearing Strata: Recent Advances*. London: Geological Society, Special Publication 32.
- Casagrande, D. J., 1985. Distribution of sulphur in progenitors of low-sulphur coal: origins of organic sulphur. In Cross, A. T., ed. *Economic Geology: Coal, Oil and Gas*. Edwardsville, Illinois: Southern Illinois University Press.
- Cloeting, S., Burov, E., Beekman, F., Andeweg, B., Andriessen, P., Garcia-Castellanos, D., De Vicente, G. & Vegas, R., 2002. Lithospheric folding in Iberia. *Tectonics*, **21** (5), p. 1041-1067.
- Colman, D. A., 1981. *The Hydrocyclone for Separating Light Dispersions*. PhD Thesis University of Southampton.
- Crangle, R. D., 2016. *USGS 2016 Minerals Yearbook: Diatomite*. [PDF] Available from: <https://s3-us-west-2.amazonaws.com/prd-wret/assets/palladium/production/mineral-pubs/diatomite/myb1-2016-diato.pdf> [11/04/2019]
- Cunha, P. P., Barbosa, B. P. & Reis, R. P., 1993. Synthesis of the Piacenzian onshore record between the Aveiro and Setúbal parallels (Western portuguese margin). *Ciências da Terra (UNL)*, **12**, p. 35-43.
- De Vicente, G., Cloetingh, S., Muñoz-Martin, A., Olaiz, A., Stich, D., Vegas, R., Galindo-Zaldivar, J. & Fernández-Lozano, J., 2008. Inversion of moment tensor focal mechanisms for active stresses around microcontinent Iberia: tectonic implications. *Tectonics*, **27**, p. 1-22.
- Dias, R. C., 2015. *Minerais pesados de areias de Rio Maior: Análise de processos de separação e concentração e caracterização de concentrados*. Dissertation Universidade de Aveiro.
- Diniz, F., 1984a. *Apports de la palynologie à la connaissance du Pliocène portugais. Rio Maior, un bassin de référence pour l'histoire de la flore, de la végétation et du climat de la façade atlantique de l'Europe meridionale*. Thesis Université des Sciences et Techniques du Languedoc.
- Diniz, F., 1984b. Étude palynologique du bassin pliocène de Rio Maior (Portugal). *Paleobiol. Cont.*, **14** (2), p. 259-267.
- Diniz, F., 2003. Os depósitos detritico-diatomíticos de Abum (Rio Maior). Novos aspectos paleoflorísticos e implicações paleoclimáticas. *Ciências da Terra (UNL)*, n° especial V, p. 7, CDRom A49-A52.
- Elliott, T., 1989. Deltaic systems and their contribution to an understanding of basin-fill successions. In Whateley, M. K. G. & Pickering, K. T., ed. *Deltas: Sites and Traps for Fossil Fuels*. Geological Society Special Publication.
- European Commission, 2014. *Non-Critical Raw Materials Profiles*. [PDF] Available from: <http://ec.europa.eu/DocsRoom/documents/7422/attachments/1/translations> [18/04/2019]
- Fauquette, S., Suc, J. P., Guiot, J., Diniz, F., Feddi, N., Zheng, Z., Bessais, E. & Drivaliari, A., 1999. Climate and biomes in the west mediterranean area during the Pliocene. *Palaeog. Palaeoclimatol. & Palaeoecol.*, **152**, p. 15-128.
- Flores, D., 1996. *Estudo petrológico e geoquímico dos carvões da Bacia de Rio Maior, Vol. I*. Porto: Universidade do Porto.
- Flores, D., 1987. *Contribuição para o estudo petrológico das lignites de Rio Maior. 2 Vols*. Porto: Universidade do Porto.
- Grupo Parapedra, 2013. *Grupo Parapedra*. [Website] Available from: <http://www.parapedra.pt> [18/03/2019]

Bibliography

- Harrell, J., 1984. A visual comparator for degree of sorting in thin and plane sections. *Journal of Sedimentary Petrology*, **54**, p. 646-650.
- Hubert, J. F., 1962. A zircon-tourmaline-rutile maturity index and the interdependence of the composition of heavy mineral assemblages with the gross composition and texture of sandstones. *Journal of Sedimentary Research*, **32** (3), p. 440-450.
- IMA-Europe, 2011. *Silica*. [PDF] Available from: https://www.ima-europe.eu/sites/ima-europe.eu/files/minerals/Silica_An-WEB-2011.pdf [22/04/2019]
- IMA-Europe, 2013. *Recycling Industrial Minerals*. [PDF] Available from: https://www.ima-europe.eu/sites/ima-europe.eu/files/publications/IMA-Europe_Recycling%20Sheets_2018.pdf [18/04/2019]
- IMR Test Labs, 2019. *X-Ray Powder Diffraction Analysis (XRD)*. [Webpage] Available from: <https://www.imrtest.com/tests/x-ray-powder-diffraction-analysis-xrd> [28/03/2019]
- Jimenez-Moreno, G., Rodríguez-Tovar, F., Pardo-Igúzquiza, E., Fauquette, S., Suc, J. P. & Müller, P., 2005. High-resolution palynological analysis in early-middle Miocene core from the Pannonian Basin, Hungary: climatic changes, astronomical forcing and eustatic fluctuations in Central Paratethys. *Palaeogeogr., Palaeoclimat. & Palaeoecol.*, **216**, p. 73-97.
- Kelly, T. D., Matos, G. R., Buckingham, D. A., DiFrancesco, C. A., Porter, K. E., Berry, C., Crane, M., Goonan, T. & Sznoppek, J., 2014. *Historical Statistics for Mineral and Material Commodities in the United States*. [Online documents] Available from: <https://minerals.usgs.gov/minerals/pubs/historical-statistics/> [23/04/2019]
- Klein, C. & Hurlbut, C. S., 1985. *Manual of Mineralogy*. 20th ed. New York: John Wiley and Sons.
- Kreiter, V. M., 1968. *Geological Prospecting and Exploration*. Honolulu, Hawaii: University Press of the Pacific. p. 13-113.
- Kullberg, J. C., Rocha, R. B., Soares, A. F., Rey, J., Terrinha, P., Azerêdo, A. C., Callapez, P., Duarte, L. V., Kullberg, M. C., Martins, L., Miranda, J. R., Alves, C., Mata, J., Madeira, J., Mateus, O., Moreira, M. & Nogueira, C. R., 2011. A Bacia Lusitaniana: Estratigrafia, Paleogeografia e Tectónica. In Dias, R., Araújo, A., Terrinha, P. & Kullberg, J. C., ed. *Geologia de Portugal no contexto da Ibéria*. Évora: Escolar Ed.
- Lewis, D. G. & McConchie, D., 1994. *Analytical Sedimentology*. London: Chapman & Hall.
- Lisiecki, L. E. & Raymo, M. E., 2005. A Pliocene-Pleistocene stack of 57 globally distributed benthic $\delta^{18}\text{O}$ records. *Paleoceanography*, **20**.
- LNEG, 2019. *Sondabase - Base de Dados de Sondagens*. [Online database] Available from: http://geoportal.lneg.pt/index.php?option=com_content&id=68&lg=pt [10/04/2019]
- Magalhães, F. & Carvalho, A. M. G., 1984. Sobre a possível origem éolica das areias brancas de Rio Maior. *Estud. Notas Trab. Serv. Fom. Min.*, **26** (1-4), p. 21-24.
- Michaud, D., 2013. *Froth Flotation Process*. [Webpage] Available from: <https://www.911metallurgist.com/blog/froth-flotation-process> [04/04/2019]
- Michaud, D., 2015. *Hydrocyclone Working Principle*. [Webpage] Available from: <https://www.911metallurgist.com/blog/hydrocyclone-workingprinciple> [04/04/2019]
- Mitchell, C., 2012. *Role of National Geological Surveys in evaluation of high-purity silica resources*. [Presentation] Available from: http://nora.nerc.ac.uk/id/eprint/18281/1/Evaluation_of_silica_Clive_Mitchell_BGS.pdf [22/04/2019]
- Moura, A. & Velho, J. L., 2012. *Recursos Geológicos de Portugal*. 1st ed. Coimbra: Palimage.

- Mouterde, R., Ramalho, R. M., Rocha, R. B., Ruget, C. & Tintant, H., 1971. Le Jurassique du Portugal. Esquisse stratigraphique et zonale. *Bol. Soc. Geol. Port.*, **18**, p. 73-104.
- Mouterde, R., Rocha, R. B., Ruget, C. & Tintant, H., 1979. Faciés, biostratigraphie et paléogéographie du Jurassique portugais. *Cien. Terra*, **5**, p. 29-52.
- Nichols, G., 1999. *Sedimentology and stratigraphy*. Oxford: Blackwell Publishing.
- Noronha, J., 2010. *Viabilidade técnica da valorização de um minério de ambligonite da Argemela através de flutuação por espumas*. Porto: Faculdade de Engenharia da Universidade do Porto.
- Pais, J., 1989. Evolução do coberto florestal em Portugal no Neogénico e no Quaternário. *Comun. Serv. geol. Portg.*, **75**, p. 67-72.
- Pais, J., 1987. Macrorrestos de gimnospérmicas dos diatomitos de Rio Maior (Portugal). In Ferreira, O. V. & Laitão, M., ed. *Da Pré-História à História. Homenagem a Octávio da Veiga Ferreira*. Lisboa: Editorial Delta.
- Pais, J., 2012. *The Paleogene and Neogene of Western Iberia (Portugal): A Cenozoic Record in the European Atlantic Domain*. Berlin: Springer-Verlag Berlin Heidelberg.
- Pais, J., 1986. Évolution de la végétation et du climat pendant le Miocène au Portugal. *Ciências da Terra (UNL)*, **8**, p. 179-191.
- Pais, J., 2010. Plantas do neogénico e paleoclimas. Evidências em Portugal. In Neiva, J. M. C., Ribeiro, A., Victor, L. M., Noronha, F., Ramalho, M., ed. *Ciências Geológicas: Ensino e Investigação. Vol. I*. Lisboa: Associação Portuguesa de Geólogos. p. 357-363.
- Pereira, V. B., 1991. Recursos nacionais em areias: panorâmica actual e perspectivas futuras. *Geonovas, Revista da Associação Portuguesa de Geólogos, n° especial*, **2**, p. 46-60.
- Pettijohn, F. J., 1975. *Sedimentary Rocks*. 3rd ed. New York: Harper and Row.
- Pettijohn, F. J., Potter, P. E. & Siever, R., 1987. *Sand and Sandstone*. New York: Springer-Verlag.
- Ramos, A. M., 2008. *O Pliocénico e o Plistocénico da Plataforma Litoral entre os paralelos do Cabo Mondego e da Nazaré*. Universidade de Coimbra.
- Ribeiro, A., Cabral, J., Baptista, R. Matias, L., 1996. Stress pattern in Portugal mainland and the adjacent Atlantic region, West Iberia. *Tectonics*, **15** (2), p. 641-659.
- RockWare, 2017. *RockWorks 17 Training Manual*. Golden, Colorado: RockWare Inc.
- SAMSA, 2019. *Glass*. [Webpage] Available from: https://www.samsa.org.uk/key_uses/glass.php [22/04/2019]
- Serpa, M. Â. J., 2018. *Caracterização Mineralógica das Areias Exploradas na Mina Via-Vai, Rio Maior*. Dissertação Universidade Nova de Lisboa.
- Silva, A. A., 1946. Diatomáceas fósseis de Portugal. Jazigos de Rio Maior, Óbidos e Alpiarça. *Bol. Soc. geol. Portg.*, **6** (1-2), p. 1-166.
- Sturm, M. & Matter, A., 1978. Turbidites and varves in Lake Brienz (Switzerland): deposition of clastic detritus by density currents. In Matter, A. & Tucker, M. E., ed. *Modern and Ancient Lake Sediments*. International Association of Sedimentologists Special Publication.
- Suc, J. P., 1984. Origin and evolution of the mediterranean vegetation and climate in Europe. *Nature*, **307**, p. 429-432.
- Suc, J. P., Bertini, A., Combourieu-Nebout, N., Diniz, F., Leroy, S., Russo-Ermolli, E., Zheng, Z., Bessais, E. & Ferrier, J., 1995. Structure of West Mediterranean vegetation and climate since 5,3 ma. *Acta zool. Cracov.*, **38**, p. 3-16.

Bibliography

- Teixeira, C., 1973. *Oreodaphne heeri* Gaud., une nouvelle espèce fossile du Pliocène de Rio Maior. *Bol. Soc. geol. Portg.*, **18** (2-3), p. 147-149.
- Teixeira, C. & Gonçalves, F., 1980. *Introdução à Geologia de Portugal*. Lisboa: Instituto Nacional de Investigação Científica.
- Tejero, R., Heydt, G. G., Vich, R. B. & García, P. F., 2010. *Long-Term evolving "Tectonic" landscapes within intra-plate domains. The Iberian Peninsula. Horizons in Earth Science Research*. 2nd ed. USA: Nova Publishers Inc. p. 103-124.
- Terrinha, P., Kullberg, J. C., Kullberg, M.C., Moita, C. & Ribeiro, A., 1996. Thin skinned and thick skinned sub-basin development, bidimensional extension and self-indentation in the Lusitanian Basin, West Portugal. *2a Conf Nac. GGET, Soc. Geol. Portugal*, p. 17-20.
- Terroso, D., 2005. *Argilas / Lamas e Águas Termais das Fumas (Açores): Avaliação das Propriedades Físicas e Químicas relevantes para a utilização em Peloterapia*. Aveiro: Universidade de Aveiro.
- Uphoff, T., Stemler, D. P., Stearns, M. J., Hogan, S. K. & Monteleone, P. H., 2002. Lusitanian basin highlights important potential in Portugal. *Oil and Gas Journal*, **100** (50), p. 32-38.
- Vegas, R., 2006. Modelo tectónico de formación de los relieves montañosos y las cuencas de sedimentación terciarias del interior de la Península Ibérica. *Bol. R. Soc. Esp. Hist. Nat. (Sec. Geol.)*, **101** (1-4), p. 31-40.
- Vieira, M. C., 2009. *Palinologia do Pliocénico da Orla Ocidental Norte e Centro de Portugal: Contributo para a compreensão da cronostratigrafia e da evolução paleoambiental*. Tese de Doutoramento Universidade do Minho.
- Vieira, M., Pais, J. & Pereira, D., 2010. Estudo Palinológico da sondagem F98 na Bacia de Rio Maior. *Revista Electrónica de Ciências da Terra*, **17** (nº 4), p. 1-4.
- Vieira, M., Poças, E., Pais, J. & Pereira, D., 2011. Pliocene flora from S. Pedro da Torre deposits (Minho, NW Portugal). *Geodiversitas*, **33** (1), p. 71-85.
- Visa, 2004. *Estudo De Impacte Ambiental Do Projecto Da Mina De Caulino De Via-Vai. Resumo Não Técnico*. Rio Maior: Sifucel - Silicas, Lda. p. 1-16.
- Wescott, W. A. & Ethridge, F. G., 1990. Fan deltas-alluvial fans in coastal settings. In Rachocki, A. H. & Church, M., ed. *Alluvial Fans: A Field Approach*. Chichester: Wiley.
- Zagwijn, W. H., 1960. Aspects of the Pliocene and early Pleistocene vegetation in the Netherlands. *Meded Geol Schicht ser C*, **3** (5), p. 78.
- Zbyszewski, G., 1966. *Carta Geológica De Portugal Na Escala De 1/50 000: Notícia Explicativa Da Folha 30-B Bombarral*. Lisboa: Serviços Geológicos de Portugal.
- Zbyszewski, G., 1943. Une reconnaissance géologique dans la région de Rio Maior: l'âge des lignites du gisement de Espadanal. *Comun. Serv. Geol. Portugal*, **24**, p. 3-21.
- Zbyszewski, G., 1967. Estudo geológico da bacia dos lignitos de Rio Maior. *Estudos Not. e Trab., S. F. M.*, **17** (3-4), p. 5-105.
- Zbyszewski, G., 1959. Étude struttural de l'aire typhonique de Caldas da Rainha. *Mem. Serv. Geol. Portugal*, **3**, p. 184.
- Zbyszewski, G. & Almeida, F. M., 1960. *Carta Geológica De Portugal Na Escala De 1/50 000: Notícia Explicativa Da Folha 26-D Caldas Da Rainha*. Lisboa: Serviços Geológicos De Portugal.